CIVIL ENGINEERING STUDIES
Illinois Center for Transportation Series No. 16-026
UILU-ENG-2016-2026
ISSN: 0197-9191

EVALUATION OF PCC PAVEMENT AND STRUCTURE CORING AND IN SITU TESTING ALTERNATIVES

Prepared By
John S. Popovics
Agustin Spalvier
University of Illinois at Urbana-Champaign

Kerry S. Hall
University of Southern Indiana

Research Report No. FHWA-ICT-16-022

A report of the findings of

ICT PROJECT R27-137
Evaluation of PCC Pavement and Structure Coring and In Situ Testing Alternatives

Illinois Center for Transportation

December 2016

TECHNICAL REPORT DOCUMENTATION PAGE

1. Report No.	2. Government Accession No.	3. Recipient's Catalog No.
FHWA-ICT-16-022	N/A	N/A

4. Title and Subtitle	5. Report Date
Evaluation of PCC Pavement and Structure Coring and In Situ Testing Alternatives	December 2016
	6. Performing Organization Code N/A

7. Author(s)	8. Performing Organization Report No.
John S. Popovics, Agustin Spalvier, and Kerry S. Hall	ICT-16-026 UILU-ENG-2016-2026

9. Performing Organization Name and Address	10. Work Unit No.
Illinois Center for Transportation Department of Civil and Environmental Engineering University of Illinois at Urbana-Champaign 205 North Mathews Avenue, MC-250 Urbana, IL 61801	N/A
	11. Contract or Grant No. R27-137

12. Sponsoring Agency Name and Address	13. Type of Report and Period Covered
Illinois Department of Transportation (SPR) Bureau of Material and Physical Research 126 East Ash Street Springfield, IL 62704	Final report, 7/1/13–12/31/16
	14. Sponsoring Agency Code FHWA

15. Supplementary Notes
Conducted in cooperation with the U.S. Department of Transportation, Federal Highway Administration

16. Abstract
The objectives of this research are to evaluate core strength correction factors considering a range of pertinent factors that are encountered in the field, and to investigate more practical core field curing practices that provide best estimates of in-place concrete strength. The effect of core condition (including presence of embedded rebar) and core conditioning procedures (dry and wet) on the measured compressive strength of the core sample was considered. Another objective of the research was to evaluate the utility of practical non-destructive testing (NDT) methods for estimating in-place concrete strength that could be used to reduce the amount of required coring or to provide an estimate of in situ strength for locations that cannot be cored, such as in precast prestressed beams. The results of in-place cylinder and core strength tests were statistically compared. This study shows that using dry-conditioned cores with the correction factors 1.05 for PV/SI cores without rebar, 1.08 for PV/SI cores with rebar, and 1.03 for PS cores without rebar yields the most confident strength estimations. Dry-conditioned core strength data show less variability than the data from wet-conditioned cores. The presence of rebar had minor effect on core strength. Non-destructive testing methods can be used to establish correlation curves to estimate in-place strength; several methods were characterized analyzing their variability and sensitivity. Results from this study can assist the Illinois Department of Transportation (IDOT) in establishing procedures to estimate the in-place strength of concrete with greater accuracy; such information could be used by IDOT to improve implementation of pay-for-performance specifications for Portland cement concrete (PCC) construction.

17. Key Words	18. Distribution Statement
Concrete, core, in-place cylinder, in-place strength, non-destructive testing, NDT, correlation curve, coring damage.	No restrictions. This document is available through the National Technical Information Service, Springfield, VA 22161.

19. Security Classif. (of this report)	20. Security Classif. (of this page)	21. No. of Pages	22. Price
Unclassified	Unclassified	72 plus appendices	N/A

ACKNOWLEDGMENT, DISCLAIMER, MANUFACTURERS' NAMES

This publication is based on the results of **ICT-R27-137, Evaluation of PCC Pavement and Structure Coring and In Situ Testing Alternatives**. ICT-R27-137 was conducted in cooperation with the Illinois Center for Transportation; the Illinois Department of Transportation, Division of Highways; and the U.S. Department of Transportation, Federal Highway Administration.

Members of the Technical Review Panel were the following:

- Douglas Dirks (Chair), IDOT
- John Albinger, IRMCA
- Dan Brydl, FHWA
- John Ciccone, IDOT
- Ryan Culton, IDOT
- Greg Heckel, IDOT
- John Huang, IDOT (subsequently retired and employed by Interra, Inc.)
- James Krstulovich, IDOT
- Matt Mueller, IDOT
- Brian Pfeifer, IDOT (employed by FHWA at start of project)
- Wayne Phillips, IDOT
- Jim Randolph, IRMCA
- Randell Riley, ACPA
- Theron Tobolski, IRMCA

EXECUTIVE SUMMARY

The objectives of this research are to evaluate core strength correction factors considering a range of pertinent factors that are encountered in the field, and to investigate more practical core field curing practices that provide best estimates of in-place concrete strength.[1]

To achieve this goal, 16 slabs were cast and tested, and the obtained results were statistically analyzed. The slabs' nominal dimensions were 5 x 5 ft (1.5 x 1.5 m) by 9 in. (23 cm) thick. Each slab produced eight core strength measurements and eight in-place strength measurements. Slabs were organized in pairs, with each pair having the same feature or effect to be analyzed. In other words, this investigation studied the effects that may occur on core strength as a result of eight characteristics or situations. These characteristics were a combination of concrete mixture design, type of moisture conditioning of cores after extraction, and presence of rebar.

Three mixture designs were used: PV/SI, PS, and PV/SI-low. The PV/SI mixture corresponded to a regular-strength concrete commonly used by the Illinois Department of Transportation (IDOT) for pavements and structures. The PS mixture corresponded to a high-strength mixture design commonly used by IDOT for prestressed members. The PV/SI-low mixture design corresponded nominally to the same mixture as PV/SI, but additional water and air-entraining admixture were added to simulate low-strength concrete.

Two types of core conditioning were employed: 1-day dry and 1-day wet. The former corresponded to placing the cores, right after extraction, in front of a fan at room humidity and temperature, for 24 hours before testing. The latter corresponded to submerging the cores in water at 73°F (23°C), right after extraction, for 24 hours before testing. The conditioning time, 24 hours was the same in all cases.

The presence of rebar was studied by embedding rebar in the slabs with a 2 in. (5.1 cm) cover depth. Two types of rebar location were studied. One was with rebar crossing the cores through the inner third of their cross-section, and the other one was with the rebar crossing the cores through the outer two-thirds of their cross-section. One pair of slabs was cast to study each of these situations.

This study shows that using dry-conditioned cores with the correction factors 1.05 for PV/SI cores without rebar, 1.08 for PV/SI cores with rebar, and 1.03 for PS cores without rebar yield the most confident strength estimations. Dry-conditioned core strength data show less variability than the data from wet-conditioned cores. The presence of rebar had minor effect on core strength. In the case of the high-strength PS mixture, strength results were more variable than in the cases of PV/SI and PV/SI-low, but the application of the factors was still applicable.

Another objective of this investigation was to evaluate the utility of practical non-destructive testing (NDT) methods for estimating in-place concrete strength that could be used to reduce the amount of required coring or to provide an estimate of in situ strength for locations that cannot be cored, such

[1] In-place strength was measured using cast-in-place cylinders that were cast inside the concrete slabs using a plastic mold inside a galvanized steel sleeve; thus, these cylinders were pulled out from the slab instead of being cored from it.

as in precast prestressed beams. Five NDT methods were employed: dynamic modulus, rebound hammer, Nitto hammer, pullout, and contactless surface wave propagation. The contactless surface wave propagation method showed very poor results as a result of experimental problems, so it was excluded from the analysis.

The obtained experimental results suggest that dynamic modulus data could substitute, in part, for some of the core strength tests. With the use of a well-constructed correlation curve, compressive strength could be estimated from the dynamic modulus of a core sample.

The rebound hammer, Nitto hammer, and pullout testing methods were analyzed separately from dynamic modulus and were compared with each other. Non-destructive testing vs. compressive strength correlation curves were built, and their quality was computed using the residual standard deviation parameter. This parameter measured the offset distance from the data points to the given correlation curve, providing an idea of how certain (or uncertain) these correlation curves were. Sensitivity of the NDT method to small strength variations was also analyzed. For each NDT method, the error that the strength estimates showed with regard to the actual measured in-place strengths was computed. Then the trend of the estimated strength errors with an increasing number of NDT locations per slab was analyzed.

First, the PV/SI and the PV/SI-low mixtures were analyzed together, and the PS mixture slabs were omitted from the analysis. It was found that the ordinary least squares (OLS) linear correlation curves for the rebound hammer and pullout testing methods were better than the power (logOLS) correlation curves. In the case of the Nitto hammer, the logOLS correlation curve was better than the OLS. In addition, when considering the entire NDT dataset (80 measurements of rebound hammer, 80 measurements of Nitto hammer, and three measurements of pullout, per slab) it was found that pullout was the most sensitive and was also the least uncertain. The rebound hammer showed results slightly poorer than pullout.

Similar observations and conclusions were found when all three mixture designs were analyzed together. In these tests, the use of power correlation curves became more accurate than when the PS was not considered.

CONTENTS

CHAPTER 1: INTRODUCTION

Determining the actual in situ strength of concrete in a pavement or structure can be difficult because it depends on curing history and the adequacy of consolidation, in addition to its inherent material qualities (Nikbin et al. 2009). Furthermore, it is well known that the standard companion test specimens are not necessarily representative of the in situ strength of the concrete product in question, which becomes an important concern when the strength test results are lower than specified. The typical solution for determining the actual in situ strength is to test core specimens taken from the suspect concrete product. However, interpreting core strength test results can be problematic depending on various factors such as the size (e.g., length-to-diameter ratio, diameter vs. maximum aggregate size) of the core specimen, its moisture condition and age at testing, any damage to the specimen caused by the coring operation (Nikbin et al. 2009), and the presence of reinforcing steel within the core (Gaynor 1965). It has also been reported that the differences between how a concrete product is poured/placed and consolidated to that of standard companion test specimens can impact the comparison of core and standard specimen strength results (Arıöz et al. 2006). Currently, the Illinois Department of Transportation (IDOT) requires core test specimens to achieve 100% of the required minimum strength regardless of these factors—a requirement that has frustrated industry and could have significant consequences for IDOT with respect to implementing pay-for-performance specifications for Portland cement concrete (PCC) construction.

Furthermore, small cores in particular are more susceptible to damage during coring and handling; for example, small cores can be more greatly affected by large aggregate particles (relative to the size of the core) being loosened during coring. Additionally, the potential impact on test results will be greater because the surface-area-to-volume ratio increases as diameter decreases (Nikbin et al. 2009). The effects of specimen size on measured strengths are well known, and methods for determining a correlation factor have been established. However, these correlation factors should be within the 95% statistical confidence level; thus, they should be established for each combination of mix design, curing condition, test age, and cylinder capping material, resulting in a minimum of 30 tests. Although practicable, alternative test methods could be more efficient without sacrificing accuracy.

The objectives of this research are to evaluate core strength correction factors considering a range of pertinent factors that are encountered in the field and to investigate a more practical core field curing practice that provides best estimates of in-place concrete strength. The effect of core condition (including presence of embedded rebar) and core conditioning procedures (dry and wet) on the measured compressive strength of the core sample was considered. Another objective was to evaluate the utility of practical non-destructive testing (NDT) methods for estimating in-place concrete strength. These NDT methods could be used to reduce the amount of required coring or to provide an estimate of in situ strength for locations that cannot be cored, such as in precast prestressed beams. The results reported here can assist IDOT in establishing procedures to estimate the in-place strength of concrete with greater accuracy. Such information could be used by IDOT to improve implementation of pay-for-performance specifications for PCC construction.

CHAPTER 2: RESEARCH SIGNIFICANCE

This research provides a useful dataset composed of 16 concrete slabs of dimensions 5 by 5 ft (1.5 x 1.5 m) by 9 in. (23 cm) thick. Each slab produced eight cast-in-place cylinders and eight cores. The in-place cylinders were regarded as representative of the in-place concrete. Thus, the concrete properties of the in-place cylinders and cores datasets could be statistically compared. The most important property studied was compressive strength; other properties analyzed were density, dynamic modulus, and other outputs from NDT methods.

The main objective of the investigation was to statistically study compressive strength populations evaluated from cores, and compare them to compressive strength populations evaluated by testing in-place cylinders. Several affecting factors were studied: mixture designs, moisture conditioning of cores during 1 day after extracting them, and presence of rebar in the cores. The investigation evaluated correction factors that could be applied to core strength in order to estimate in-place strength for a particular concrete mixture, moisture core conditioning, and presence of rebar.

The use of dynamic modulus tests and other NDT methods was analyzed and the results were compared. Correlation curves to estimate in-place concrete strength from the NDT data were built for each case; recommendations are provided for building and using new correlation curves for other cases.

CHAPTER 3: EXPERIMENTAL PROCEDURES

This research project involved casting and testing 17 concrete slabs[2]. Each slab produced eight cast-in-place cylinders and eight cored cylinders. Several NDT methods were carried out on each cylinder and to the top surface of the slabs on day 16 after casting. Cast-in-place cylinders and cored cylinders were tested under compression at day 16 after casting to obtain strength measurements.

3.1 MATERIALS DESCRIPTION

3.1.1 Concrete Mixtures

Three concrete mixture designs were employed in the project: PV/SI, PS, and PV/SI-low, per IDOT nomenclature. The mixture PV/SI-low was nominally the same as the mixture PV/SI except that additional mixing water and an air-entraining agent (AEA) were added to emulate a low-strength concrete. Table 1 contains the target properties of these mixture designs. Table 2 contains the nominal mixture design proportions of the three mixtures.

Table 1: Mixture Designs Target Properties

	PV/SI	PS	PV/SI-Low
Compressive strength, psi (MPa)	3500 (24)(i)	5000 (34)(ii)	< 3500 (24)
w/cm	0.42	0.35	0.50
Slump, in. (cm)	3.5 to 4.5 (8 to 12)	3.5 to 4.5 (8 to 12)	unspecified
Corrected air content, %	5 to 8	5 to 8	8 to 10

(i) Minimum acceptable compressive strength at day 14 after casting according to IDOT specifications, 2012.

(ii) Minimum acceptable compressive strength at day 28 after casting according to IDOT specifications, 2012.

Table 2: Mixture Design Nominal Proportions

	Content per yd^3 (m^3) of concrete		
	PV/SI	PS	PV/SI-Low
Coarse Agg. 1 - CM16(i)-Kankakee, lb (kg)	364 (216)	1820 (1080)	364 (216)
Fine Agg. - FA-Mid-America-Mahomet, lb (kg)	1227 (728)	1108 (657)	1227 (728)
Coarse Agg. 2 - CM11(ii)-Kankakee, lb (kg)	1450 (860)	—	1450 (860)
Fly Ash - C-MRT Labadie, lb (kg)	145 (86)	—	145 (86)
Portland cement type I, lb (kg)	435 (258)	705 (418)	435 (258)
Water, gal (L)	29.2 (145)	29.6 (147)	34.8 (173)
	Admix. content per 100 lb (kg) of cementitious material(iii)		
Air-entraining admixture, oz (mL)	1.9 to 2.0 (56 to 59)(iv)	1.0 (30) (iv)	Variable(iv)
Water reducer Pozzolith 80, oz (mL)	4.0 (118.3)	4.0 (118.3)	4.0 (118.33)

(i) Aggregate CM16 corresponds to 100% passing the 0.5 in. aperture sieve. The complete aggregate gradation is given in Appendix F.

(ii) Aggregate CM11 corresponds to 100% passing the 1 in. aperture sieve. The complete aggregate gradation is given in Appendix F.

(iii) Cementitious material stands for the combination of Portland cement and any other finely divided materials.

(iv) Different quantities were added at every batch to meet the air content specification.

[2] One of the slabs (initially named R15 and then re-named as R15A) was cored on the wrong day; therefore, its core results were not included in the analysis and another slab (R15B) was cast to substitute for it. However, the NDT analyses of both slabs were valid, so both NDT datasets were retained and analyzed.

3.1.2 Formwork

Two sets of reusable forms were employed. Both were built from plywood sheets and were supported and reinforced using 2 × 4 wood bars and steel angles.

3.1.3 Water Bath

A water bath was employed to moist-cure the concrete specimens. The bath was set to hold water at 73°F (23°C), but the real measured water temperature ranged between 70°F and 73°F (21°C and 23°C).

3.1.4 Concrete Internal Vibrator

An internal vibrator with a 1 in. (2.5 cm) diameter was employed to consolidate concrete. The vibrator generated 14,000 vibrations per minute (vpm).

3.1.5 Galvanized Steel Bracer

Galvanized steel bracers, commonly used as wall hangers for pipes and vents, were used to hold the galvanized steel sleeves and plastic molds to generate in-place cylinders (see Section 3.1.9, “In-Place Cylinder Holder”). The bracer is capable of holding pipes or tubes of 4 in. (10.2 cm) diameter, and it has a screw to adjust its mouth for tightening or loosening the grip. Figure 2 (bottom of next page) shows a photograph of the galvanized steel bracer together with other elements.

3.1.6 Galvanized Steel Sleeve

Galvanized steel sleeves were made using sheets of 0.02 in. (0.5 mm) thickness. These sheets were cut and bent to form 9 in. (22.9 cm) tall tubes with a 4.25 in. (10.8 cm) inner diameter. The tubelike shape was formed by applying three welding points along the superposed sheet’s edges. Figure 1 shows a scheme of the galvanized sheet bent to form the sleeve and the approximate position of the welding points.

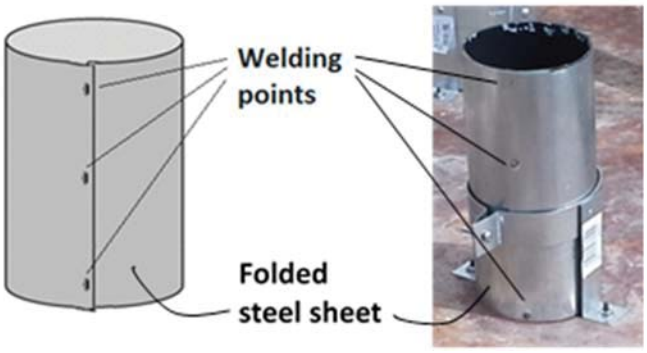

Figure 1: Galvanized steel sheet forming the sleeve, with three welding points.

3.1.7 Foam Pad Disc

Discs 4 in. (10.2 cm) in diameter were cut from 1 in. (2.5 cm) thick extruded polystyrene (foam) sheets. These were used to support the plastic molds inside the steel sleeve, forming the cast-in-place cylinder holder.

3.1.8 Cylinder Plastic Molds

Two sizes of commercially available plastic molds (4 × 8 in. and 6 × 12 in.) were used to produce concrete cylinders of nominal dimensions equal to 4 in. (10.2 cm) diameter and 8 in. (20.3 cm) height, and 6 in. diameter (15.2 cm) and 12 in. (30.5 cm) height, respectively.

3.1.9 In-Place Cylinder Holder

Each of these holders was assembled using one galvanized steel bracer, one galvanized steel sleeve, one foam pad disc, and one 4 × 8 plastic mold. The procedure to prepare holders was as follows: Each bracer was initially fixed to the form floor (plywood formwork of the slab) using screws. The foam pad was then put inside the sleeve, toward one of the ends. Next, the sleeve was set into the bracer, with the foam pad disc in contact with the form floor; the bracer was tightened to hold the sleeve firmly but without deforming it. The inner face of the sleeve was greased using form oil. Then the plastic mold was slid into the sleeve. If every piece of the cast in-place cylinder holder was prepared and assembled correctly, the total height of the holder would be 9 in. (22.9 cm), with the plastic mold and sleeve top edges level. In addition, there would remain a gap of around 0.08 in. (2 mm) between the plastic mold and the sleeve; the top part of that gap was covered with Vaseline to prevent concrete seeping in during casting.

Figure 2 depicts the three main elements of the in-place holder. The foam pad is not seen because it was placed inside the sleeve in contact with the form surface and below the plastic mold. Figure 3 shows the geometric configuration of the eight in-place holders attached to the formwork.

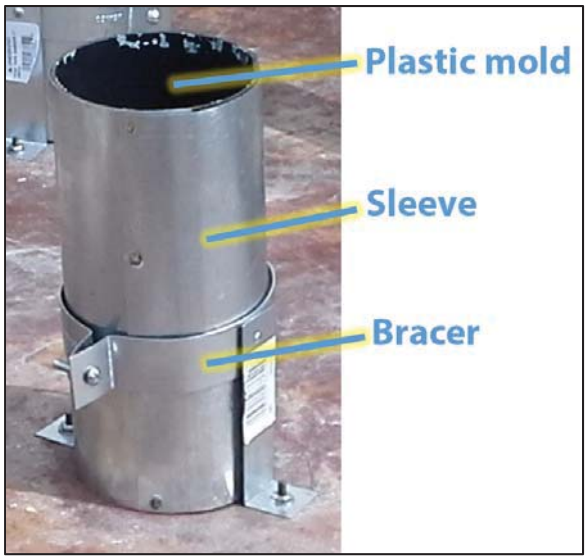

Figure 2: In-place cylinder holder.

Figure 3: Formwork with cast-in-place cylinder holders fixed.

3.1.10 Steel Rebar

Certain slabs included embedded steel rebar (see testing matrix in Table 3). These bars were epoxy-coated #5 bars, with a 2 in. (5.1 cm) top cover, to simulate a real bridge deck.

3.2 SPECIMEN DESCRIPTIONS

3.2.1 Slabs

To produce each slab, concrete components were batched and mixed in a ready-mix plant, producing a 4 yd^3 (3 m^3) concrete batch. Concrete was transported to the laboratory in concrete mixer trucks. Some amount of the water-reducing admixture was added at the plant and some on site to achieve the desired slump. Most AEA was added at the plant; additional AEA was added on site in case it was needed to achieve the desired air content. Each batch was used to produce one slab and five companion cylinders. More detail about the companion cylinders is provided in Section 3.2.4. Each slab produced eight cores and eight cast-in-place cylinders.

The nominal dimensions of the slabs were 5 × 5 ft (1.5 × 1.5 m) surface by 9 in. (0.23 m) thickness. Figure 4 shows a slab during casting, indicating its nominal dimensions.

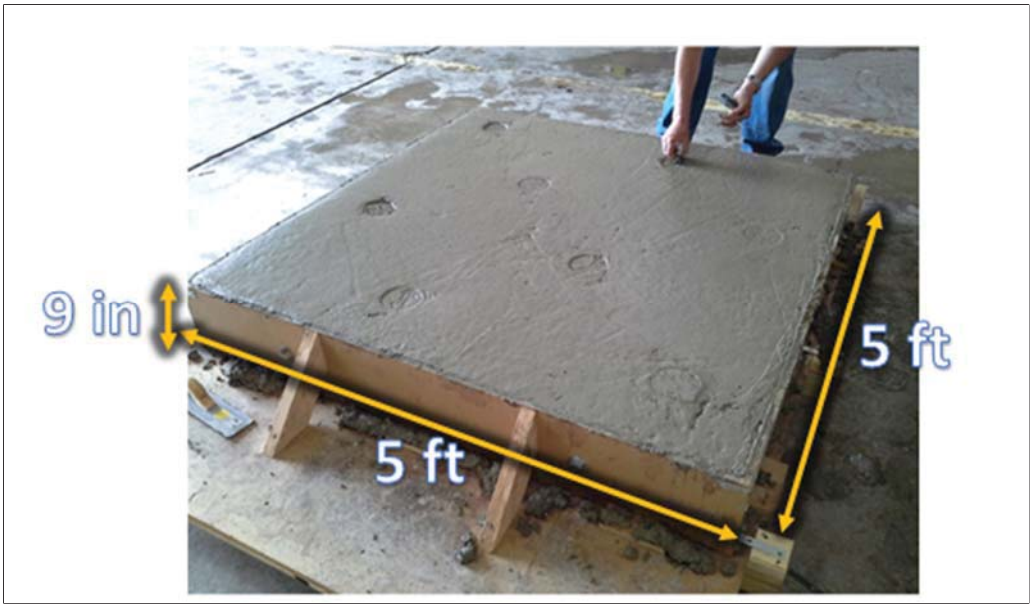

Figure 4: Slab dimensions.

Table 3 presents the experimental testing matrix, describing the main testing features of each slab.

Table 3: Experimental Testing Matrix

Slab Name	Mixture	Core Treatment	Rebar?
R1	PV/SI	1-day dry	No
R2	PV/SI	1-day dry	No
R3	PV/SI	1-day wet	No
R4	PV/SI	1-day wet	No
R5	PV/SI	1-day dry	Yes, inner*
R6	PV/SI	1-day dry	Yes, inner*
R7	PV/SI	1-day dry	Yes, outer**
R8	PV/SI	1-day dry	Yes, outer**
R9	PS	1-day dry	No
R10	PS	1-day dry	No
R11	PS	1-day wet	No
R12	PS	1-day wet	No
R13	PV/SI-low	1-day dry	No
R14	PV/SI-low	1-day dry	No
R15A	PV/SI-low	1-day wet	No
R16	PV/SI-low	1-day wet	No
R15B	PV/SI-low	1-day wet	No

* Inner means that the rebar passed through the inner one-third (area-based computation) of the core.

** Outer means that the rebar passed through the outer two-thirds (area-based computation) of the core.

Figure 5 is a graphic representation of the testing matrix detailed in Table 3.

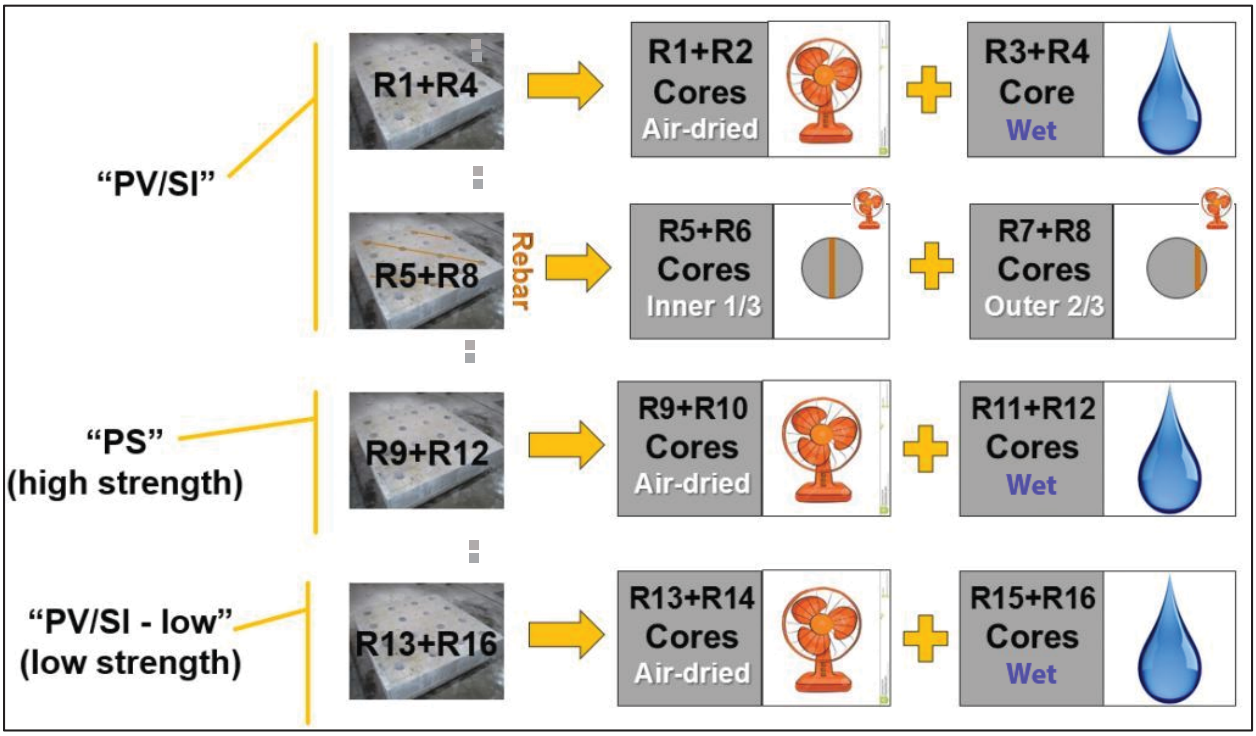

Figure 5: Slab testing matrix. The fans represent slabs with cores 1-day dry, the water drops represent slabs with cores 1-day wet, and the circle with the bar represent the slabs with rebar embedded.

3.2.2 Cored Cylinders

Cored cylinders, also called cores, were extracted from the concrete slabs at day 15 after casting. Each slab produced eight cores. Cores were extracted using diamond-tipped core bits with an inner diameter of approximately 4 in. (10.2 cm). Cores were drawn from the top side of the slabs through their full thickness, yielding cores of 9 in. (22.9 cm) height. After extraction, cores were conditioned (see Section 3.4.7 about core conditioning) for 24 hours before being tested under compression.

To prepare cores for the compressive strength test, the bottom 1 in. (2.5 cm) was saw-cut, yielding cores of 8 in. (20.3 cm) height. Thus, the final nominal dimensions of each core were 4 in. (10.2 cm) diameter and 8 in. (20.3 cm) height. Compressive strength tests were carried out at day 16 after casting, following ASTM C 39/C 39M (2012) and AASHTO T 22. Figure 6 shows photographs of eight cores extracted from one of the slabs cast during this investigation.

Figure 6: Picture of eight cores extracted from one of the slabs.

3.2.3 In-Place Cylinders

In-place cylinders are also referred to as cast-in-place cylinders. Before each concrete slab was cast, eight in-place cylinder holders were fixed to the bottom of the plywood formwork. The in-place cylinders were cast by filling the molds in two layers and rodding (and tapping) each layer, as specified in ASTM C 192/C 192M (2013a) and AASHTO R 39; this was done immediately before pouring the concrete into the rest of the form to produce the slab. The research team carried out a side study to confirm that the consolidation of the in-place cylinders using the rodding procedure yielded equivalently consolidated concrete as the rest of the slab. Details of that study are provided in Appendix C. In-place cylinders were removed from the slab by pushing them from the bottom on day 16 after casting. Their final nominal dimensions were 4 in. (10.2 cm) diameter and 8 in. (20.3 cm) height. In-place cylinders were tested under compression the same day of extraction. Compressive strength tests were carried out following ASTM C 39/C 39M (2012) and AASHTO T 22. Figure 7 shows photographs of eight in-place cylinders of one of the slabs cast during this investigation.

Figure 7: Photograph of eight in-place cylinders of one of the slabs.

3.2.4 Companion Cylinders

Five companion cylinders were cast from each concrete batch (which also produced the concrete slab). Three of them had nominal dimensions of 4 in. (10.2 cm) diameter and 8 in. (20.3 cm) height, while the remaining two were 6 in. (15.2 cm) diameter and 12 in. (30.5 cm) height. The objective of casting companion cylinders was to have a direct measurement of the compressive strength capacity of the concrete batch in standard conditions.

Companion cylinders were produced following ASTM C 192/C 192M (2O13a) and AASHTO R 39. They were demolded 24 hours after casting and then submerged under water at 73°F (23°C) until they were tested under compression at day 14 after casting. Compressive strength tests were carried out following ASTM C 39/C 39M (2012) and AASHTO T 22.

3.3 TEST DESCRIPTIONS

3.3.1 Slump

Slump tests were carried out upon concrete arrival, following ASTM C 143/C 143M (2015) and AASHTO T 119.

3.3.2 Air Content and Unit Weight

Air content and unit weight tests were carried out upon concrete arrival, following ASTM C 231/C 231M (2016) and AASHTO T 152, obtaining the uncorrected air content measurement. The corrected air content measurement was calculated by subtracting 0.4% from the uncorrected measurement; 0.4% accounted for the air content in the aggregate. This percentage was provided by the concrete supplier.

3.3.3 Compressive Strength

Compressive strength tests were carried out following ASTM C 39/C 39M (2012) and AASHTO T 22. In the cases of cores and in-place cylinders, special attention was paid to obtain flat end faces (i.e., to the perpendicularity of the end faces with regard to the lateral face; some faces were saw-cut to reach the correct level of perpendicularity required by IDOT[3]).

All compressive strength tests were carried out using steel caps with 60 durometer neoprene pads.

3.3.4 Longitudinal Dynamic Modulus

Longitudinal dynamic modulus tests (resonance tests) were carried out on cores and in-place cylinders to obtain their longitudinal dynamic moduli. These tests were performed following ASTM C 215 (2002a). The dynamic moduli data were used as an additional parameter to monitor material mechanical properties.

Longitudinal dynamic moduli were obtained from cores and in-place cylinders. Special care was taken to maintain the moisture condition of the samples throughout the testing period. Three resonance signals were obtained from each sample by measuring acceleration amplitude in time, following ASTM C 215 guidelines (2002a). The sampling rate was set at 1 MHz, yielding a time interval of 1 µs. Each signal was composed of 100,000 data points. From each signal, the longitudinal fundamental frequency was selected by carrying out a fast Fourier transform to obtain the amplitude spectrum in the frequency domain of the signal. For each sample, the three resonant frequencies were averaged and, from that average, the longitudinal dynamic modulus of the sample was computed.

3.3.5 Rebound Hammer

Slabs were tested using the Proceq N-34 159279 (provided by the manufacturer, Proceq) rebound hammer equipment in vertical position, at eight testing locations. Ten replicates were collected at each testing location, with each replicate collected at least 1 in. (2.5 cm) away from the others, as specified in ASTM C 805 (2002b). Figure 8 is a picture of the rebound hammer employed in this investigation.

Figure 8: Photograph of the rebound hammer.

[3] ASTM C 39/C39M (2012) and AASHTO T 22 indicate that "neither end of test specimens shall depart from perpendicularity to the axis by more than 0.5° (approximately equivalent to 1 mm in 100 mm)," which is extremely restrictive. Upon consultation with the Technical Review Panel for this project, the research team was informed that up to a 3 mm departure from perpendicularity would be allowed. This was permitted because the Technical Review Panel suspected the perpendicularity is not always followed in the field.

3.3.6 Nitto Hammer

Slabs were tested with the CTS-02V4 hammer equipment, provided by the manufacturer (Nitto Company).

The Nitto equipment is composed of a hammer that contains a force cell and an accelerometer; when the hammer is used to strike a surface, the impact force and acceleration are measured over time. These data are then processed internally, yielding an output parameter that is termed reactive impedance (Zr). This parameter was the one used in this investigation. The physical unit of Zr is not provided by the manufacturer, so all measurements carried out with the Nitto hammer correspond to the Nitto Zr parameter and are treated as unitless indices.

Nitto Zr measurements were acquired at eight testing locations per slab. Ten replicates were collected at each testing location on a slab by impacting at the exact same spot. As recommended by the manufacturer, the first three replicate measurements were discarded, and only the last seven replicates were used for further analysis.

Figure 9 shows a photograph of the Nitto hammer used during this investigation.

Figure 9: Photograph of the Nitto hammer in use.

3.3.7 Pullout[4]

Pullout tests were carried out using the CAPO-Test provided by Germann Instruments. Each slab was tested at three testing locations[5]. One pullout test was carried out at each testing location, constituting one single testing replicate per testing location. Pullout tests were carried out following ASTM C 900 (2013b), always pulling in the vertical direction. This unit yielded pullout force measurements in units of kN. Figure 10 shows two photographs of the equipment used to carry out the pullout tests.

[4] Because the pullout test causes some superficial surface damage as part of its use, it is not considered a completely non-destructive test.

[5] For one of the slabs, pullout tests were carried out at five locations instead of three. This was done because of potential experimental errors observed during testing; therefore, extra measurements were taken. See Chapter 5 for more details.

(a)

(b)

(c)

Figure 10: (a) and (b) are pictures of the pullout device CAPO-Test, and (c) is a picture of the concrete surface after carrying out the pullout test.

3.3.8 Surface Waves

Ultrasonic surface waves were sent through the top surface of the slabs using an electrostatic air-coupled transducer, Series 600 Smart Sensor, provided by SensComp. The center frequency of the narrow-band pulse was approximately 50 kHz. The wave was detected using micro-electromechanical systems (MEMS) Zero Height Ultra-Mini SiSonic microphones provided by Knowles Acoustics. The MEMS used in this project were sensors capable of detecting pressure changes in air, from which the velocity of propagation was calculated.

The procedure consisted of generating surface waves in the concrete by inclining the sending transducer approximately 8° to 10° from the slab's surface. The propagating wave was then detected using four MEMS set in an array, at known relative positions. These were located approximately 3.5 in. (9 cm) away from the sending transducer and approximately 0.2 in. (0.5 cm) away from the concrete surface. The data were collected using a National Instruments DAQ, with a sampling frequency of 2 MHz. The signals collected with each sensor provided the time delay from one to the other, which allowed the wave speed to be calculated based on the known relative distances between sensors.

In general, surface wave data were collected at eight testing locations per slab. In each testing location, 300 signals were time-averaged with each sensor. These signals were then processed to yield surface wave velocity measurements.

Figure 11 presents pictures of the ultrasonic sending/sensing device utilized to produce and sense ultrasonic surface waves during this investigation.

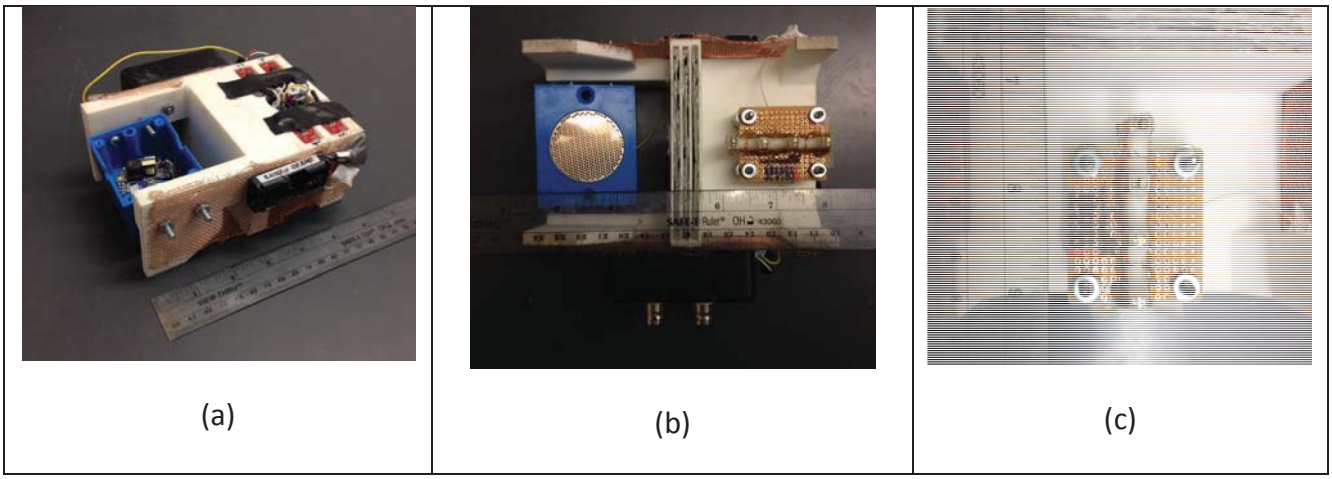

(a) (b) (c)

Figure 11: Photographs of the ultrasonic sending/sensing homemade device: (a) the frame holding the blue transducer set in position to test, (b) a bottom view the sending transducer and receivers (MEMS), and (c) receiver array.

3.3.9 Temperature Monitoring

Temperature was monitored using the TC-08 data logger, provided by Omega. Type-K thermocouple wires were employed. Figure 12 shows a photograph of the TC-08 data logger. Internal concrete temperatures were monitored to ensure that concrete within the in-place cylinders and in the body of the slab experienced similar temperature histories.

Figure 12: Photograph of the TC-08 data logger for temperature monitoring.

3.4 GENERAL CASTING PROCEDURE

Figure 13 illustrates the general casting and testing procedure for each slab. Figure 14 shows the relative positions of in-place cylinders and cores in a regular slab (without rebar) and the relative positions of rebar and cores in a slab with rebar.

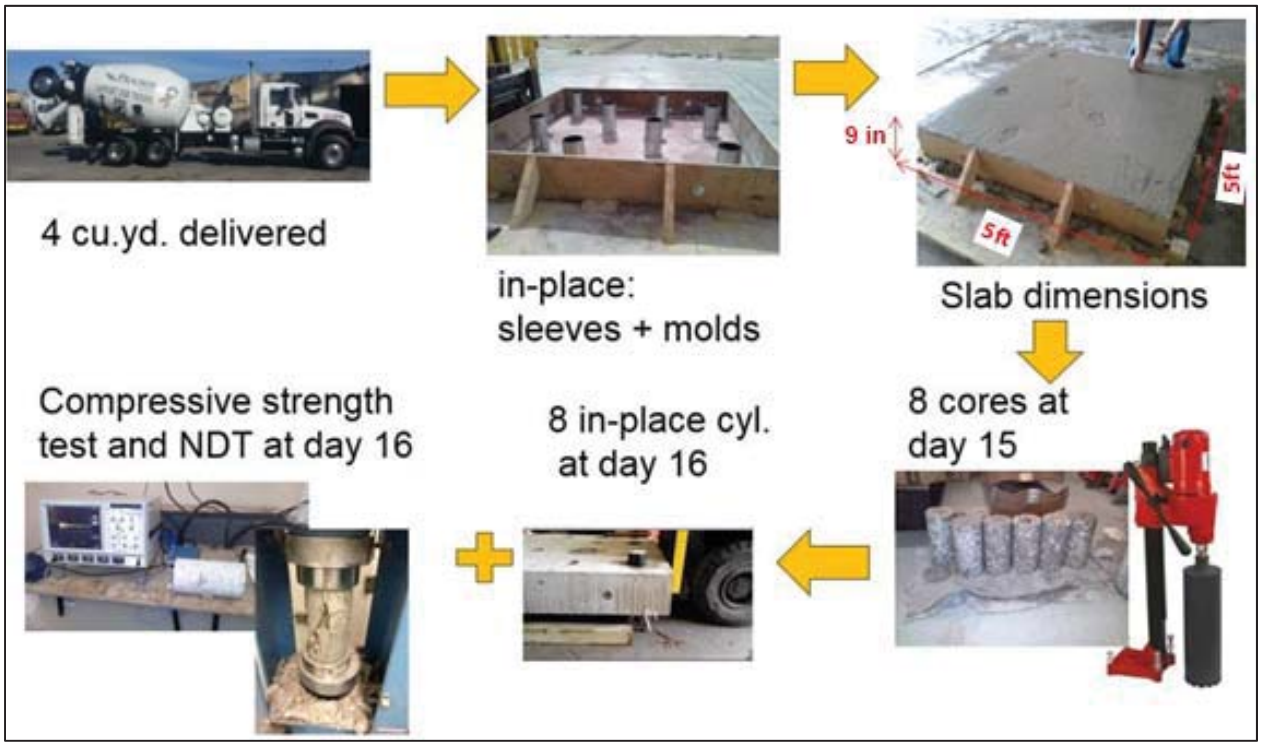

Figure 13: General casting and testing procedure.

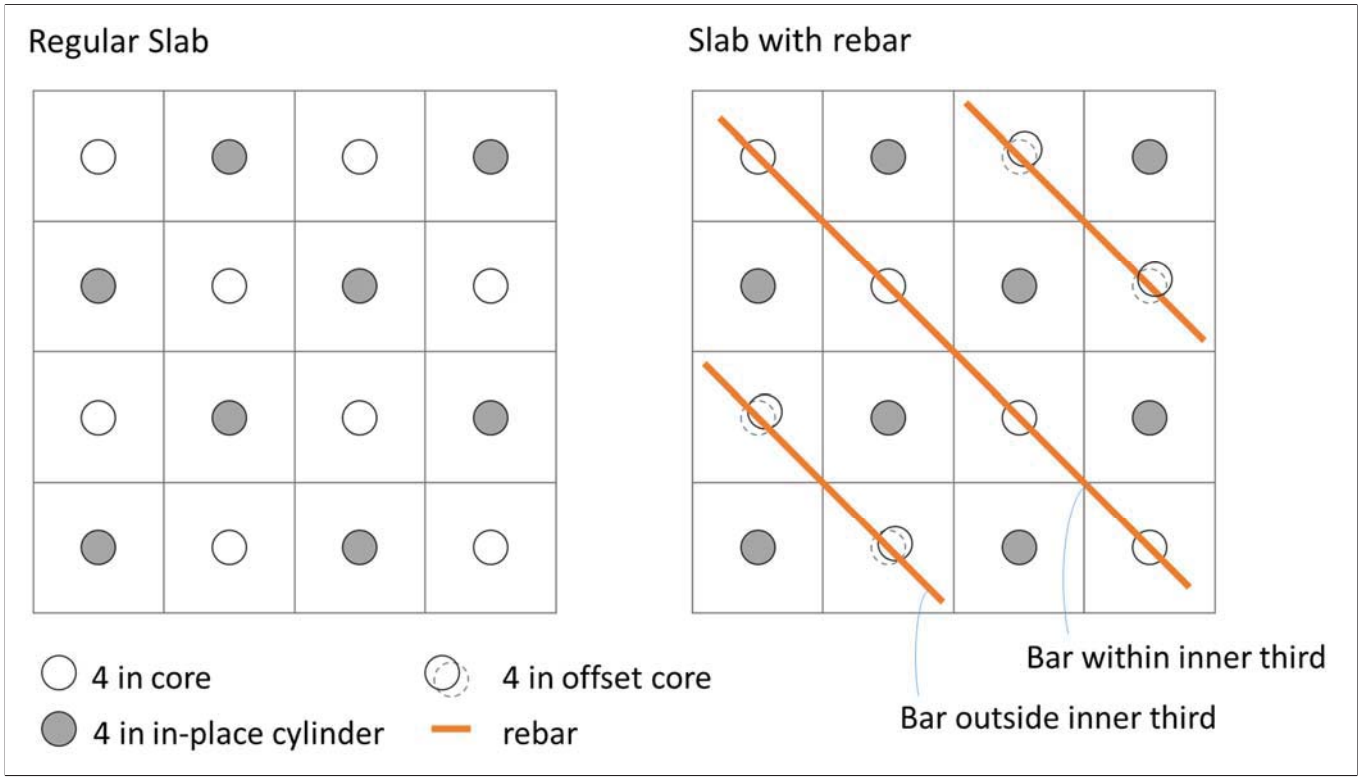

Figure 14: Plan view of a slab showing nominal relative positions between cores and in-place cylinders, and between cores and embedded rebar. Inner one-third rebar cores and outer two-thirds cores were in separate slabs.

3.4.1 Step 1: Preparation

Preparation began with cleaning and assembling the formwork. Some slabs had embedded rebar; in those cases, the steel bars were set in position during this step.

On the pouring day, burlap bags were submerged in water. The clean formwork was set outdoors and leveled. Galvanized steel bracers were fixed in position. Galvanized steel sleeves had been previously constructed. Foam pad discs, sleeves, and plastic molds were set into the bracers following the description presented in Section 3.1.9, “In-Place Cylinder Holder.”

A demolding agent (form oil) was sprayed on the inside of the form. The outside of the galvanized steel sleeve was wetted with water.

3.4.2 Step 2: Casting

Concrete was delivered by a concrete mixer truck. Slump, air content, and unit weight tests were carried out upon arrival to determine whether to accept or reject the batch. Occasionally, additional AEA and/or a water-reducing admixture or high range water-reducing admixture was added to increase the air content and/or the slump, respectively, to meet the requirements of the specific mixture design (see Table 1 for target properties).

Once the batch was accepted, the cast-in-place cylinders were cast first, following the procedure described in Section 3.2.3, "In-Place Cylinders." The rest of the concrete was then poured into the form. Immediately after the concrete was poured, the form (holding the fresh concrete) was moved indoors onto a leveled floor. There, the concrete was vibrated using the internal vibrator following recommended practice: the vibrating head was inserted vertically downward into the concrete at a rapid rate, but without touching the bottom of the form, and then more slowly lifted vertically to the surface (Mindess et al. 2003). After vibration, the screeding process was performed using a wood 2 × 4, followed by steel troweling to improve the finished surface.

Five companion cylinders were cast at the same time as the slab was being poured.

One thermocouple wire was inserted into one of the in-place cylinders to monitor temperature at mid depth. Another thermocouple wire was inserted into the slab's concrete (outside any in-place cylinder) to monitor concrete temperature at mid depth. Air temperature was monitored using a third thermocouple wire. Temperature measurements were collected at a rate of one measurement every 30 seconds during at least 66 hours after casting.

3.4.3 Step 3: Curing Slab and Demolding Companion Cylinders

Curing was performed by wetting burlap and using plastic sheets to prevent evaporation. The slabs made of concrete mixtures PV/SI and PV/SI-low were moist-cured for 3 days, except for slab R15B, which was moist-cured for 4 days[6]. The slabs made of the concrete mixture PS were moist-cured for 1 day. Companion cylinders were demolded the day after casting and were immediately put in the water bath.

3.4.4 Step 4: Form Removal

Forms were removed from the concrete slabs no earlier than day 3 after casting.

3.4.5 Step 5: Companion Cylinder Tests

The five companion cylinders were tested under compression on day 14 after casting, following ASTM C 39/C 39M (2012) and AASHTO T 22. Measurements collected were visual inspection, height, diameter, roughness, perpendicularity, mass, maximum load, and type of break; these data are presented in Appendix A.

3.4.6 Step 6: Coring

Eight cores were extracted on day 15 after casting. To perform this task, the slabs were moved and leveled outdoors. A polystyrene sheet was placed below the slab to avoid damaging the cores by impacting the underlying pavement. Coring was carried out by positioning the core bit onto the slab and letting it fall downward by self-weight as the drilling progressively advanced. The eight cores were then moved indoors for moisture conditioning.

[6] Note that IDOT requires 7-day moist curing for SI mixtures and 3-day moist curing for PV mixtures.

3.4.7 Step 7: Core Conditioning

Two types of moisture conditioning were performed in this investigation: 1-day wet (submerging the cores in a water bath) and 1-day dry (placing the cores in front of a three-speed fan with speed set to medium in the laboratory under uncontrolled room temperature and moisture conditions). Figure 15 depicts the configuration during the core's air drying.

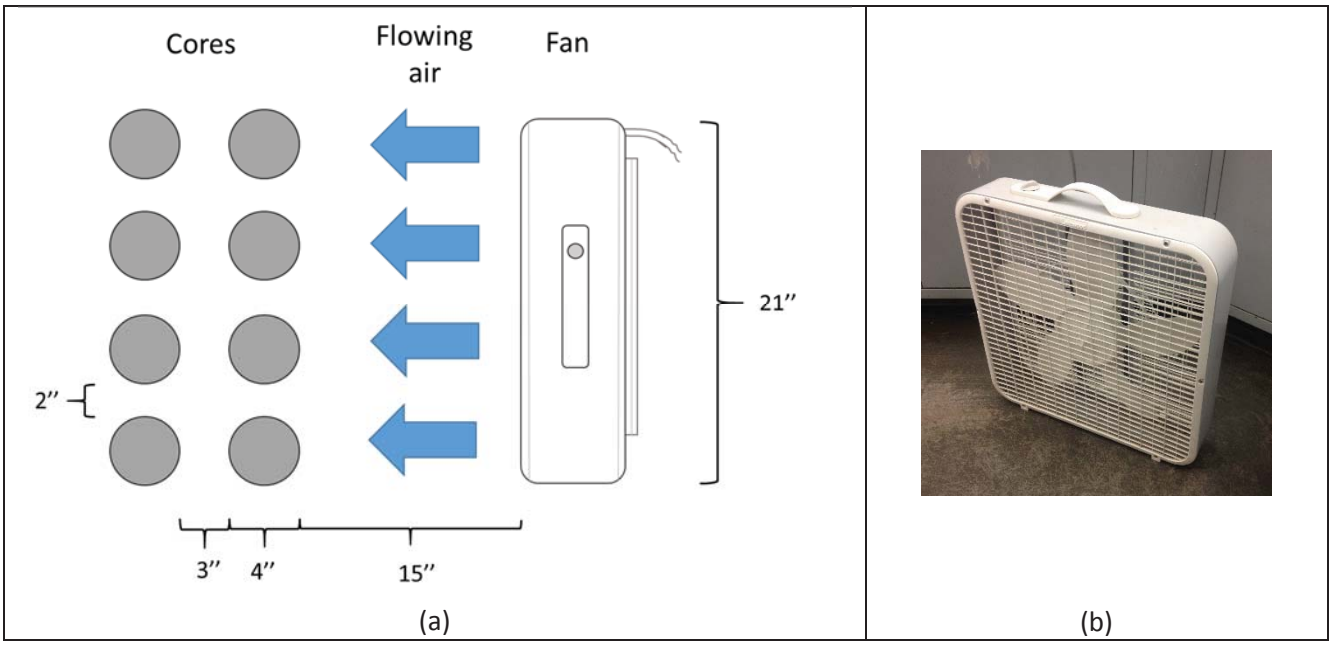

Figure 15: (a) geometric configuration of fan and cores used during the air-drying conditioning (1-day dry core conditioning), and (b) a photograph of the box fan used.

3.4.8 Step 8: Saw-Cutting Cores

Because the slab thicknesses were 9 in. (22.9 cm), the bottom 1 in. (2.5 cm) of the cores were saw-cut to obtain 4 in. (10.2 cm) diameter by 8 in. (20.3 cm) high cores. This task was carried out on day 16, before the other tests were carried out. If a core's top surface happened to be out of perpendicularity, a thin slice was saw-cut from it to improve that characteristic. Perpendicularity measurements are presented in Appendix A.

3.4.9 Step 9: Extracting In-Place Cylinders

In-place cylinders were extracted on day 16 after casting. To perform this task, the slab was lifted up about 3 ft (1 m) from the floor using a truck lifter (Bobcat). A wood 2 × 2 was set in contact with the in-place cylinder bottom and the floor. Then the slab was slowly moved down so that the plastic mold (containing the in-place cylinder) would slide out from the galvanized steel sleeve (fixed to the rest of the slab) and thus be held up by the wood 2 x 2.

After the in-place cylinders had been extracted, they were demolded and moved to the testing section of the laboratory. Some in-place cylinders had an excess of concrete at their top end; this excess was either saw-cut out or ground out to obtain the appropriate cylindrical dimensions.

3.4.10 Step 10: Cores and In-Place Cylinder Testing

Cores and in-place cylinders were tested on day 16 after casting. By that point, the cores had been conditioned for 24 hours and then saw-cut; also, the in-place cylinders had been extracted from the slab and then demolded.

The first measurement collected was perpendicularity. In the case of unacceptable perpendicularity (see Section 3.3.3, “Compressive Strength”), the cylinder was saw-cut or grounded down to improve this property. Then the cylinders were weighed, and geometrical dimensions were measured as in accordance with ASTM C 39/C 39M (2012) and AASHTO T 22.

Special care was taken to maintain the cores’ moisture condition; thus, cores were kept either submerged or in front of the fan when they were not being measured.

Longitudinal dynamic elastic modulus tests were then carried out on cores and in-place cylinders. Finally, cores and in-place cylinders were tested under compression, following ASTM C 39/C 39M (2012) and AASHTO T 22, to obtain the failure force and type of breaking.

3.4.11 Step 11: NDT Testing in Slab

The undamaged parts of the slab were used to carry out the NDT. Eight testing locations were defined for each of the three NDT methods (rebound hammer, Nitto hammer and surface waves). Three testing locations were defined for carrying out the NDT pullout tests.

CHAPTER 4: ANALYTICAL PROCEDURES

4.1 DATA PROCESSING ASSOCIATED WITH THE EXPERIMENTS

4.1.1 Slump

No processing was done with the slump measurements.

4.1.2 Air Content and Unit Weight

The air content test yielded an uncorrected air content measurement. The corrected air content measurement was calculated by subtracting 0.4% from the uncorrected air content measurement, to account for the air content in the aggregate. This number was provided by the concrete supplier.

The unit weight measurement was obtained using a scale to measure the weight of the fresh concrete in the specified metal bucket of known volume. The unit weight was calculated by directly dividing the measured weight by the known volume.

4.1.3 Compressive Strength

The procedures described here were applied to all cylindrical test samples, including core, in-place and companion samples. The compressive strength tests included several subtests to measure the sample's roughness, perpendicularity, height, diameter, failure load, type of break, and final compressive strength. All these parameters were measured following ASTM C 39/C 39M (2012) and AASHTO T 22.

The perpendicularity of each edge face was estimated by setting a square at the angle formed by the cylinder's edge face and lateral face, pressing the square firmly to the flat lateral side of the cylinder. The maximum air gap formed between the square and the edge face, measured at the diametrically opposed side of where the square was set, was considered to be the perpendicularity measurement.

The roughness of each edge face was measured by setting a ruler on each edge face and estimating the air gap distance between the uneven surface and the ruler. These measurements provided an estimation of the distance between peaks and valleys of the uneven concrete surface.

Three height measurements were taken using a caliper. Two diameter measurements were collected using a caliper—both at the cylinder's mid height but on two diameters 90° from each other. In the case of the 6 × 12 companion cylinders, the caliper could not be used because of the large dimensions of the cylinders, so a metric tape was employed to measure height and a measuring clamp was employed to measure diameter.

The cross-section area of each cylinder was computed from the average of the measured diameters.

The failure load was obtained from the compressive strength failure load. The type of break was based on visual inspection of the failed sample after the compressive strength test.

The compressive strength of each cylinder was computed by dividing the failure load by the cross-sectional area.

4.1.4 Longitudinal Dynamic Modulus

The sample's longitudinal dynamic modulus was obtained by analyzing the collected signals as specified in ASTM C 215 (2002a). The longitudinal fundamental frequency of vibration was obtained from each sample by performing a fast Fourier transform of time-domain signals. Three time-domain signals per sample were processed in this way, and the average of the three frequencies composed the final fundamental frequency of the sample.

Once the fundamental frequency was computed, the longitudinal dynamic modulus $E_{l,d}$, in units of Pascals, was calculated as follows:

$$E_{l,d} = 5.093 \frac{L}{d^2} Mf^2 \qquad \text{(Equation 1)}$$

where *L* is the cylinder's length in meters, *d* is the diameter in meters, *M* is the mass in kilograms, and *f* is the longitudinal fundamental frequency of vibration in Hertz.

4.1.5 Rebound Hammer

The data collected with the rebound hammer were processed as specified in ASTM C 805 (2002b).

As explained in Section 3.3.5, in general, each slab was tested with the rebound hammer at eight testing locations, and ten measurement repetitions were collected at each testing location. Each repetition was therefore one real reading given by the apparatus in a specific test, with each of the readings taken from a different physical spot, at least 1 in. (2.5 cm) away from the others. The first processing of that set was to take the mean (average) of those ten measurements; then, if any one of the ten measurements was six units or more away from the mean, that particular measurement was discarded, and a new mean was calculated from the remaining nine measurements. If any one of the nine remaining measurements was six units or more away from the new calculated mean, the entire set was discarded.

To summarize, the final outputs of rebound hammer tests were, for each slab, eight rebound numbers, collected from eight locations of the slab. These eight rebound numbers were the only ones that were further analyzed and discussed for each slab.

4.1.6 Nitto Hammer

The data collected with the Nitto hammer were processed as recommended by the manufacturer.

As explained in Section 3.3.6, each slab was tested with the Nitto hammer at eight testing locations, and ten measurement repetitions were collected at each testing location. Each of these repetitions was a reactive impedance (Zr) reading given by the equipment. Within testing locations, all ten measurement repetitions were collected by striking the hammer at the exact same spot. Then the first three repetitions were discarded from the set, and the last seven repetitions were averaged to compute the final average of the set.

Therefore, the final outputs of Nitto hammer tests were, for each slab, eight Zr, collected from eight locations of the slab. These sets of eight Zr were the only ones that were further analyzed and discussed

4.1.7 Pullout

As explained in Section 3.3.7, each slab was tested at three testing locations (in this case, one testing location corresponds to one testing replicate). These three pullout measurements of each slab were used for further analysis and discussion.

4.1.8 Surface Waves

As explained in Section 3.3.8, each slab was tested at eight testing locations by collecting ultrasonic surface wave signals using a sending transducer and four sensors.

At each of these locations, four time-domain signals were collected, each signal associated with one sensor. At each testing location, it was possible to obtain the relative time delay of the wave arrival between signals (between sensors). Because the relative distances between sensors was known, it was possible to calculate the velocity of wave propagation by fitting a linear trend between the relative time delays and the relative distances between sensors; the slope of that best-fit line was used as the surface wave velocity.

4.1.9 Temperature Monitoring

No additional processing was carried out with the temperature data.

4.2 USE OF BOXPLOTS

Boxplots are used to graphically show the statistical variation of a dataset. As it can be seen in Figure 16, the boxplot scheme is composed of two horizontal lines indicating the maximum and minimum values of the dataset; a box, whose edges indicate the 75th and 25th percentiles of the dataset; and another horizontal line inside the box, which indicates the median. In addition, crosses indicate the outliers of the dataset. Unless otherwise specified, throughout this report, the criterion to define a certain data value as a statistical outlier was as follows: if a data point was at least 2.7 times the standard deviation of the dataset away from the median, that point was considered an outlier. It should be noted that other data points could have been discarded for other reasons. Every time a data value was discarded, the justification for doing is explicitly provided in this report (see Chapter 5).

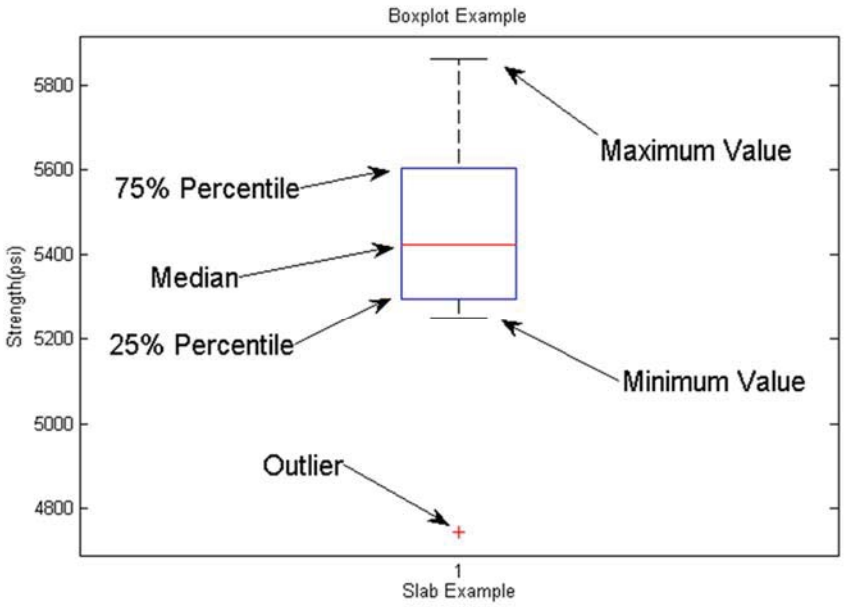

Figure 16: Explanation of boxplot.

4.3 STATISTICAL ANALYSIS

Analysis of variance (ANOVA) is used to evaluate whether groups of strength data are statistically equivalent. This approach is an extension of the two-sample t-test for means assuming normally distributed datasets but unequal variance among the compared populations. Hypotheses are often employed in statistical analysis to express results. In this study, we assumed the following null hypothesis: "Population samples for a particular type of core condition or from an NDT test have the same mean value as that from the molded in-place cylinder samples for a given concrete mixture and condition." The alternative hypothesis is then "Population samples have different mean values." In this study, the hypothesis analysis was carried out at a 95% confidence level, meaning only a 5% chance of a false positive reading. If the null hypothesis was rejected, then the alternative hypothesis was accepted and we stated, with a 95% confidence level, that the population sets had different mean values; in that case, we developed a correlation between the strength values. If the null hypothesis was not rejected, then we stated that the mean values of the population sets were not significantly different, with 95% confidence. These analyses were carried out separately for each material type and test case.

Figure 17 describes the procedure to obtain the possible correction factors associated with the compared populations for slab R3. Core strength multiplied by different correction factors (shown at top of graph) and populations were compared to determine whether they were statistically different, under certain assumptions. Orange circles represent the compressive strengths of the cores multiplied by the corresponding correction factor, and blue circles represent the compressive strengths of the in-place cylinders ("InCyl"). The word "different" is used to designate populations

that were statistically different at a 95% confidence level. When two populations that each contained eight cylinders were compared, the parameter limit F was 4.6 for 95% confidence. By applying different correction factors to the core data and then comparing them with the in-place strengths, we see that the optimal correction factor (F-score is equal to zero) for this particular dataset is near the value of 1.15. The 95% confidence range of correction factors and the optimal correction factor for each slab are computed and discussed in Section 5.9.1 of this report.

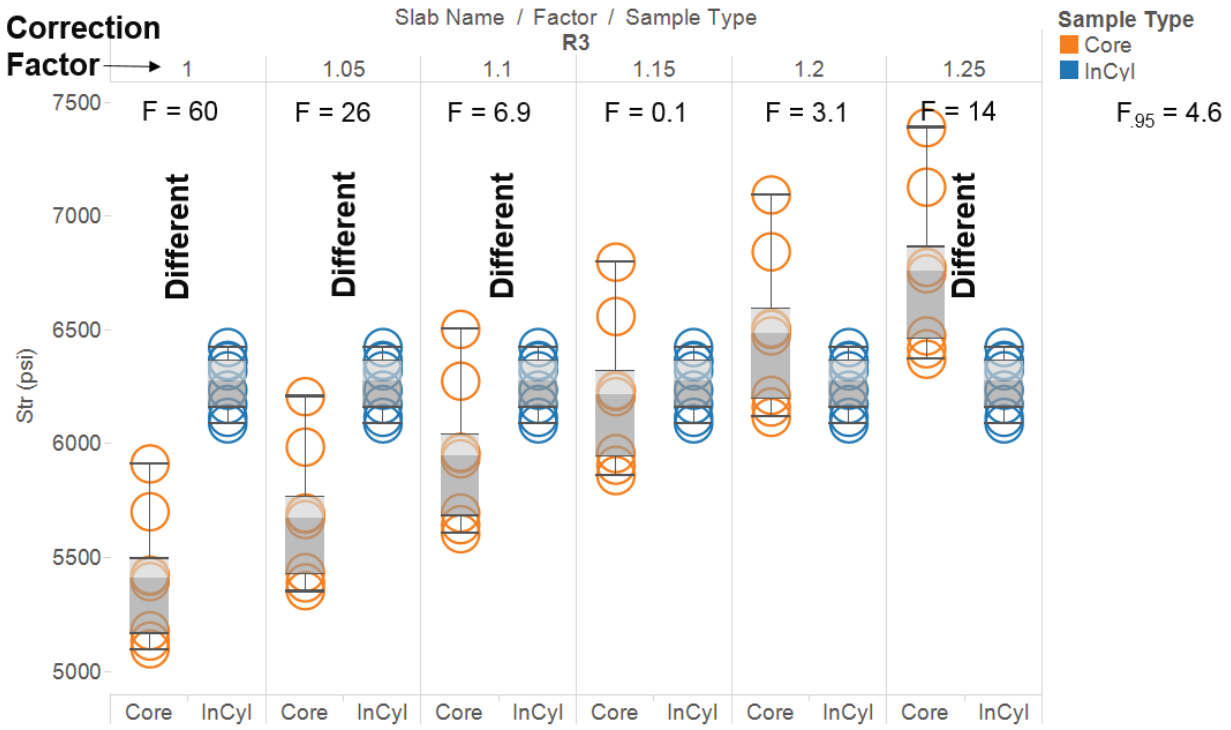

Figure 17: Example of correction factor calculation (slab R3) using ANOVA analysis.

4.4 RANDOM SAMPLING ANALYSIS

Random sampling analysis studies how the error between measured and estimated strengths is reduced when additional strength estimates are considered. The strength estimates are obtained from an indirect measurement to which a certain correlation curve or correction factor is applied. These indirect measurements could be core strength measurements or NDT measurements.

Results from cores and each NDT method were studied individually. To explain the analysis, consider strength estimation method from core samples obtained from one particular slab. Several cores were drawn from the slab and tested (or several testing locations for the case of NDT methods) yielding several core strength values. One can randomly select one of those core strength values and transform it to an estimated strength using the corresponding correction factor (or OLS correlation curve for the case of the NDT methods) already calculated. Then the difference between the measured strength and estimated strength can be quantified with the absolute error (*Abs.Err*):

$$Abs.Err(\%) = 100 \times \frac{|Y_{est} - Y_{meas}|}{Y_{meas}} \qquad \text{(Equation 2)}$$

where Y_{est} corresponds to the strength estimated using the core strength and Y_{meas} is the measured strength using the in-place cylinders (average of eight cylinders per slab).

The use of the absolute value of the strength estimate errors gives an idea of how off the strength predictions are from the real strength, but it does not differentiate which "side" the error is located. In other words, using the absolute value does not indicate if the prediction overestimates (non-conservative estimate) or underestimates (conservative estimate) the actual in-place strength.

To study the statistical behavior of the absolute error values, every possible core strength result was considered, one at a time, and one absolute error value was calculated from each of them using Equation 2. The obtained dataset corresponds to absolute strength error associated with considering one core strength value at a time (i.e., *# Cores = 1*).

One can expect that if two cores are tested and averaged, the resulting estimated strength would yield a lower expected error than when estimating the strength from a single core. The analysis thus continued by calculating all possible combinations of core strength values, taking them in pairs; each pair was averaged, yielding as many Y_{est} as there were possible combinations of core strength values. Then the strength absolute errors were calculated from the new Y_{est} data (associated with *# Cores = 2*). This new dataset corresponded to strength absolute errors associated with *# Cores* = 2. This procedure was further carried out by considering all possible combinations of three core strength values, successively up to N_{loc}, where N_{loc} is the total number of core values for a specific slab.

Then the *Abs.Err*. values were calculated for each slab and aggregated to form a different data population for each of the *# Cores*. One histogram was constructed for each of the datasets associated with each *# Cores*. The metric named $Abs.Err_{95}$ was computed for each histogram (each histogram associated with each *# NDT locations* for every NDT method). The metric $Abs.Err_{95}$ corresponded to the absolute error of the histogram that leaves 95% of those errors below it and 5% higher; in other words, $Abs.Err_{95}$ corresponds to the 95th percentile of the population at each histogram. In an analogous procedure, the metrics $Abs.Err_{85}$ and $Abs.Err_{75}$ were also computed.

The same analysis applies for the three NDT methods by substituting # Cores with "# NDT locations, and noting that the strength estimates come from the application of a certain correlation curve instead of a single correction factor. Also, for the NDT cases, N_{loc} = 8 for rebound hammer and Nitto hammer, and N_{loc} = 3 for pullout.

The random sampling analysis allows obtaining the expected strength error curves which show how the expected error of the strength prediction varies with increasing number of tested cores (or NDT locations). For the case of the cores, the expected strength error curves are plotted at three different confidence percentiles: 75%, 85%, and 95%. For the NDT cases, only the 95% confidence percentile is carried out, but using three different correlation curves.

Particularly for the core's random sampling analysis, an additional analytical approach was carried out using the aggregated data of strength errors previously mentioned. In this case, instead of prescribing

a fixed confidence percentile and observing how the expected strength error drops with increasing number of cores, the expected strength error is now prescribed and the confidence is then calculated. The expected strength error was defined as 5%, and confidence of the estimation was computed by calculated the percentage of strength estimations that have an error lower than 5%. As more cores are considered to compute the strength estimation, the confidence of having a 5% error or lower increases.

An example of the application of random sampling analysis is presented in Appendix D which provides more detail and explanation for the reader.

4.5 ANALYSIS OF NDT VS. IN-PLACE CYLINDER COMPRESSIVE STRENGTH

This analysis studied the correlation of NDT carried out on the concrete slabs vs. the compressive strength of in-place cylinders.

4.5.1 NDT vs. Compressive Strength Relationships

Four sets of data were obtained from each slab. The first dataset corresponded to the averaged values of in-place cylinders (i.e., one strength value per slab, each being the average of the eight cylinders). The other three datasets corresponded to NDT location values of rebound hammer, Nitto hammer, and pullout tests, respectively.

NDT vs. strength relationships (correlation curves) were calculated using the described datasets by following the specifications given in ACI 228.1R (2003). For each NDT method, two regression methods were computed to obtain two types of correlation curves. These were the ordinary least squares method (OLS) and the natural logarithm ordinary least squares method (logOLS). The OLS method is a linear approximation, whereas the logOLS method is a power approximation.

Therefore, the application of the OLS method yields an equation that correlates NDT values to strength values as

$$Y = aX + b \qquad \text{(Equation 3)}$$

where *X* is an NDT value, *Y* is an estimated strength value, and *a* and *b* are the slope and Y-intercept of the correlation curve, respectively. In the case of the logOLS method, the correlating equation is

$$Y = AX^B \qquad \text{(Equation 4)}$$

where *A* and *B* are the parameters characteristic of the logOLS fit.

4.5.2 NDT Variability

The variability of the NDT results is composed of two variability sources. One corresponds to the inherent variability of the NDT method, and the other to the variability of the structure's material (i.e., the slab's concrete). These types of variability were analyzed together and are generically called NDT variability. The NDT variability was assessed by taking the range of NDT location results in each

slab. Non-destructive testing variability at each slab was graphically represented either with a boxplot, as shown in Figure 36, Figure 37, and Figure 38, or with horizontal error bars, as shown in Figure 39. To quantify the NDT variability across all slabs, the metric average range (*Avg.Range*) was calculated as

$$Avg.Range = \frac{\sum_{i=1}^{N} Range_i}{N} \qquad \text{(Equation 5)}$$

where $Range_i$ corresponds to the range of the NDT location values of slab *i*, and *N* is the total number of slabs tested.

4.5.3 Correlation Curve Uncertainty

The residual standard deviation (RSD) is a parameter that ACI 228.1R (2003) proposes for quantifying the uncertainty of a linear regression analysis. The RSD was estimated as

$$RSD \quad \sqrt{\frac{\sum_{i\ 1}^{N} \left(Y_i - f(X_i)\right)^2}{N-2}} \qquad \text{(Equation 6)}$$

where *N* is the total number of slabs, Y_i is the computed strengths of each slab (average of eight compressive strength values in general), X_i is the NDT average values of each slab, and $f(X_i)$ is estimated strength values computed by applying the corresponding correlation curve to the X_i values. In other words, the values $Y_i - f(X_i)$ correspond to the deviations from the measured average strengths and estimated average strengths of slab *i*.

4.5.4 NDT Sensitivity

The sensitivity of an NDT method is a metric that characterizes its ability to predict strength. More sensitive methods are able to distinguish between concretes with closer strength values. One way to quantify sensitivity is to use the slope of a linear best-fit line. In this report, the slope of the ordinary least OLS best-fit line was employed to evaluate sensitivity. In the case of non-linear trend lines, their range of slopes could be used to assess sensitivity.

A NDT vs. strength relationship with lower slope indicates higher sensitivity of the NDT method, where the NDT data are the independent variable (horizontal axis) and the estimated strength is the dependent variable (vertical axis).

4.5.5 NDT Random Sampling Analysis

The random sampling analysis uses the NDT and strength data to compute the expected errors that occur as a result of using NDT for strength prediction. The analytical procedure was carried out as explained in Section 4.4.

CHAPTER 5: RESULTS AND DISCUSSION

5.1 OUTLIERS OR EXCLUDED DATA

Before presenting the results, it should be noted that the testing matrix included two slabs designated R15: R15A, which was cast first; and R15B. The cores and in-place cylinders of R15A were drawn from the slab 1 day earlier than they should have been owing to a scheduling miscommunication with the assigned technician. Therefore, it was decided to cast a replicate of R15 and not to analyze R15A. However, the NDT of R15A was carried out normally, so it was decided to include those results in the NDT analysis.

The following is a summary of specific missing and excluded data:

- The value of mass of the in-place cylinder identified as InCyl_1 from slab R7 is significantly higher than the rest, yielding a density value statistically different from the rest of the set. As a result, the dynamic modulus result would also be flawed, so it was also excluded from the analysis.
- The 4 × 8 companion cylinder identified as Comp_3 of slab R2 was not tested under compression because it the mold deformed during curing so the cylinder had an ellipsoidal cross-section instead of circular.
- The 6 × 12 companion cylinder identified as Comp_4 of slab R4 suffered damage during transportation, so it was not tested under compression.
- The compressive strength of the core identified as Core_6, the in-place cylinder InCyl_4, and the in-place cylinder InCyl_6 (all from slab R10) could not be recorded because the loading machine had an electrical problem during testing.

The exclusion of these limited data are not expected to have any significant effect on the analysis of the remaining data. The results of slab R7 showed unusual and different trends from the rest of the slabs. Section 5.8 is a specific analysis of R7; it was decided to reject those results and exclude them from the rest of the discussion and analysis.

5.2 FRESH CONCRETE PROPERTIES AND TEMPERATURE MONITORING

5.2.1 Fresh Concrete Properties

Table 4contains the fresh concrete experimental results of all slabs. Other fresh concrete experimental data can be found in Table A.1 and Table A.2 in Appendix A. The fresh concrete properties included in Table 4 were employed to accept or reject the delivered concrete at the moment of casting. No additional analyses were carried out using the fresh concrete properties.

Table 4: Fresh Concrete Experimental Results*

Slab Name	Mixture	Core Treatment	Rebar?	Slump, in. (cm)	Corrected Air, %	Unit Weight, lb/ft^3 (kg/m^3)
R1	PV/SI	1-day dry	No	4.5 (11)	8	134
R2	PV/SI	1-day dry	No	4.25 (11)	4.9	144
R3	PV/SI	1-day wet	No	4.25 (11)	5.8	142
R4	PV/SI	1-day wet	No	4 (10)	5.8	146
R5	PV/SI	1-day dry	Yes, inner	4.75 (12)	6.6	142
R6	PV/SI	1-day dry	Yes, inner	4.5 (11)	5.8	144
R7	PV/SI	1-day dry	Yes, outer	3.25 (8)	7.6	142
R8	PV/SI	1-day dry	Yes, outer	3.5 (9)	5.6	144
R9	PS	1-day dry	No	4.75 (12)	6.6	140
R10	PS	1-day dry	No	4 (10)	5.1	146
R11	PS	1-day wet	No	3.75 (10)	6.1	—
R12	PS	1-day wet	No	7 (18)	7.9	—
R13	PV/SI-low	1-day dry	No	8.5 (22)	9.1	138
R14	PV/SI-low	1-day dry	No	8.75 (22)	9.6	134
R15	PV/SI-low	1-day wet	No	8 (20)	8.1	—
R16	PV/SI-low	1-day wet	No	8 (20)	9.1	136
R15B	PV/SI-low	1-day wet	No	7.75 (20)	8	142

* Specific mixture performance observations are included in Table A.2 in Appendix A.

5.2.2 Temperature Monitoring

Figure 18, Figure 19, and Figure 20 present the temperature monitoring results in slabs R1, R9, and R15, respectively. These slabs exemplify the concrete mixtures PV/SI, PS, and PV/SI-low, respectively.

All temperature monitoring results can be found in Appendix B.

In the three figures, it can be seen that the air temperature was much lower than both sources of internal concrete temperature. The InSlab and the InCylinder concrete temperatures overlap, indicating that the in-place cylinder had a curing temperature very similar to the rest of the slab. Finally, sudden drops in the measured temperatures may have occurred as a result of gusts of cold air entering the lab when the main gates were opened.

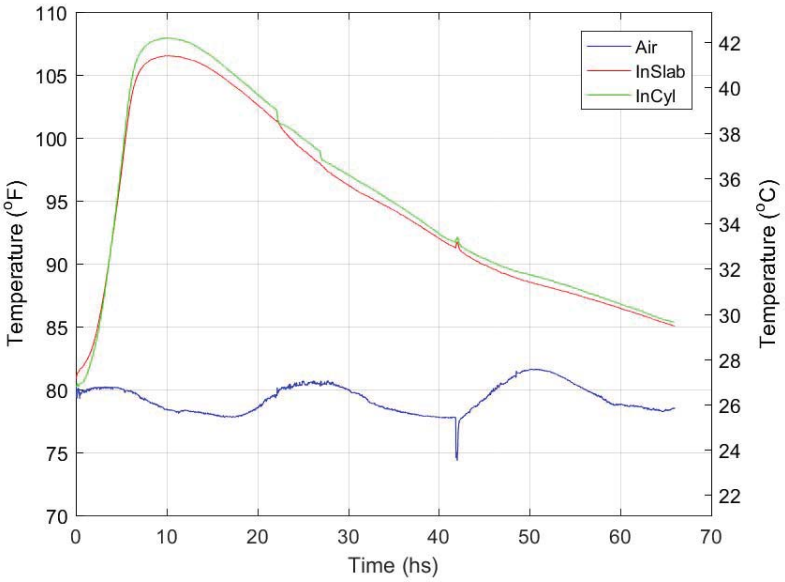

Figure18: Temperature monitoring of slab R1. "Air" corresponds to air temperature measurements close to the slab. "InSlab" corresponds to temperature measurements collected by a thermocouple inserted in the slab concrete outside any in-place cylinder at mid depth. "InCyl" corresponds to a thermocouple inserted into an in-place cylinder at mid depth.

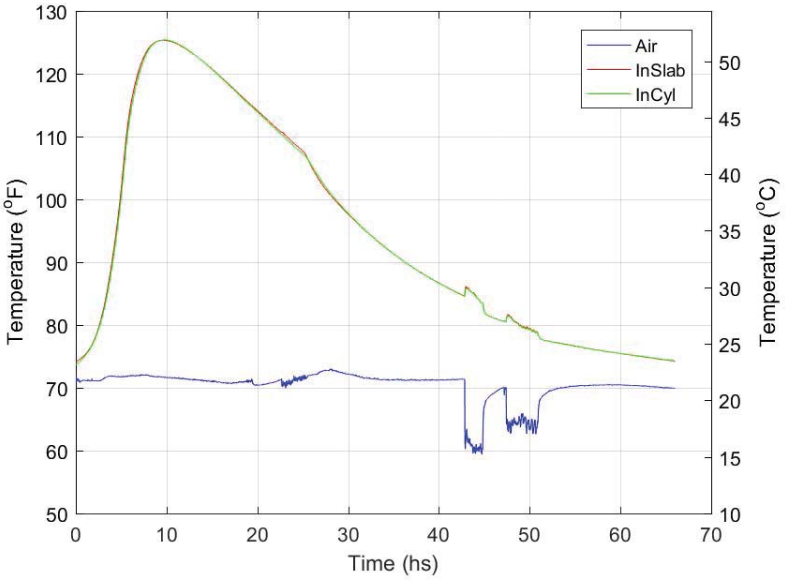

Figure 19: Temperature monitoring of slab R9. "Air" corresponds to air temperature measurements close to the slab. "InSlab" corresponds to temperature measurements collected by a thermocouple inserted in the slab concrete outside any in-place cylinder at mid depth. "InCyl" corresponds to a thermocouple inserted into an in-place cylinder at mid depth.

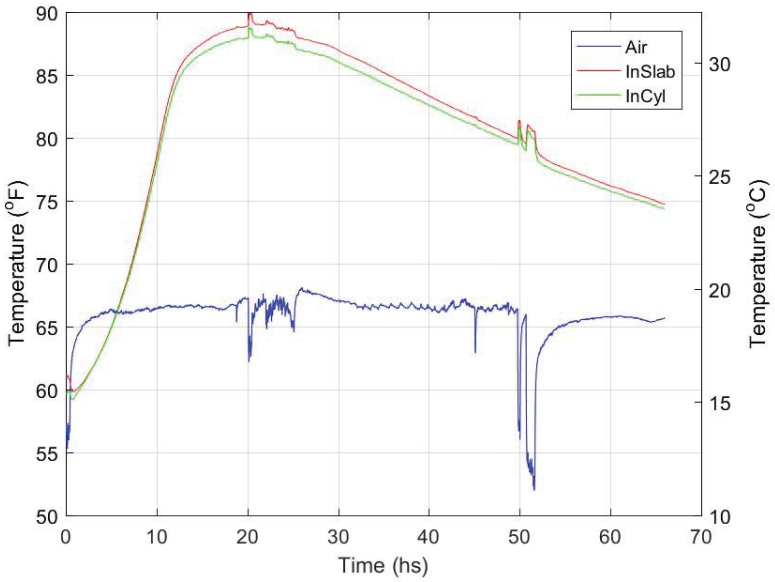

Figure 20: Temperature monitoring of slab R13. "Air" corresponds to air temperature measurements close to the slab. "InSlab" corresponds to temperature measurements collected by a thermocouple inserted in the slab concrete outside any in-place cylinder at mid depth. "InCyl" corresponds to a thermocouple inserted into an in-place cylinder at mid depth.

5.3 COMPANION CYLINDER DENSITY RESULTS

Figure 21 shows the density results of the companion cylinders, which were measured and tested on day 14 after casting.

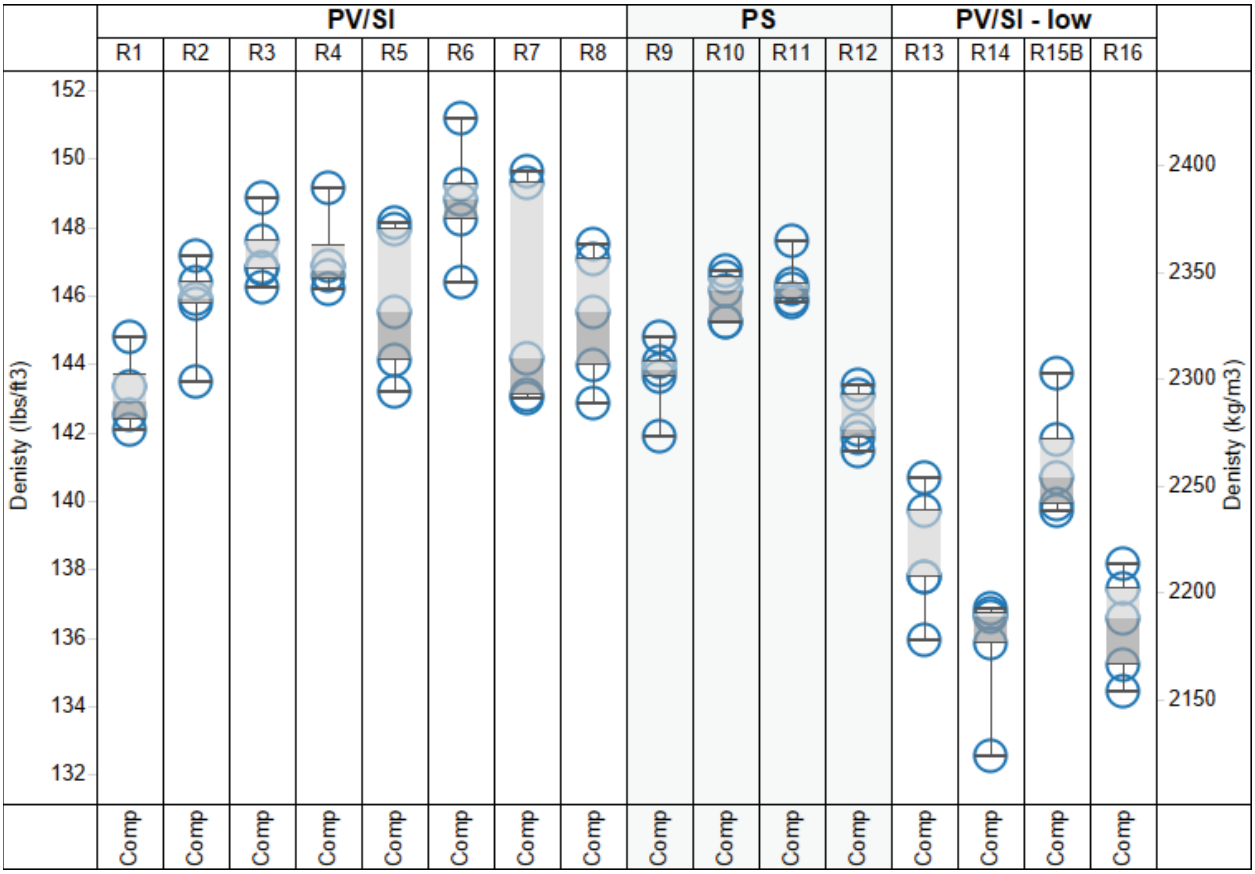

Figure 21: Density results of companion cylinders. Measurements and tests carried out on day 14 after casting immediately before testing. Boxplots superimposed.

5.4 IN-PLACE CYLINDER AND CORES DENSITY RESULTS

Figure 22 shows the density results of the in-place cylinders and core samples, which were measured and tested on day 14 after casting.

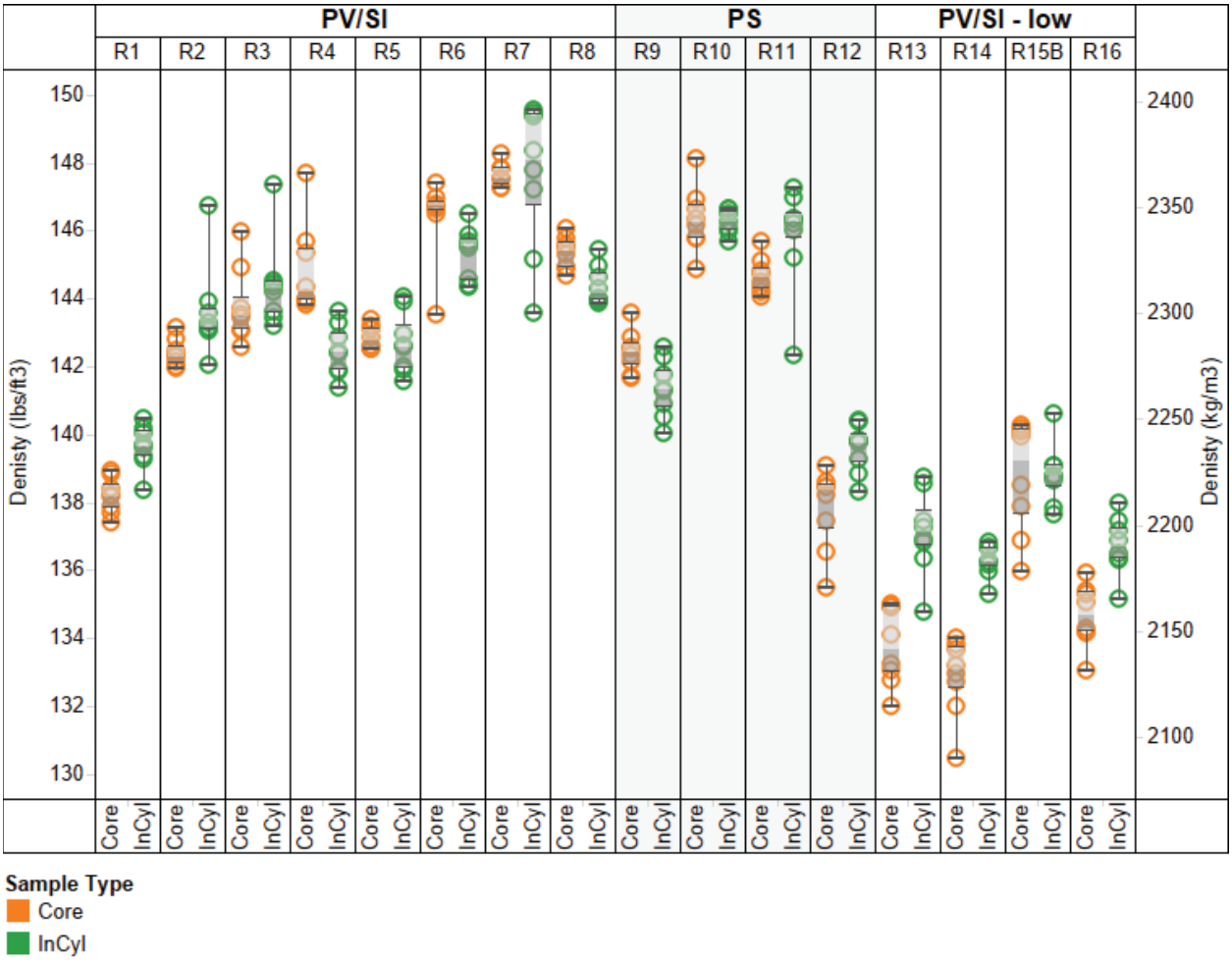

Figure 22: In-place cylinder ("InCyl") and core density results indicated by green and orange circles measured immediately before testing. Boxplots are superimposed.

5.5 COMPANION CYLINDER STRENGTH RESULTS

Figure 23 contains the compressive strength results of the 4 × 8 and 6 × 12 companion cylinders, tested on day 14 after casting. The strength results that come from both sizes of cylinders are shown combined together as no statistical difference in strength value was found between them. Moreover, the goal of testing companion cylinders was to characterize the quality of the concrete mixture and not to compare the strength results populations of testing the cylinder size.

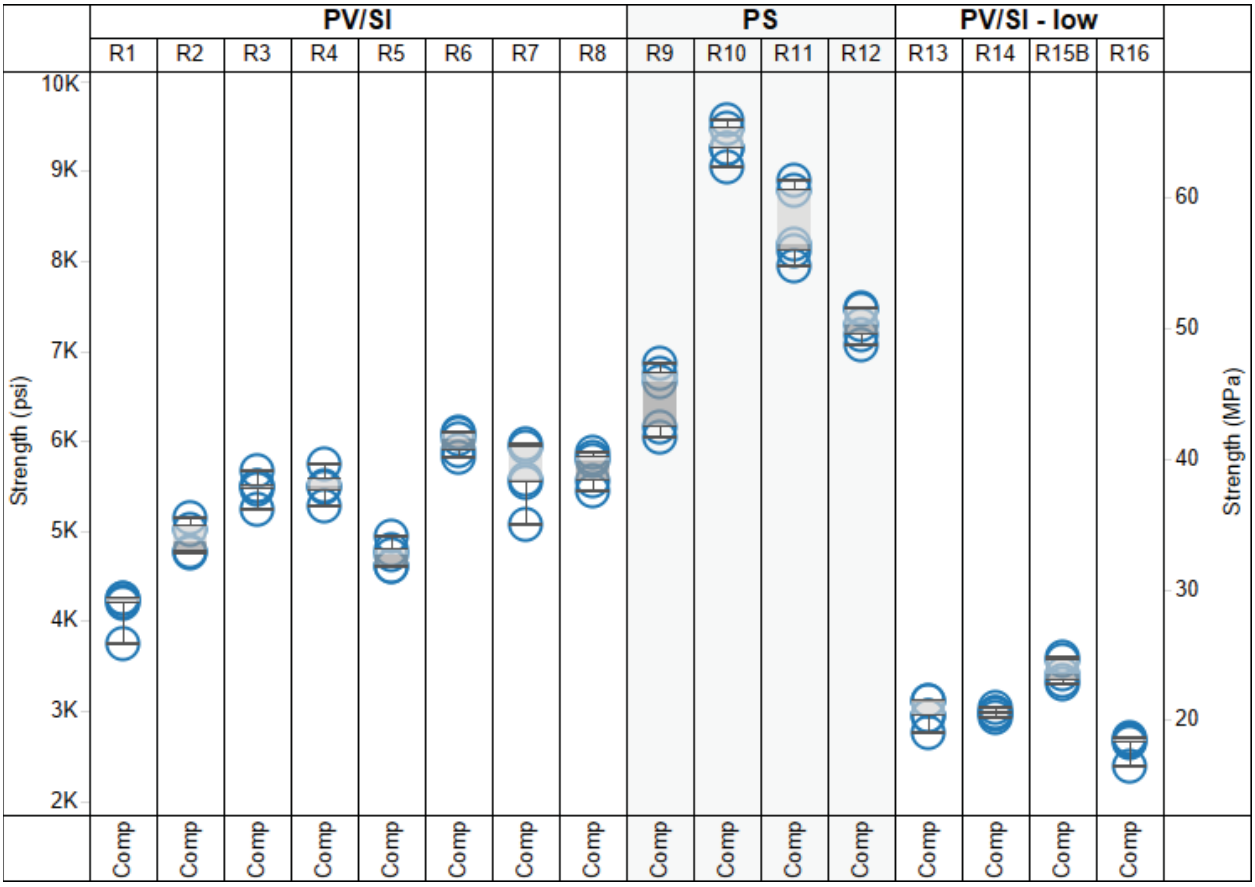

Figure 23: Compressive strength results of 4 × 8 and 6 × 12 companion cylinders, tested on day 14 after casting.

5.6 IN-PLACE CYLINDER AND CORE COMPRESSIVE STRENGTH RESULTS

Figure 24 contains the compressive strength data of in-place cylinders and cores, tested in day 16 after casting.

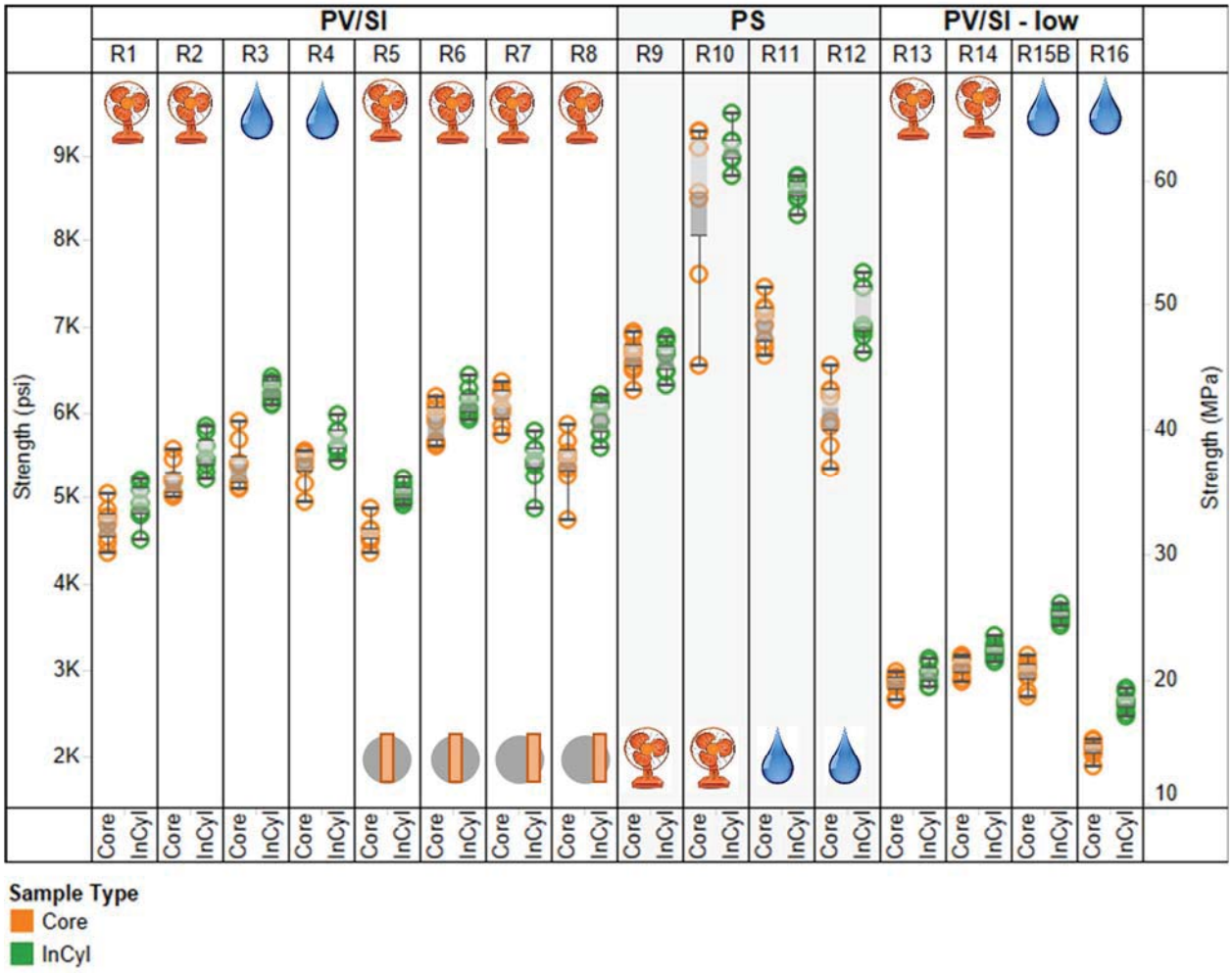

Figure 24: In-place cylinder ("InCyl") and core compressive strength results indicated by green and orange circles. Boxplots are superimposed. The fan and the water droplet indicate the 1-day dry and 1-day wet slabs. The gray circle with the superimposed orange bar indicates the slabs with rebar and whether the rebar was in the inner third or outer two-thirds of the cores.

5.7 IN-PLACE AND CORE DYNAMIC MODULUS RESULTS

Figure 25 contains the longitudinal dynamic elastic modulus results of in-place cylinders and cores, tested on day 16 after casting.

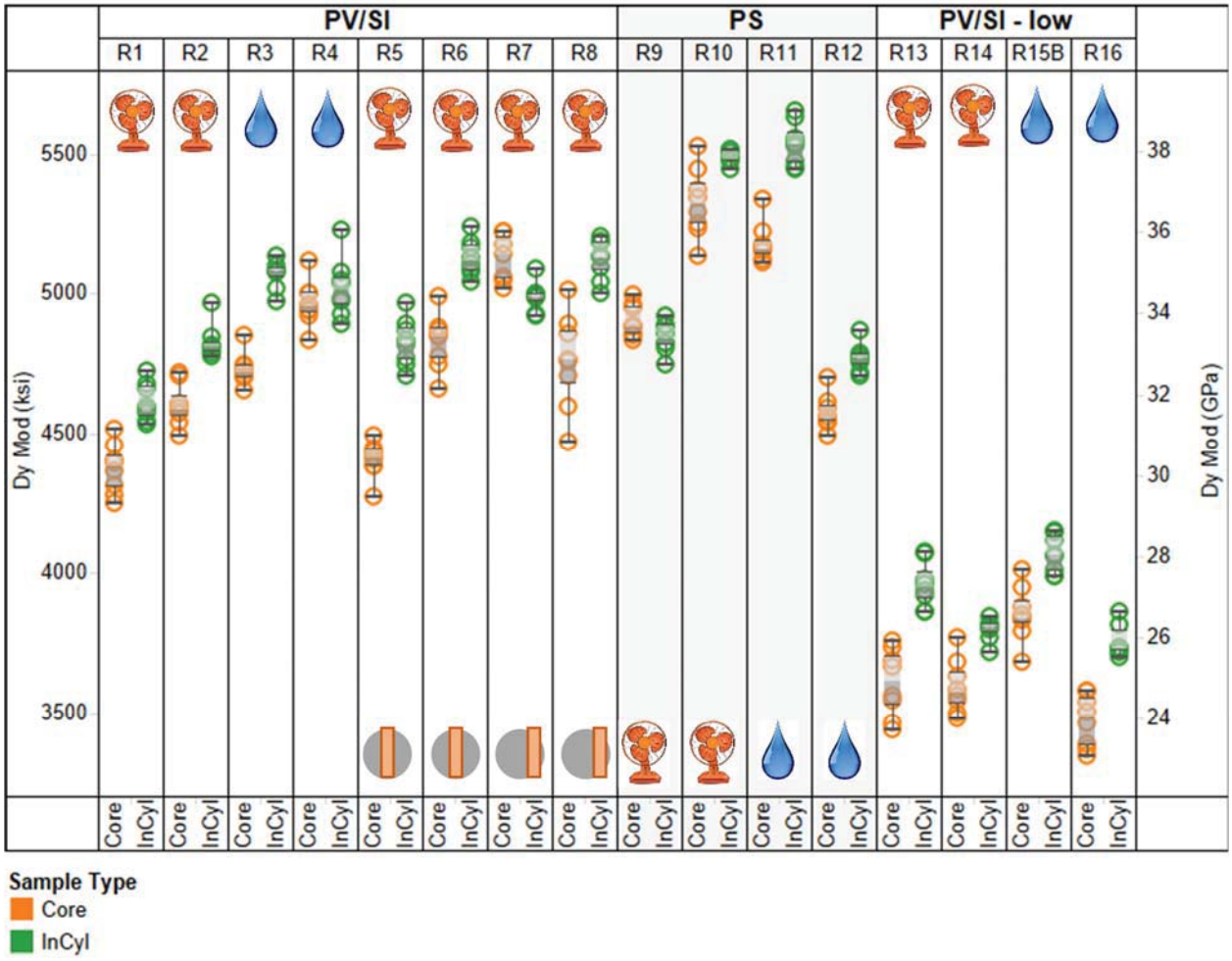

Figure 25: In-place cylinder ("InCyl") and core longitudinal dynamic modulus results indicated by green and orange circles. Boxplots are superimposed. The fan and the water droplet indicate the 1-day dry and 1-day wet slabs, respectively. The gray circle with the superimposed orange bar indicates the slabs with rebar and whether the rebar was in the inner third or outer two-thirds of the cores.

5.8 EXCLUSION OF SLAB R7

5.8.1 Fresh Concrete Properties

Slab R7 corresponded to the third slab cast with embedded rebar, and the first one in which rebar was located at the cores' outer two-thirds. The fresh concrete properties included in Table 4 were employed to accept or reject the delivered concrete at the moment of casting. No additional analyses were carried out with the fresh concrete property data.

Table 4 shows that almost all the measured fresh concrete properties of R7 were within specifications. The measured slump was 3.25 in. (8.3 cm), only 0.25 in. (0.6 cm) below the minimum required slump of 3.5 in. (8.9 cm), so it was decided to accept the mixture.

5.8.2 Flawed Diameter Measurements

During the processing stage of the investigation, it was noted that the diameters of the R7 in-place cylinders were measured incorrectly. These errors were probably caused by the use of an electronic caliper with low battery, which did not zero out correctly (see red circle in Figure 26).

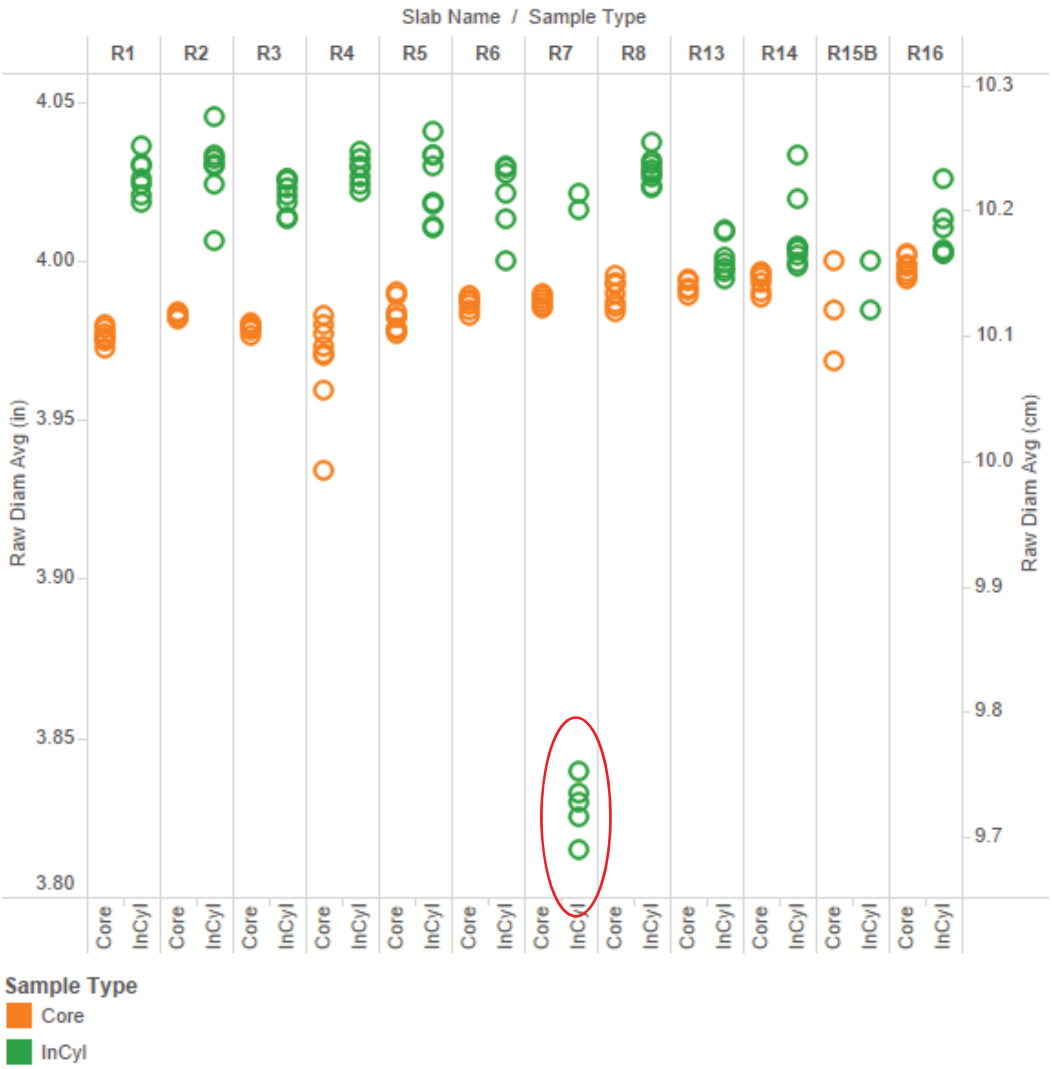

Figure 26: Measured diameters of cores and in-place cylinders ("InCyl"), of PV/SI and PV/SI-low mixtures, including the flawed measurements of R7 in-place cylinder diameters. The red oval indicates the flawed measurements.

5.8.3 Compressive Strength Analysis

R7 was the only slab of the entire set in which in-place cylinder strength was significantly lower than core strength. This fact is depicted in Figure 27 from a qualitative point of view (statistical analysis confirmed this observation). It should be noted that R7 and R8 cores had steel rebar in the outer two-thirds, and R5 and R6 cores had rebar in the inner third; the rest of the slab cores did not have rebar.

This unusual result in which the in-place cylinders of R7 yielded a compressive strength statistically lower than the cores suggested a problem other than the error in the diameters. In addition, looking at slabs R5, R6, and R8, which also contained cores with embedded rebar (as R7 did), it can be seen in Figure 27 that cores always yielded compressive strengths significantly lower than in-place cylinders did. Thus, it can be presumed that the presence of rebar did not increase the compressive strengths of the cores; instead, the problem should have been in the in-place cylinders.

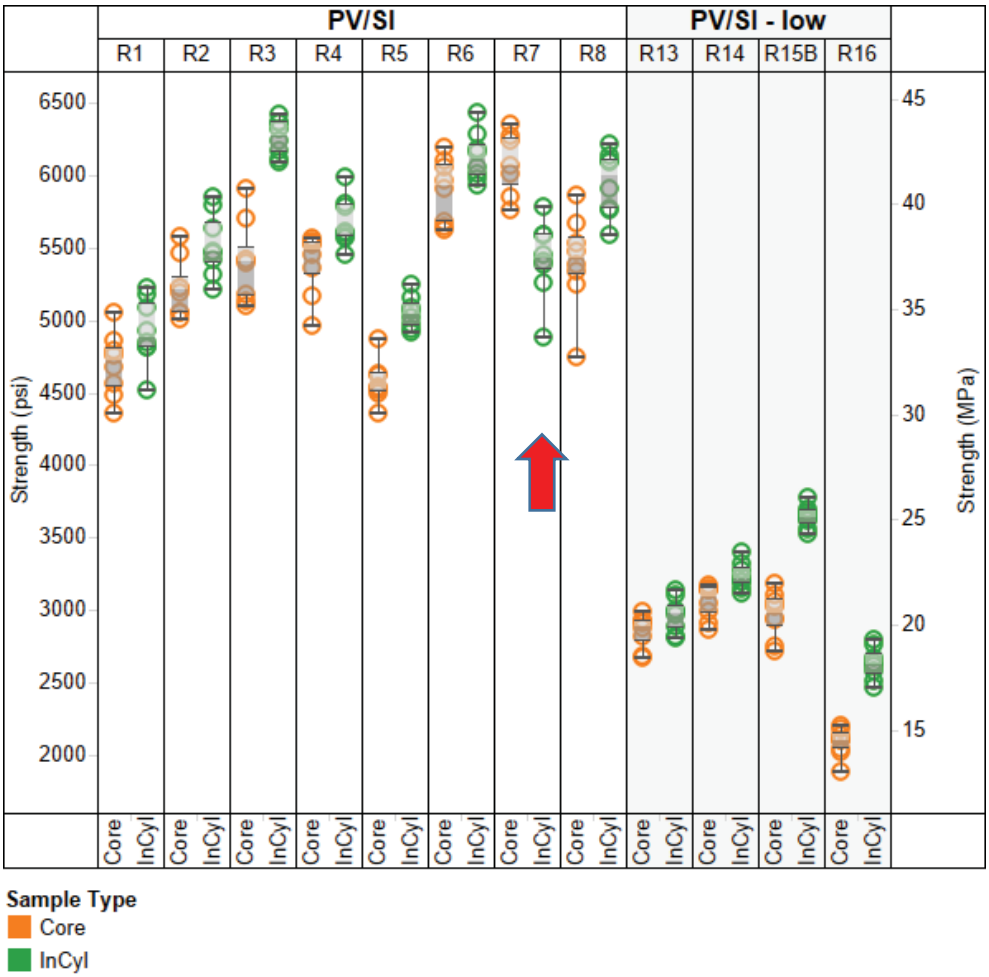

Figure 27: Compressive strength of cores and in-place cylinders ("InCyl"), of PV/SI and PV/SI-low mixtures, assuming 4 in. (10.2 cm) diameter of the R7 in-place cylinders to calculate compressive strength. The red arrow indicates the R7 dataset showing that the in-place cylinder's compressive strength population was significantly lower than that of the core population.

5.8.4 Longitudinal Dynamic Modulus Analysis

Figure 28 presents the dynamic modulus computation of cores and in-place cylinders, focusing on the mixtures PV/SI and PV/SI-low.

It can clearly be seen in Figure 28 that slab R7 was the only one in which in-place cylinders had a dynamic modulus dataset significantly lower than the cores (statistical analysis confirmed this observation). In addition, looking at slabs R5, R6, and R8, which also contained cores with embedded rebar, it can be seen that cores always yielded dynamic moduli significantly lower than in-place cylinders (statistical analysis confirmed this observation). Thus, it can be presumed that the presence of rebar did not increase the dynamic moduli of the cores; this confirmed that the problem should have been in the in-place cylinders.

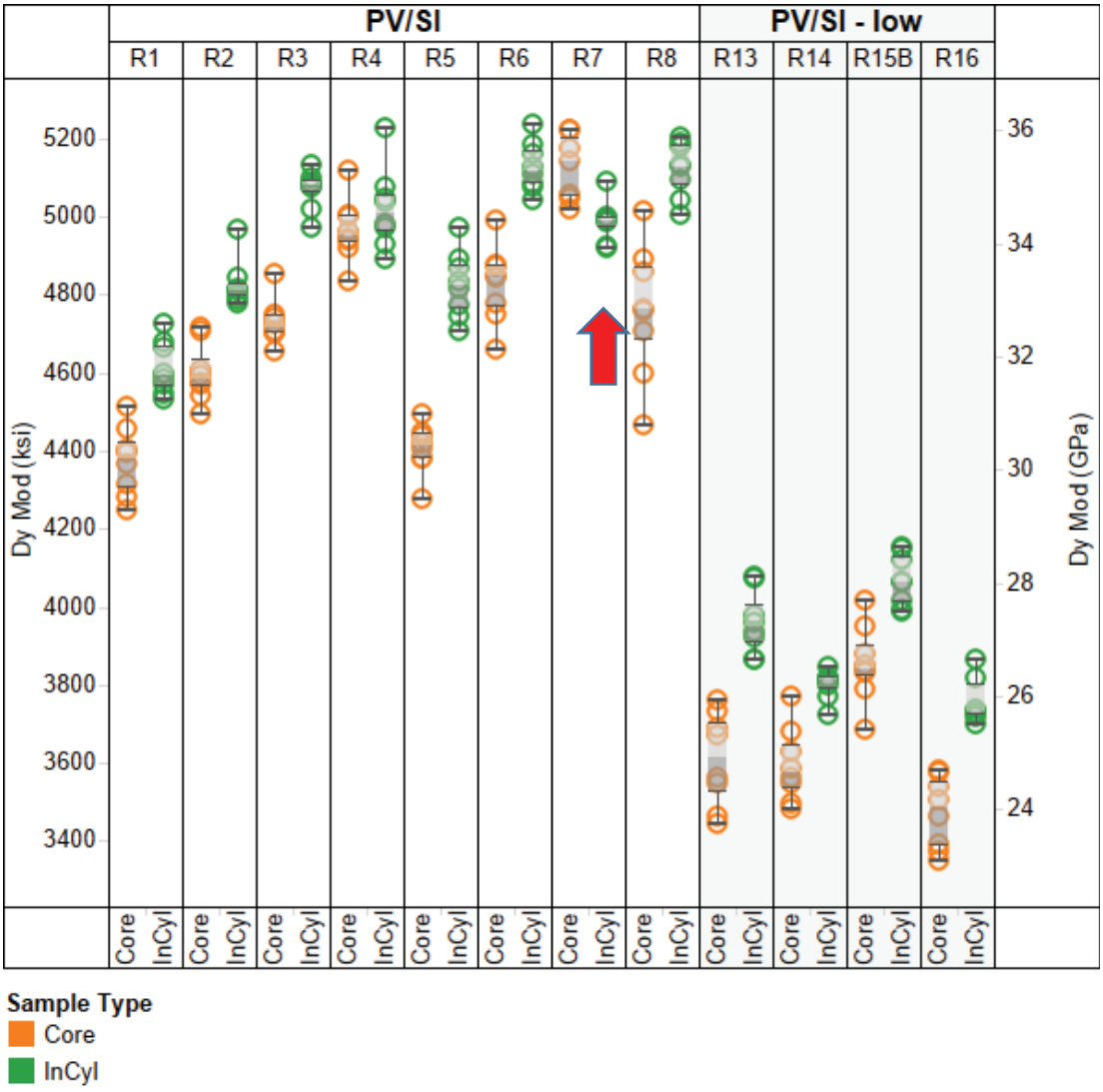

Figure 28: Dynamic modulus of cores and in-place cylinders ("InCyl"), of PV/SI and PV/SI-low mixtures, using exactly 4 in. (10.2 cm) as the diameter of the R7 in-place cylinders to calculate dynamic modulus.

5.8.5 NDT Analysis

Non-destructive tests carried out on the slab were compared with the in-place cylinder compressive strength results to illustrate NDT vs. compressive strength relationships as correlation curves. These analyses are described in detail in Section 5.12.

The goal of including the correlation curves in this section is to give additional support that the in-place cylinder compressive strength results of slab R7 were flawed and that they should be excluded from the analysis.

Figure 29 depicts the relationship between the rebound hammer test results and in-place compressive strength results. The dotted line in that figure is an OLS best-fit line computed for the data without considering R7. The blue dot pointed out by the blue arrow corresponds to R7, which is significantly far from the rest of the population. Assuming that the rebound hammer data were collected accurately, the position in which the R7 blue dot appears suggests that the real R7 average compressive strength should be higher. This explanation suggests that the measured values of compressive strength using the in-place cylinders were lower than the compressive strength of the concrete that remained in the slab.

A similar graph was obtained when analyzing the pullout test results, with the R7 blue dot being to the right of the graph and significantly away from the rest of the data points. This fact confirms that the NDT measurements taken at the slab's concrete were accurate and that the in-place compressive strengths were inaccurate.

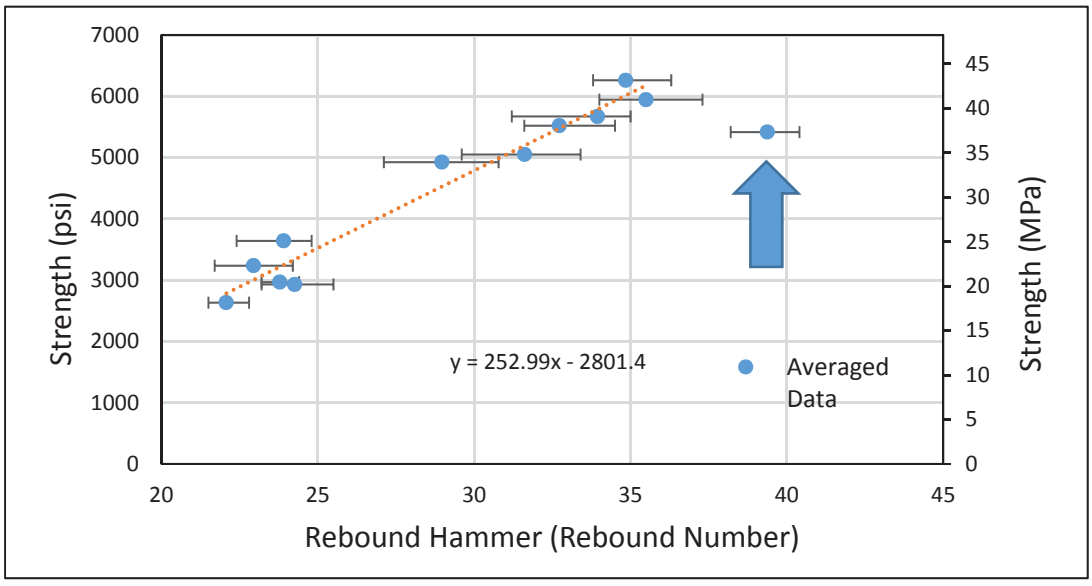

Figure 29: Rebound hammer vs. in-place compressive strength relationship. Blue dots represent the average rebound number vs. average in-place compressive strength of each slab. The black horizontal error bars show the variability of all rebound number testing location values. The dotted red line is an OLS best-fit line computed without considering R7 results. Blue arrow indicates the averaged data point of R7.

5.8.6 Section Conclusions

The compressive strength values of the in-place cylinders of slab R7 are not representative of the real in-place strength of the slab's concrete. This statement is supported by analyzing compressive strength, dynamic modulus, and rebound hammer test results. The analysis of density comparing in-place cylinders to cores and in-place cylinders to companion cylinders, yielded results less clear than the ones presented above. However, it was observed that the in-place cylinders of R7 have lower densities than they should have, based on a qualitative analysis.

It can also be affirmed that, if the in-place cylinders' strengths should have been higher than the measured ones. It is presumed that the concrete exhibited a sticky and dry consistency and thus were more difficult to consolidate within the in-place cylinders. This explanation justifies the fact that compressive strength and dynamic modulus of the in-place cylinders were significantly and statistically lower than the compressive strength and dynamic modulus of the cores, respectively, and that their densities were also slightly lower. This fact also explains the findings from the NDT analyses.

As a result of this specific study of slab R7, it was decided to exclude all R7 measurements from the rest of the analysis, discussion, and conclusions.

5.9 STATISTICAL ANOVA ANALYSIS OF IN-PLACE CYLINDERS VS. CORE STRENGTH

The analysis procedure described in Section 4.3 was applied to each group of data to evaluate the range of correction factors that would make the core strengths not statistically different from the in-place cylinder strengths. The results of these analyses are described in this section.

5.9.1 Correction Factors

Examining the ranges of correction factors that are applicable to each slab individually, as shown in Figure 30, it is evident that no one correction factor will work for all cores. In particular, the strengths of the wet core treatment required larger and less consistent correction factors to make them statistically similar to the in-place strengths. Subsequent figures will compare ranges of correction factors applicable to subsets of slabs. Table 5 lists the values of correction factors needed to satisfy a 95% statistical confidence level (giving an F-score less than or equal to 4.6) for the individual slabs, and combinations thereof, shown in Figure 30. The optimal correction factor (giving an F-score equal to zero) is also provided for each case. A correction factor score is not provided for the R3 and R4 slab pair because no one factor satisfies both sets of data; as seen in Figure 30, the R3 and R4 slab datasets show no overlap in correction factor value.

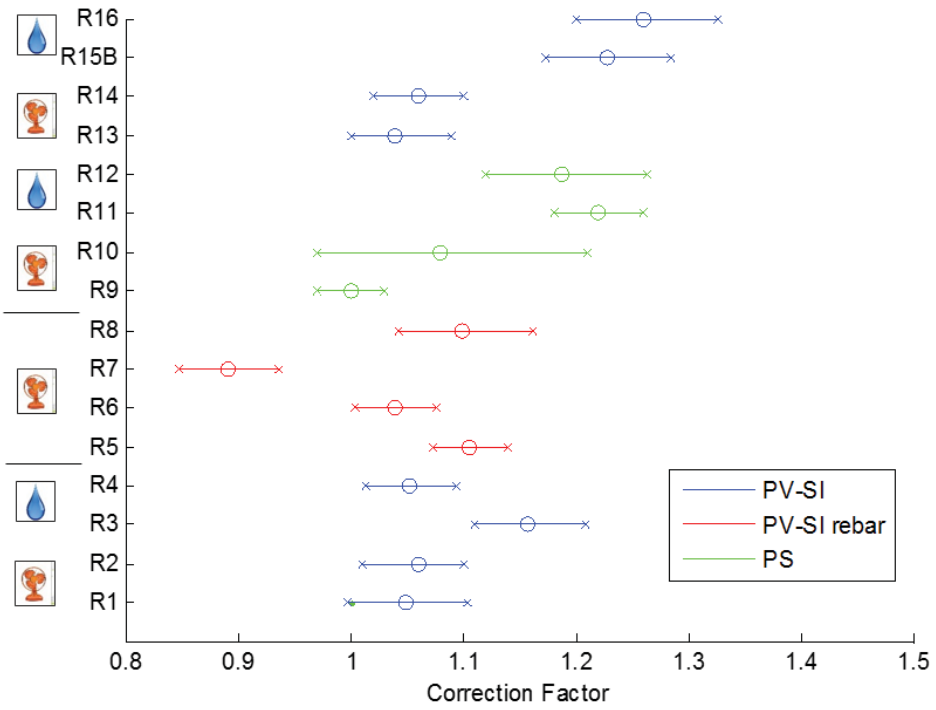

Figure 30: Correction factors applied to core strengths of each slab to make them not statistically different from the in-place strengths.

Table 5: Correction Factors Needed to Meet ANOVA Requirements for 95% Confidence Level

	Corrections			
	Min	Best	Max	For pair
R1	1.00	1.05	1.11	1.05
R2	1.02	1.06	1.11	
R3	1.12	1.16	1.22	n.a.
R4	1.02	1.06	1.10	
R5	1.08	1.11	1.15	1.08
R6	1.01	1.04	1.09	
R8	1.05	1.10	1.17	1.10
R9	0.97	1.00	1.04	1.03
R10	0.98	1.09	1.22	
R11	1.19	1.22	1.27	1.21
R12	1.12	1.19	1.27	
R13	1.00	1.04	1.10	1.05
R14	1.03	1.06	1.11	
R15B	1.18	1.23	1.30	1.24
R16	1.21	1.26	1.34	

The ranges of correction factors applicable to the dry core treatments without rebar are shown in Figure 31. By isolating this subset of slabs, it becomes noticeable that a factor of 1.05 would provide a good prediction of in-place strength from core strength for the dry core treatments of PV/SI. This is reliable even if extra water were added to lower the strength, as in slabs R13 and R14. With a correction factor of 1.05, the greatest average error of the PV/SI slabs was 0.9%. A factor of 1.03 would be applicable to all six of these slabs, including the higher-strength PS mix, but with larger overall average errors in prediction. In other words, a correction factor of 1.03 works for all six slabs shown in Fig. 31, but a correction factor of 1.05 provides lower average error in prediction for all slabs except slab R9.

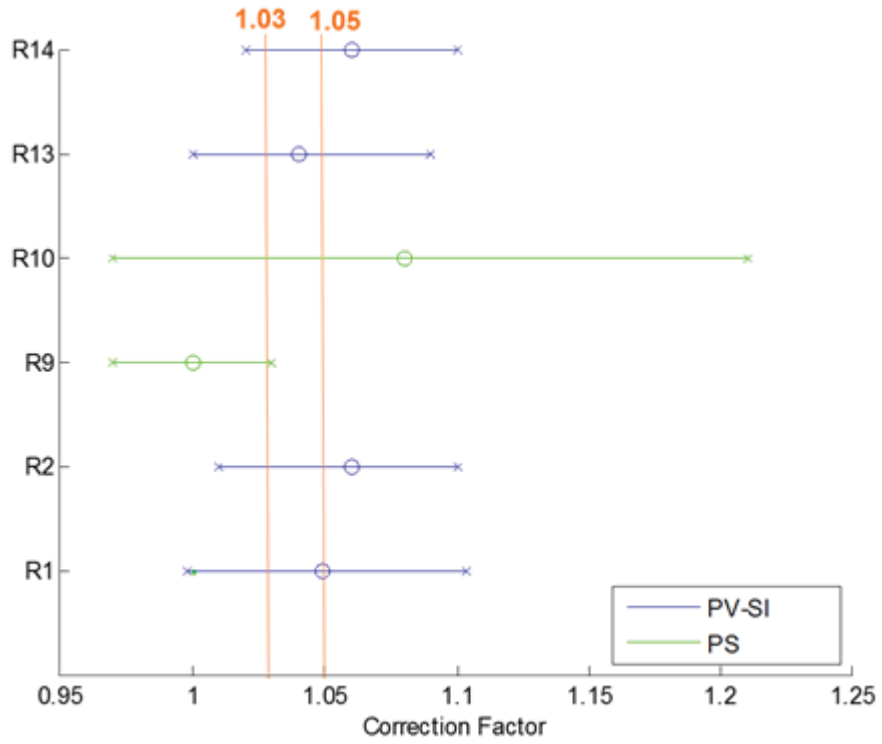

Figure 31: Correction factors applied to dry core strengths of each slab to make them not statistically different from the in-place strengths.

The ranges of correction factors applicable to the wet core treatments without rebar are shown in Figure 32. A factor of 1.21 would provide a statistically equivalent prediction of in-place strength from core strength for most but not all of the wet core treatments. The average errors in prediction of in-place strengths would be significantly higher for those slabs than for the dry core treatment predictions. For slab R4, a factor of 1.21 applied to the core strengths leaves them statistically different from the in-place strengths.

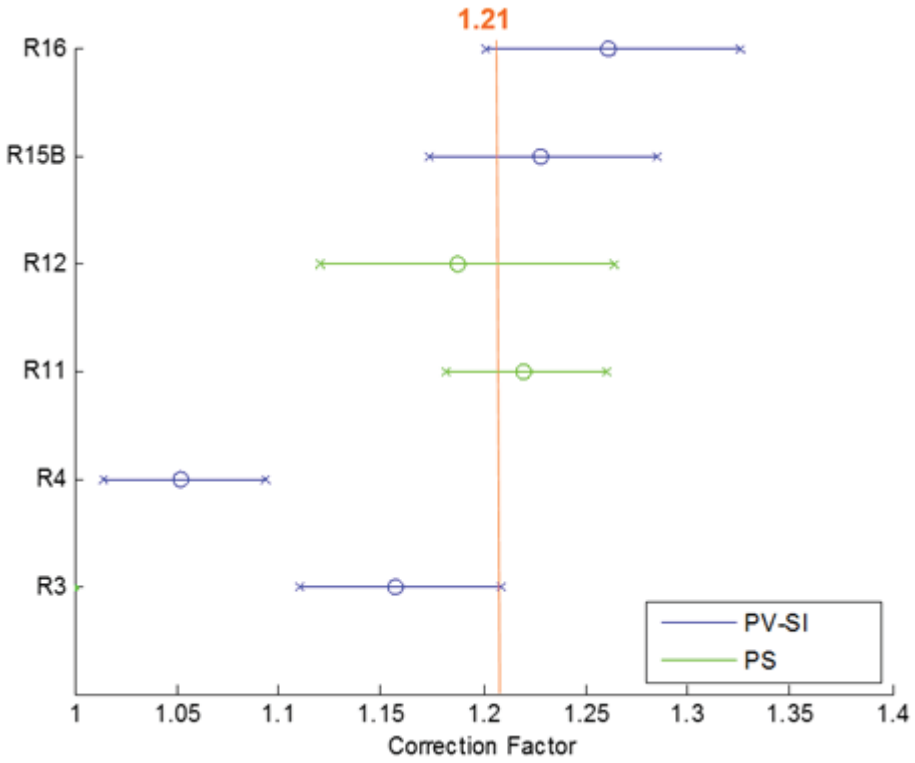

Figure 32: Correction factors applied to wet core strengths of each slab to make them not statistically different from the in-place strengths.

The ranges of correction factors applicable to the slabs with dry core treatments with rebar are shown in Figure 33. By isolating this subset of slabs, it becomes noticeable that a factor of 1.08 would provide a statistically equivalent prediction of in-place strength from core strength for the dry core treatments with rebar, except for slab R7, which has been rejected as previously explained. Furthermore, the location of the rebar in the core (located within the inner third of core radius in slabs R5 and R6 and within the outer two-thirds of the core radius in slab R8) did not significantly affect the correction factor needed to make the core strengths similar to the in-place strengths. The average errors in prediction of in-place strengths would be significantly higher for these cores with rebar, but the populations are statistically equivalent to the respective in-place strengths.

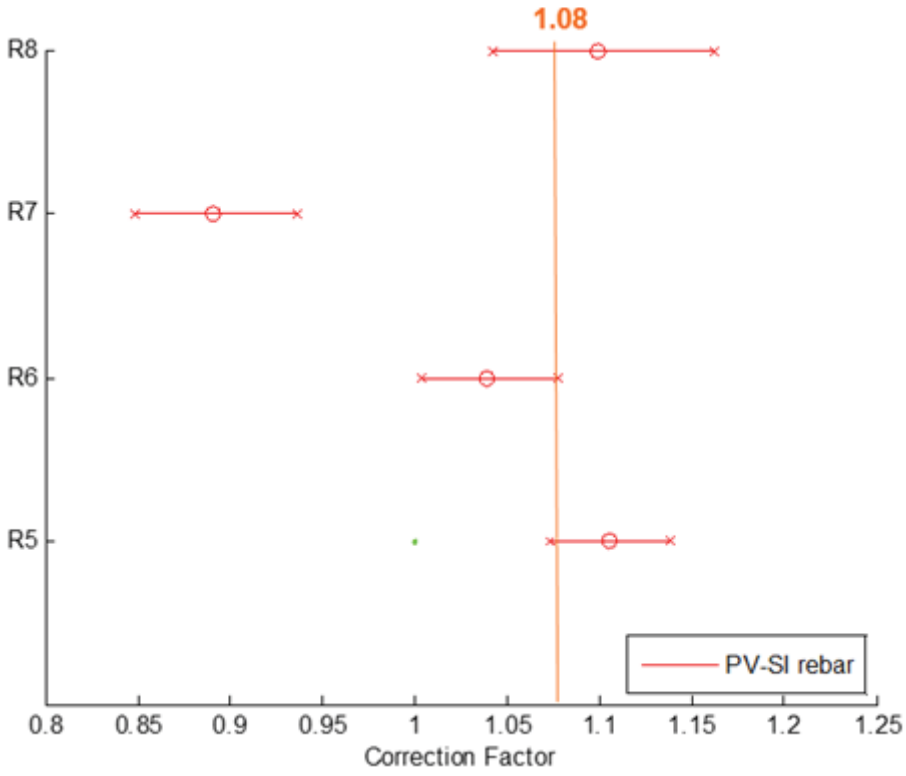

Figure 33: Correction factors applied to dry core strengths of slabs containing rebar to make them not statistically different from the in-place strengths.

5.9.2 Linear Fit

In order to predict the in-place strength more accurately, a linear fit was also considered to relate the core strength to the in-place strength. When applied to the dry core data without rebar, the linear fit equation 0.96*(Core Strength) + 337psi yielded strength predictions that were statistically equivalent to the in-place strength for all six slabs. The greatest average error in the predicted strengths was only 3.7% (Figure 34).

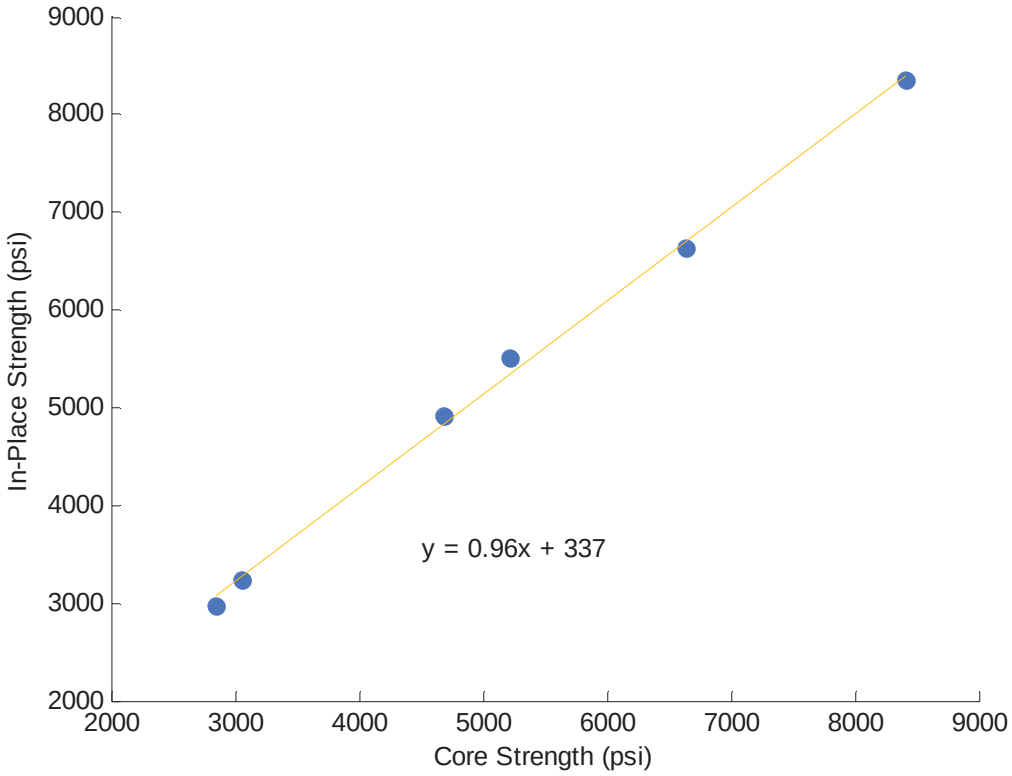

Figure 34: Linear fit to dry core strengths of slabs without rebar to make them not statistically different from the in-place strengths.

5.9.3 Discussion

The results showed high variability between slabs. The most consistent results were achieved by dry conditioning of the cores for the PV/SI mix. For that subset of slabs, the in-place cylinder strength could be predicted accurately by applying a 1.05 correction factor to the dry core strength. Rebar generally lowers core strengths and increases errors in prediction, but a factor of 1.08 provides strengths that are not statistically different from the in-place strengths. High-strength mixes showed more variability, as did the cores with the wet treatment. A linear fit of the data provides a good strength prediction from the cores for both mixes.

5.10 CORE STRENGTH RANDOM SAMPLING ANALYSIS

This section presents the results obtained from applying the random sampling analysis by estimating in-place strength using cores. Ten different analyses are presented, each corresponding to using a different subset of slabs. These analyses are named alphabetically from A to J, as shown and described in Table 6.

Table 6: Core Random Sampling Analyses Description

Analysis Name	Corr. Factor	Slabs	Description
A	1.05	R1,R2,R13,R14	PV/SI and PV/SI-low, no rebar, air dried.
B	1.05	R1,R2,R5,R6,R8,R13,R14	PV/SI and PV/SI-low, with and without rebar, air dried.
C	1.05	R1,R2	PV/SI only, without rebar, air dried.
D	1.05	R13,R14	PV/SI-low only, without rebar, air dried.
E	1.08	R5,R6,R8	PV/SI with rebar only, air dried.
F	1.03	R9,R10	PS only, no rebar, air dried.
G	1.05	R1-R2-R9-R10-R13-R14	PV/SI, PV/SI-low and PS, no rebar, air dried.
H	1.05	R1-R2-R5-R6-R8-R9-R10-R13-R14	PV/SI, PV/SI-low and PS, with and without rebar, air dried.
I	1.03	R1-R2-R5-R6-R8-R9-R10-R13-R14	PV/SI, PV/SI-low and PS, with and without rebar, air dried.
J	Var.*	R1-R2-R5-R6-R8-R9-R10-R13-R14	PV/SI, PV/SI-low and PS, with and without rebar, air dried.

* In analysis J, different correction factors were applied depending on the origin of the strength estimation (i.e., depending of which slab was the core from). The applied correction factors were 1.05 for slabs R1, R2, R13 and R14, 1.08 for slabs R5, R6 and R8, and 1.03 for slabs R9 and R10.

In these analyses it should be noted that the correction factors were computed from the same data that now are being analyzed to quantify the error in strength predictions. Thus, the errors in strength predictions shown here are likely lower than if these factors are applied to a situation with different conditions (e.g. varying mixture design and aggregate size and gradation, different testing age, different sample size, different core conditioning, etc.). It should also be noted that the different analyses consider different number of slabs, which makes the dataset's sizes to be different, which in turn affect the results' confidence.

Figure 35 contains the expected error curves of analyses A, B, G, H, I and J. The rest of the expected error curves for analyses C, D, E, and F, as well as the corresponding histograms for all analyses are presented in Appendix E.

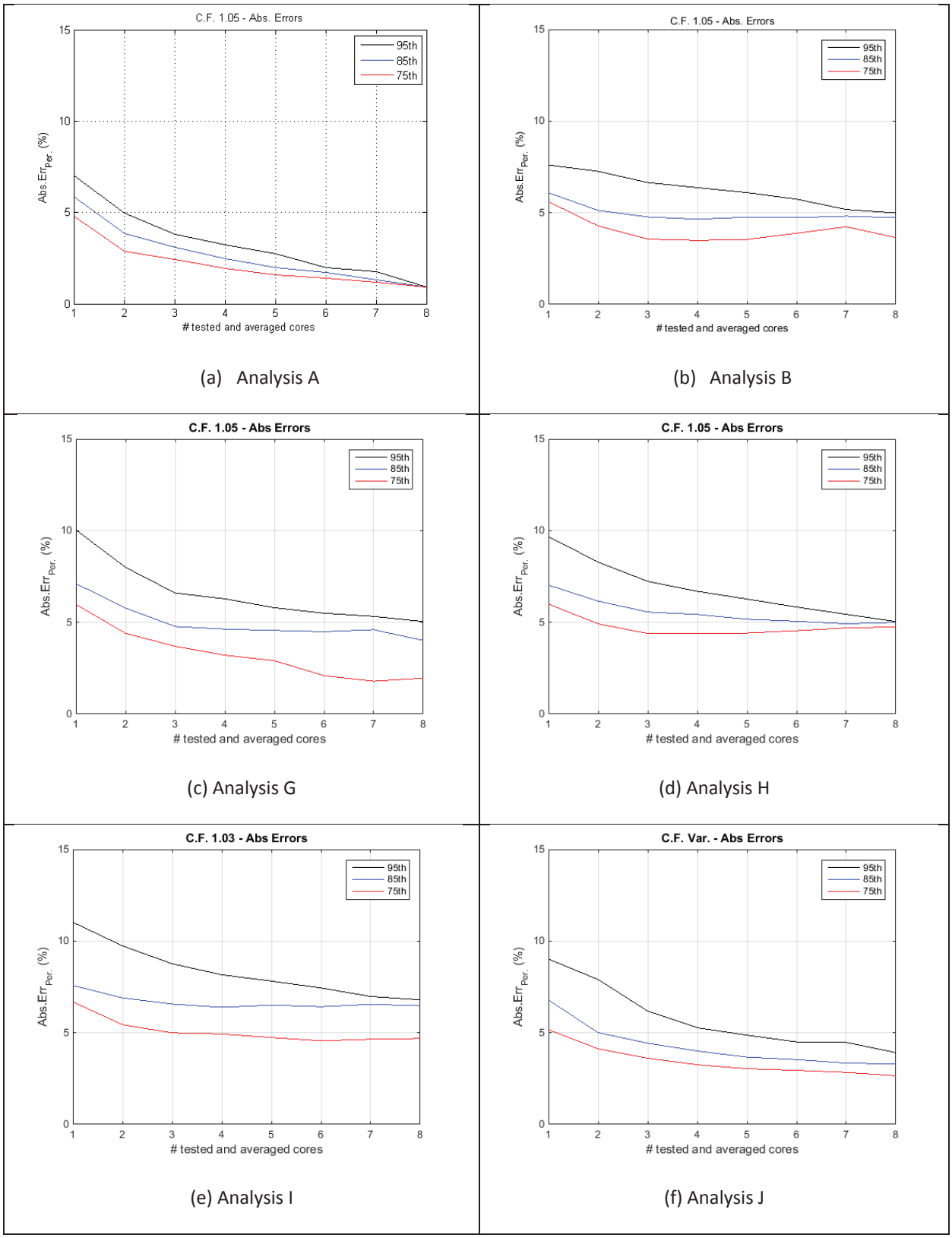

Figure 35: Expected error curves results of analyses (a) A, (b) B, (c) G, (d) H, (e) I, and (f) J.

The following is a brief description of how to interpret Figure 35.

First it should be noted that theoretically, the expected error curves should never increase with increasing number of cores. This occurs because, for a given level of confidence (a constant percentile in this case), the strength estimation will have a lower error. However, it can be seen in Figure 35, that sometimes the expected error curves tend to increase after six or more *# tested and averaged cores* are considered; this is an artifact that happens due to the use of limited amount of data, becoming a problem at higher *# tested and averaged cores*. The $Abs.Err._{per}$ calculated for 7 and 8 *# tested and averaged cores* is not as reliable as those obtained for 1 to 6. A well-established expected error curve would be one that comprises a sufficiently big dataset to provide statistically reliable results. The number of samples considered for each analysis and at each *# tested and averaged cores* is shown in the corresponding histograms in Appendix E.

To analyze Figure 35, the reader should first select one of the three plotted confidence levels, here quantified as percentiles 75th, 85th and 95th. As an example, consider the 85th percentile, the blue curve in Figure 35. Then choose a value of *# tested and averaged cores*, for example the value 2. Then the blue curve correlates the value 2 to an expected strength estimation error ($Abs.Err._{85}$) in the Y-axis. That value corresponds to the expected error that has approximately an 85% chance of not being exceeded when averaging two cores. In other words, the error of your strength estimation has an approximately 85% probability of being that obtained error or lower.

A 5% expected error was used under an 85% confidence. It should be noted that previously the correction factors were obtained using a statistical analysis under a 95% confidence level. Those factors were computed comparing populations between in-place cylinders and cores' strengths, and using a much more rigorous mathematical/statistical approach. In the analysis presented in this section the approach is less rigorous, as the confidence is only being quantified using the dataset's percentile. To summarize the difference between these concepts, the computation of every given correction factor was obtained using a 95% confidence level, and in this section, the analysis focuses on the confidence of the strength estimation, which is evaluated using the computed strength error's dataset's percentiles.

Figure 35 illustrates that the 85th percentile expected error curves of analyses H and I do not reach 5 % error for any *# tested and averaged cores*. This fact indicates that considering one single correction factor for all the slabs may not be the most accurate approach. For instance, analysis J contains the same slabs but the correction factors varied depending on the slab; as expected, analysis J had a lower 85th percentile expected curve which intersects the 5% expected error at *# tested and averaged cores* = 2.

Table 7 has been constructed to provide a better and easier understanding of the results presented in Figure 35, and can be used to draw conclusions by comparing analyses A through J. Table 7 contains the percentage of strength estimations of the random sampling analysis that had a strength error lower than 5% (*% Data < 5% error*), when considering varying number of tested and averaged cores, for each of the mentioned analyses A to J. In other words, the values presented in Table 7 are the approximate probabilities of obtaining a strength estimation from a core that has an error of 5% or lower, for a given number of averaged cores. For example, using the dataset of analysis A, when two

cores are selected randomly from a random slab, and that slab's in-place strength is estimated by taking the strength average of those two cores, there is approximately a 96% probability that strength estimation has a 5% error or lower.

The color code in Table 7 indicates the *% Data < 5% error* lower than 75% exclusively in red, between 75% and 85% exclusively in yellow, and 85% or higher in green.

Table 7: Core Random Sampling Analyses Results

				Number of cores used to estimate strength							
		C.F.	Slabs	1	2	3	4	5	6	7	8
%Data < 5% error	A	1.05	R1,R2,R13,R14	78	96	100	100	100	100	100	100
	B	1.05	R1,R2,R5,R6,R8,R13,R14	70	84	86	87	88	88	91	100
	C	1.05	R1,R2	81	95	100	100	100	100	100	100
	D	1.05	R13,R14	75	96	99	100	100	100	100	100
	E	1.08	R5,R6,R8	71	79	85	90	93	96	100	100
	F	1.03	R9,R10	60	69	75	81	86	91	100	100
	G	1.05	R1-R2-R9-R10-R13-R14	66	81	86	88	89	90	90	80
	H	1.05	R1-R2-R5-R6-R8-R9-R10-R13-R14	63	77	80	82	83	84	86	88
	I	1.03	R1-R2-R5-R6-R8-R9-R10-R13-R14	58	72	75	75	77	77	77	75
	J	Var.	R1-R2-R5-R6-R8-R9-R10-R13-R14	72	84	90	93	95	97	100	100

Table 7 clearly shows that the best analyses are A, C and D, where the probability of having a strength estimation error lower than 5% exceeds 85% when using 2 cores. In other words, the green cell with the lowest number of cores occurs at two in these analyses. In these three analyses, only PV/SI and PV/SI-low were considered, and only the 1.05 correction factor was used. When the rebar slabs are added in analysis B, the first green cell moves one core to the right, but still when taking two cores the result is 84% probability, almost 85% (almost green). Analysis B shows slightly better results than E, which only considers rebar slabs and uses 1.08 correction factor; the reason is because in the latter case the dataset size is much lower than in the former. Similarly, analysis F, which considers PS mixes only, is worse than analysis G—which combines all slabs without rebar. Analysis I, where the 1.03 correction factor is applied to all slabs, shows the poorest results. Analysis H is slightly better than I, and the green cell is achieved only when using 7 cores. Finally, analysis J, which uses the correction factors 1.05 for PV/SI and PV/SI-low slabs with no rebar, 1.08 for PV/SI slabs with rebar, and 1.03 for PS slabs with no rebar, shows very good results, reaching the green cell at three cores—but with an 84% probability (almost 85%) at two cores.

This study clearly shows that using the correction factors 1.05 for PV/SI cores without rebar, 1.08 for PV/SI cores with rebar, and 1.03 for PS cores without rebar yield the most confident strength estimations. The study also shows that at least two cores are needed, but three are strongly recommended, to reach an approximate 85% confidence of obtaining a strength error of 5% or lower, where the confidence level was quantified using the 85th percentile of the dataset. However, it should be noted that both PS slabs, R9 and R10 showed anomalous behavior which reduces the

reliability of the 1.03 correction factor. In the case of R9, the in-place strength population was very similar to the core strength population, to the point that its optimum correction factor is around 1.00 (see Figure 31). In addition, the R9 in-place cylinders had statistically lower dynamic moduli than the cores. These facts suggest that some of the R9 in-place cylinders may have been consolidated poorly. In the case of R10, the core strength results showed large variability (see Figure 24), which made the range of applicable correction factors be much higher than the other slabs, as depicted in Figure 31.

5.11 NDT RESULTS

Before presenting the NDT results, the authors acknowledge that the surface wave results were poor because of experimental problems. The analysis of these results shows that the data had problems; thus, the authors have chosen not to present them nor to show any analysis that may misguide potential upcoming research.

Table 8 presents the number of testing locations per slab and the number of testing replicates per location for each NDT method.

Table 8: Testing Locations per Slab and Testing Replicates per Location for Each NDT

NDT Method	Testing Locations per Slab	Testing Replicates per Location	Total Number of Measurements per Slab
Rebound	8	10	80
Nitto	8	10	80
Pullout	3*	1	3

*Slab R1 was tested with pullout at five testing locations. Extra tests were carried out because experimental errors occurred that prevented the researchers to collect pullout data on day 16. Thus three pullout measurements were collected on day 17 and two more on day 18 in order to study a potential change due to the hardening concrete in one day. No differences were seen among the collected data, so all five measurements were accepted as valid representation of day 16 data.

Figure 36, Figure 37, and Figure 38 contain the NDT results, divided between mixtures and slabs.

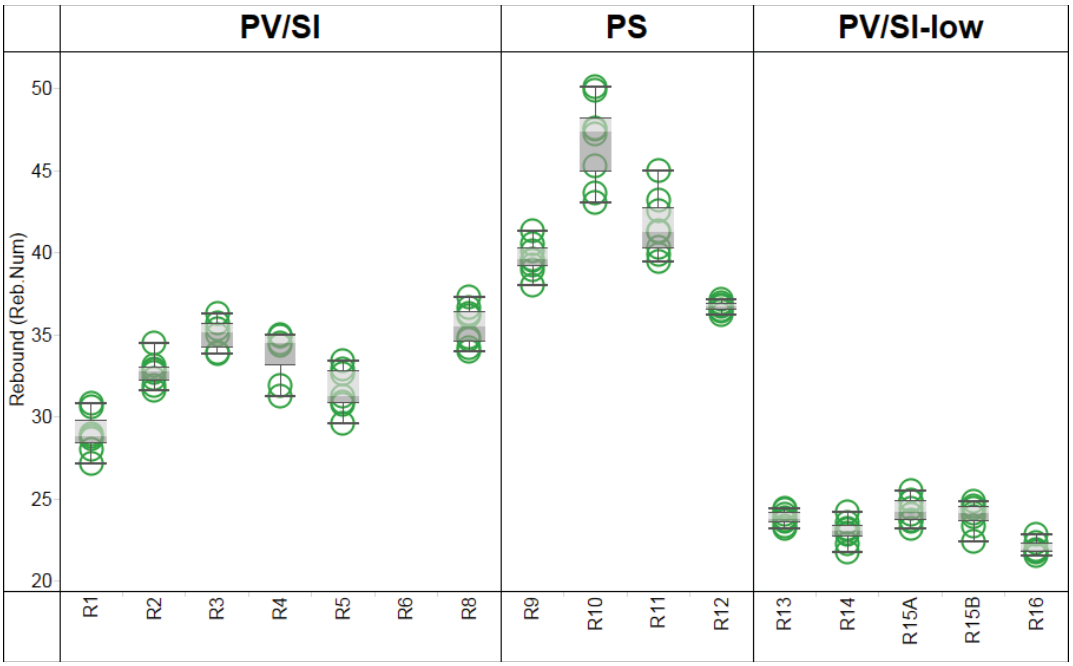

Figure 36: Rebound hammer test results. The green circles represent each testing location result at each slab. Boxplots are superimposed on the testing location results.

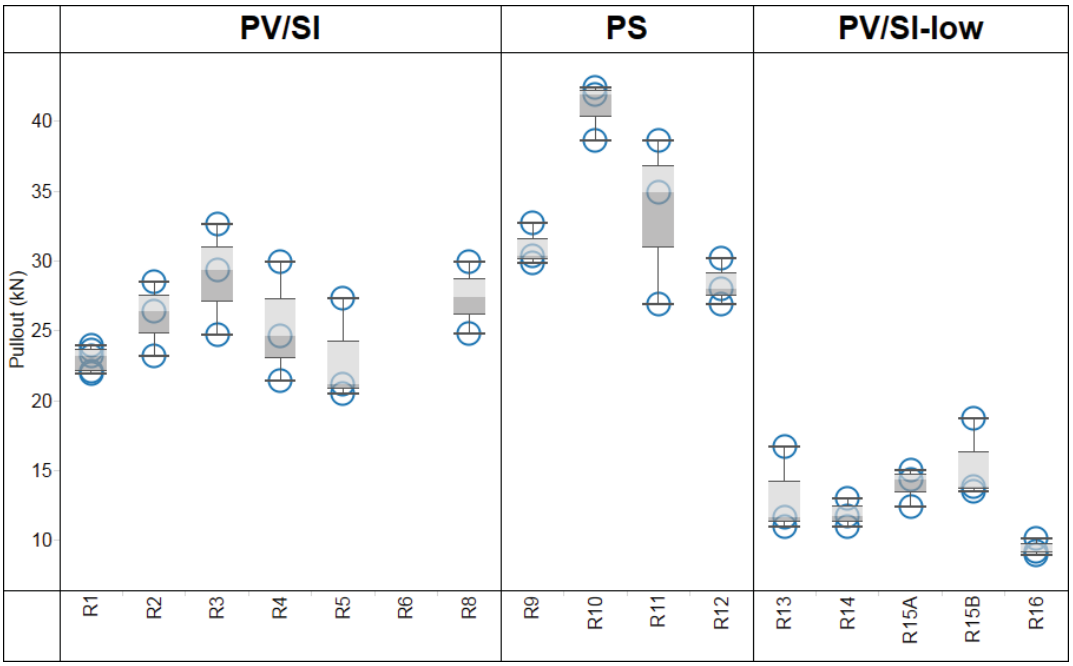

Figure 37: Pullout test results. The blue circles represent each testing location result at each slab. Boxplots are superimposed on the testing location results.

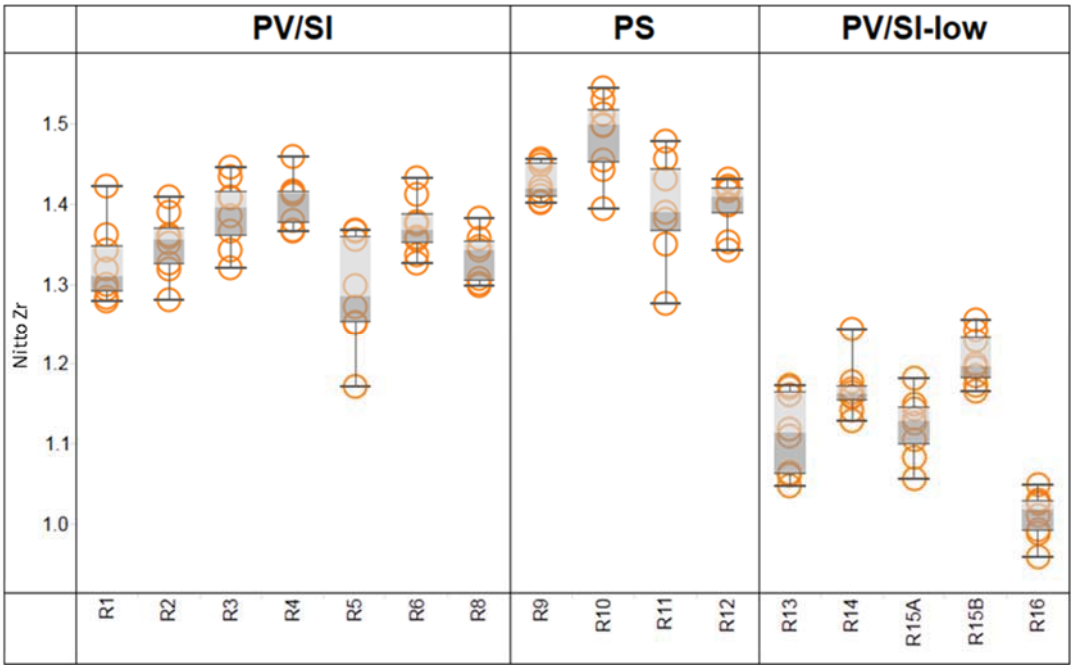

Figure 38: Nitto hammer test results. The orange circles represent each testing location result at each slab. Boxplots are superimposed on the testing location results.

5.12 ANALYSIS OF NDT VS. IN-PLACE CYLINDER COMPRESSIVE STRENGTH OF PV/SI AND PV/SI-LOW MIXTURES

5.12.1 NDT vs. Compressive Strength Relationships

Figure 39 presents the NDT vs. strength relationships (correlation curves) for the rebound hammer, Nitto hammer, and pullout tests. Each blue dot corresponds to the average NDT values (average of testing location values) plotted against the average in-place compressive strength values, for every slab. The horizontal error bars mark the minimum and maximum NDT location values for each slab. Ordinary least squares and logOLS best-fit lines have been computed and are also shown in Figure 39.

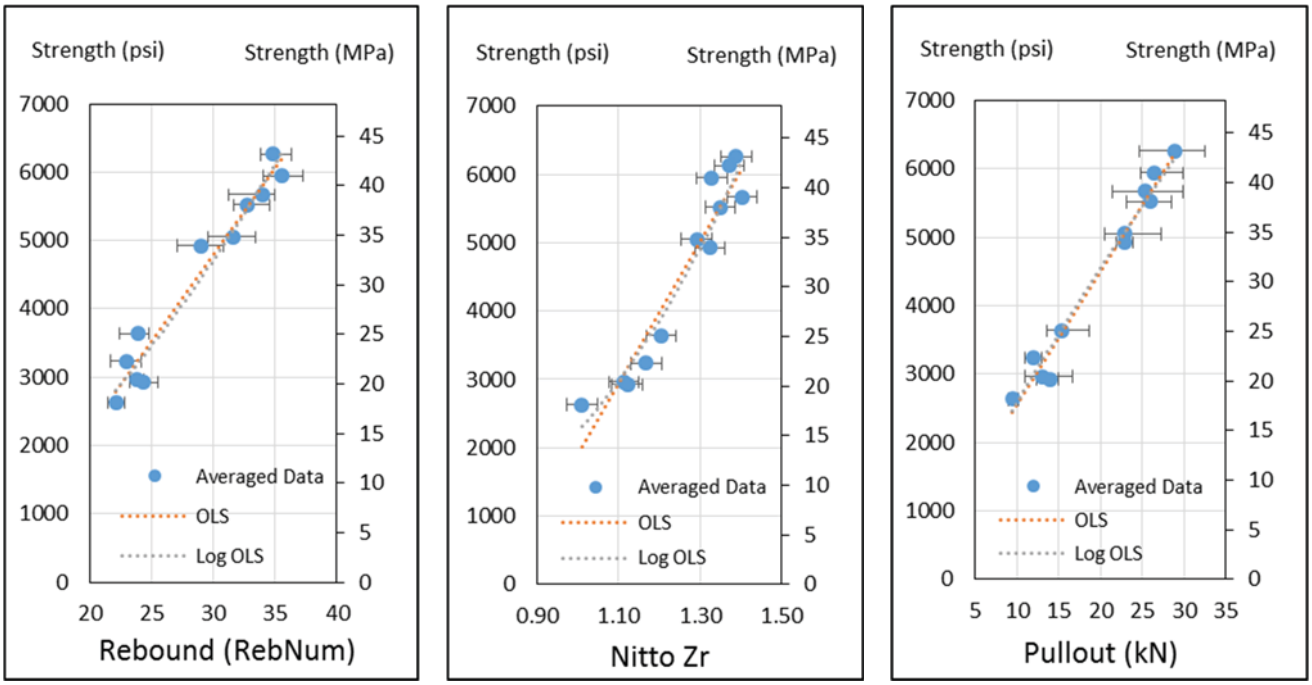

Figure 39: NDT vs. strength correlation curves for (a) rebound hammer, (b) Nitto hammer, and (c) pullout test, considering PV/SI and PV/SI-low mixtures only. Blue dots indicate average NDT and strength results of each slab. Horizontal error bars indicate data range (testing location results) for every slab. Red dotted lines are the best-fit OLS correlation curves. Gray dotted lines are best-fit logOLS correlation curves.

It can be seen in Figure 39 that in the cases of the rebound hammer and pullout, the OLS and logOLS best-fit lines almost overlap. In the case of the Nitto hammer, there are larger differences between the best-fit lines.

Table 9 contains the useful parameters for the computed OLS and logOLS NDT vs. strength relationships.

Table 9: Computed Parameters for OLS and LogOLS NDT vs. Compressive Strength Relationships

	Parameter	Rebound, rebound number	Pullout, kN	Nitto, Zr
OLS	Slope, psi/NDT (MPa/NDT)	253 (1.7)	194 (1.3)	10380 (71.6)
	Y-intercept, psi (MPa)	–2801 (–19.3)	628 (4.3)	–8464 (–58.4)
LogOLS	Factor A	14.78*	393.8*	2236.4*
	Exponent B	1.69*	0.817*	3.00*

* Values calculated and valid only for strengths in units of psi.

Figure 40, Figure 41, and Figure 42 contain the correlation curves computed from the experimental data overlapped with the correlation curves recommended by the corresponding manufacturers. For the case of the rebound hammer (Figure 40) the correlation curve was read from the device. In the case of Nitto hammer, the manufacturer's recommended correlation curve was

$$f = 145 \times 11.53 \times (Z_r)^4 \qquad \text{(Equation 7)}$$

where the factor 145 corresponds to a unit conversion factor, and f is the strength estimated from the tested Z_r.

In the case of pullout test, the manufacturer's recommended correlation curve was

$$f = 145 \times 0.60 \times (pullout)^{1.12} \qquad \text{(Equation 8)}$$

It should be noted that the manufacturer's recommended formulas did not necessary apply to the conditions of this investigation. For instance, the rebound hammer recommended correlation curve relates rebound number to f'_c (compressive strength of standard cured cylinders at 28 days), which is definitely not the case of this investigation where strength was computed from cast-in-place cylinders at day 16. The same fact applies for pullout and Nitto.

The purpose of presenting Figures 40, 41, and 42 is to emphasize that manufacturer's recommended correlation curves for compressive strength estimation may not be accurate for conditions that differ from those present when they were computed.

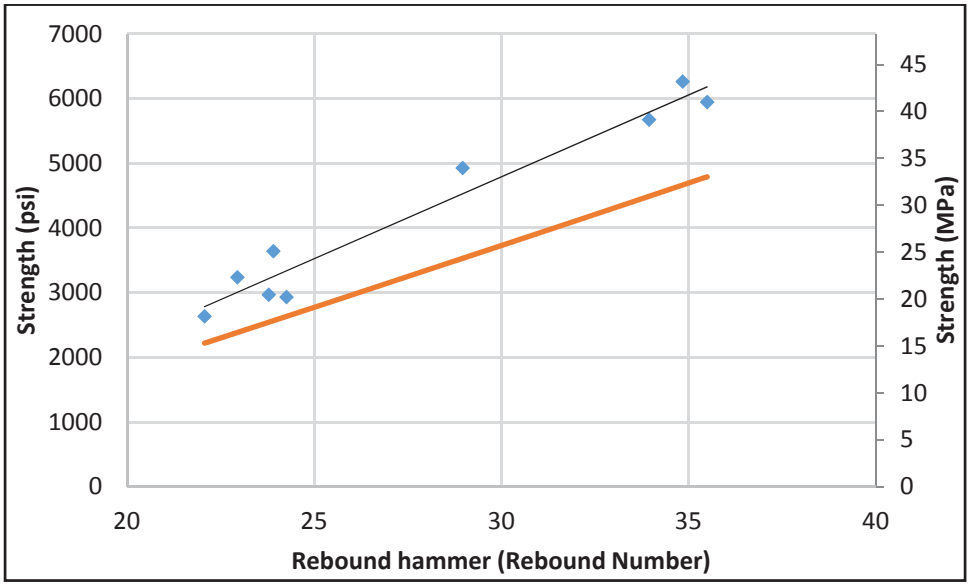

Figure 40: Rebound number vs. strength experimental data (blue marks) overlapped with OLS correlation curve (black line) and manufacturer's recommended correlation curve (orange line).

It can be seen in Figure 40 that the manufacturer's recommended correlation curve is clearly different from the one experimentally computed.

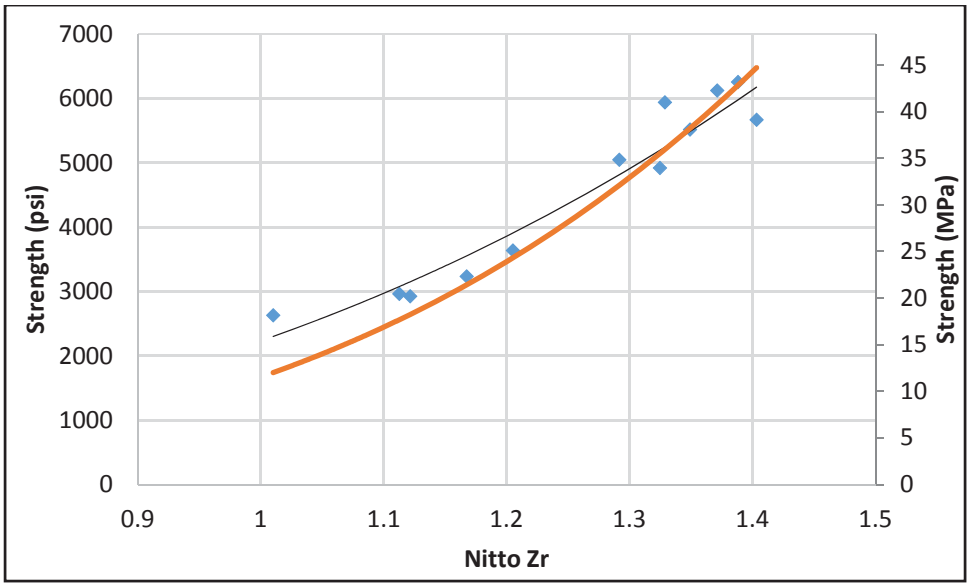

Figure 41: Nitto hammer Zr vs. strength experimental data (blue marks) overlapped with logOLS correlation curve (black line) and manufacturer's recommended correlation curve (orange line).

Figure 41 shows that the manufacturer's recommended correlation curve overlaps with the one experimentally calculated at higher strengths but it differs at low strengths.

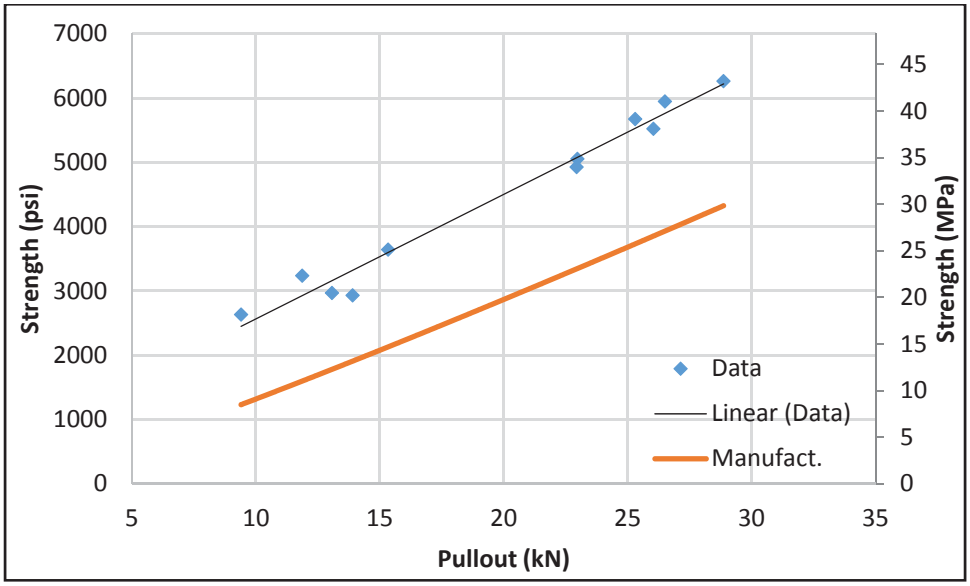

Figure 42: Pullout vs. strength experimental data (blue marks) overlapped with logOLS correlation curve (black line) and with manufacturer's recommended correlation curve (orange line).

Figure 42 shows that the pullout manufacturer's recommended correlation curve is significantly different from that one experimentally computed. However, the two best-fit lines are practically parallel, which indicates that a minor modification to the manufacturer's formula would yield a better

correlation. Such difference between correlation curves could be due to curing differences between the manufacturer's and this research project's tested cylinders; such differences could be curing time, curing temperature and even the nature of the concrete cylinders. This research uses in-place cylinders and not standard cured companion cylinders.

5.12.2 NDT Variability

The NDT variability can be qualitatively assessed by observing the horizontal error bars shown previously in Figure 29. Those bars indicate the data dispersion of each slab, where each bar extends from the minimum testing location value to the maximum testing location value of each slab (i.e., each error bar is a graphical representation of the range of testing locations for each slab).

Figure 42 contains the average normalized NDT location ranges among slabs for each NDT method. In other words, each bar shown in Figure 42 represents the average of all the error bar's widths shown in Figure 29 for each NDT method and normalized with regard to the value of slab R5.

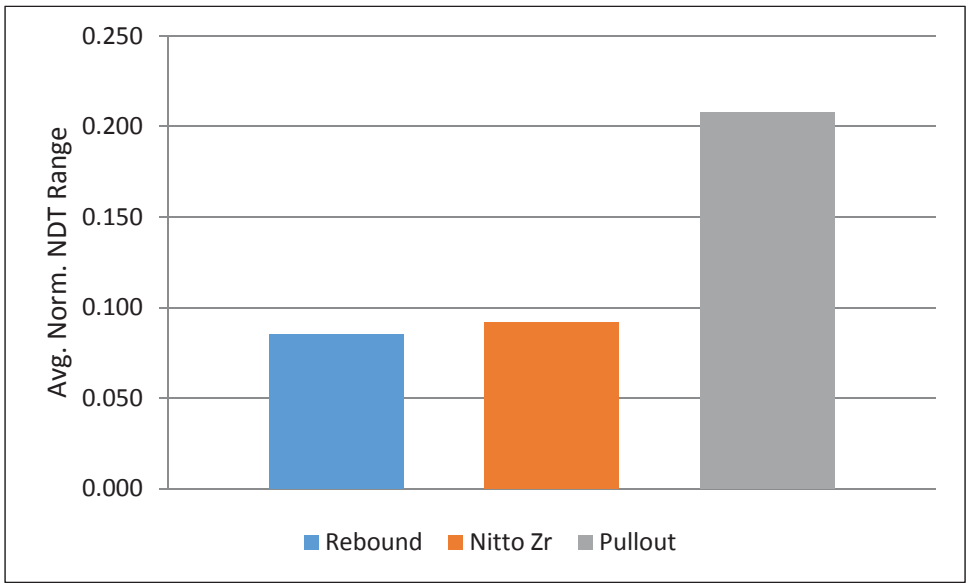

Figure 43: Average NDT location ranges (error bar width) of each NDT method normalized with regard to the average NDT location value of slab R5 (mixtures PV/SI and PV/SI-low).

Figure 43 clearly shows that the pullout's variability (normalized range) is more than double that of the other two NDT methods. It should be noted that this variability is a measurement that describes the in-test variability of the NDT methods, coupled with the material variability of the slabs' concrete. The variability of NDT location values influences the quality of the correlation curve but not directly or significantly; it occurs because the NDT vs. compressive strength correlation curves were computed using the average of the testing location values, not the entire dataset. In other words, a group of NDT datasets (of testing location values) can each have a wide range, indicating high data variability of the NDT method, but if their averages follow a specific trend consistently, then the correlation curve would be of high quality (low uncertainty).

5.12.3 Correlation Curve Uncertainty

The uncertainty of the computed correlation curves can be assessed using the RSD parameter, as defined in Section 4.5.3 and by ACI 228 1.R (2003). Figure 44 shows the RSD computed for each NDT method using both the OLS and the logOLS methods.

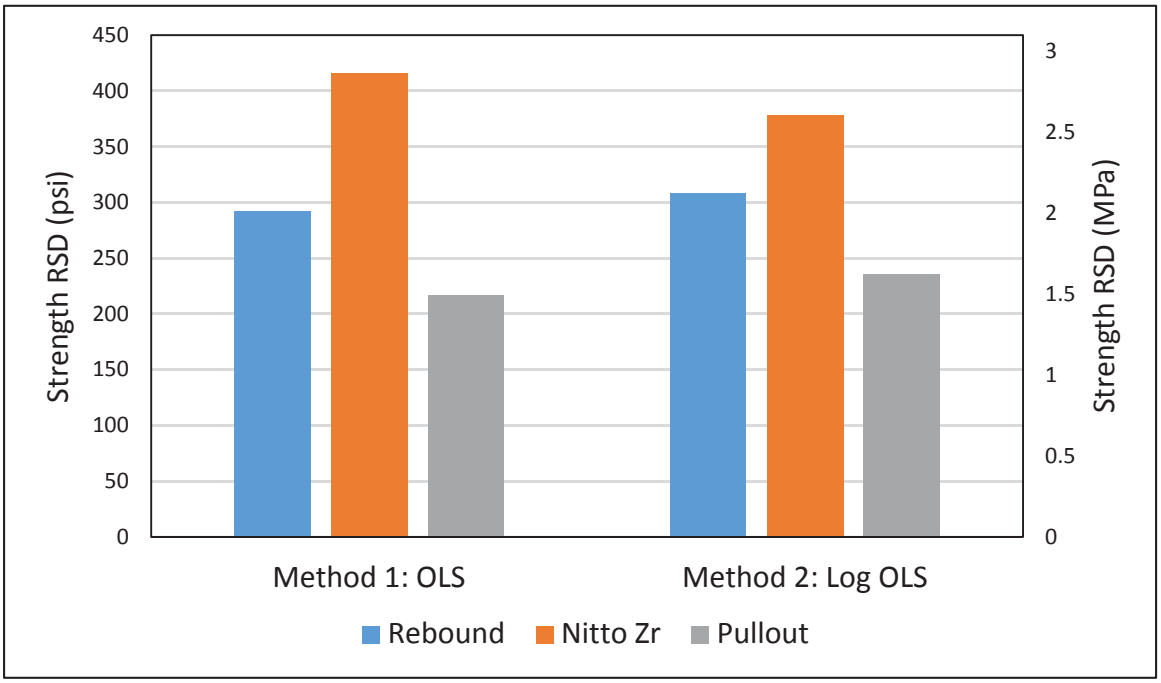

Figure 44: Residual standard deviation of OLS and logOLS correlation curves relating NDT to in-place cylinder compressive strength data (mixtures PV/SI and PV/SI-low).

Figure 44 clearly shows that for both correlation curves, the pullout test has the lowest RSD and the Nitto has the highest. In the case of the OLS computation, the rebound and Nitto hammer tests yielded RSDs 35% and 92% higher, respectively, than the RSD of the pullout. In comparing the RSD results obtained with the logOLS method and the OLS method, it was observed that the RSD of Nitto was reduced, whereas for the rebound and pullout tests, the RSD increased. This fact suggests that using OLS is better for approximating the relationship of the rebound hammer and pullout tests vs. compressive strength, but it is more accurate to use logOLS in the case of Nitto.

5.12.4 NDT Sensitivity

Figure 45 shows the normalized OLS and logOLS NDT vs. strength relationships for the rebound hammer, pullout, and Nitto hammer tests. The pullout test has the lowest slope (or range of slopes for the case of logOLS), followed by the rebound hammer and then the Nitto hammer. This means that the pullout test is the most sensitive, and the Nitto is the least sensitive of the NDT methods.

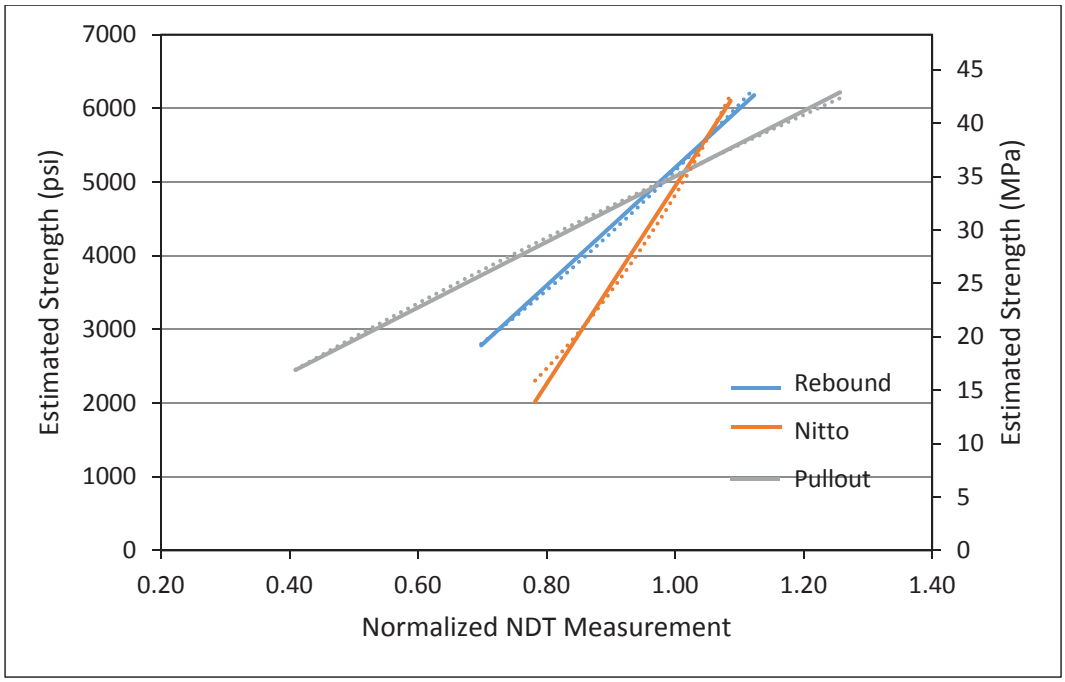

Figure 45: Analysis of sensitivity showing estimated strength vs. NDT measurements normalized with regard to slab R5. Solid lines and dotted lines correspond to the OLS and logOLS methods, respectively (mixtures PV/SI and PV/SI-low).

The use of OLS or logOLS did not significantly affect the overall sensitivity of each method of strength determination. Thus, to ease the analysis, sensitivity can be quantified only by observing the slopes of the OLS correlation curves of each NDT method. For the OLS best-fit lines, a lower slope indicates higher sensitivity than a higher slope.

Table 10 summarizes the normalized slopes of the OLS correlation curves. The pullout test had a normalized slope of 4447 psi (31 MPa) per normalized NDT unit; the normalized slopes of the rebound hammer and Nitto hammer OLS correlation curves were 80% and 200% higher, respectively, than that of pullout test. This analysis clearly shows that pullout test is the most sensitive of the three studied NDT methods.

Table 10: Normalized OLS Slopes and Slopes' Relative Differences

	Rebound	Nitto	Pullout
Slope, psi/normalized unit (MPa/normalized unit)	7998 (55)	13,407 (92)	4447 (31)
Relative difference (%)	80	201	0

5.12.5 Random Sampling Analysis

The studies presented in the previous sections described the NDT vs. strength relationships and considered their uncertainty. Another study, also discussed previously, assessed the variability of

each NDT method separately. Those two studies were not combined because they were computed separately. Thus, in general terms, the analysis of the uncertainty of NDT vs. strength relationships could be used to yield an estimated strength from NDT data, but it does not consider the NDT variability. The random sampling analysis combines both approaches by analyzing the trend of the error between real and estimated strengths when additional testing locations are carried out.

Figure 46 contains the results of the random sampling analysis applied when using both types of correlation curves (OLS and logOLS). The *Abs.Err*$_{95}$ metric is the value of error between the estimated strength that leaves 95% of the population below it (see Section 4.4 for details on this metric).

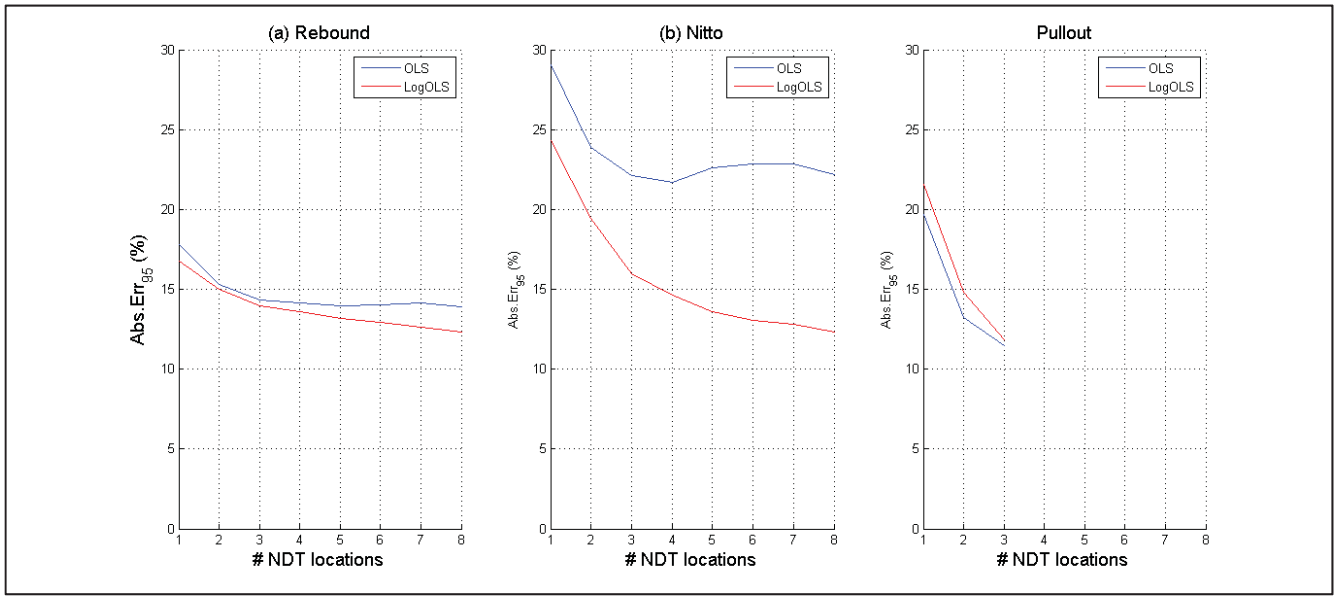

Figure 46: Random sampling analysis of (a) rebound hammer, (b) Nitto hammer, and (c) pullout, showing the behavior of *Abs.Err*$_{95}$ vs. the considered *# NDT locations* (mixtures PV/SI and PV/SI-low).

In the cases of the rebound hammer and pullout tests, the random sampling curves associated with the OLS and logOLS methods are very similar. However, for the Nitto hammer, the logOLS yielded *Abs.Err*$_{95}$ values much lower than those of the OLS. This fact is in agreement with the uncertainty analysis shown in Figure 44, where the RSD of the Nitto hammer Zr vs. compressive strength logOLS correlation curve was lower than the RSD of the Nitto hammer Zr vs. compressive strength OLS correlation curve. Thus, this analysis confirms that logOLS is a better approximation method for the Nitto hammer, whereas both OLS and logOLS could be used for the rebound and pullout tests without much difference. Therefore, to simplify the discussion, the OLS results will be further analyzed for rebound hammer and pullout tests, and the logOLS results for the Nitto.

In the case of one testing location, the *Abs.Err*$_{95}$ values were 18% for rebound OLS, 24% for Nitto logOLS, and 20% for pullout OLS.

For the rebound hammer, when additional testing locations were considered, the $Abs.Err_{95}$ first decreased and then became constant at *# NDT locations* equal to three, reaching an $Abs.Err_{95}$ of 14%. Thus, with the data collected in this investigation, taking more than three rebound hammer testing locations did not reduce the expected strength error significantly.

For the Nitto hammer, the $Abs.Err_{95}$ decreased with increasing *# NDT locations* and did not become constant within the eight possible *# NDT locations.* Only at *# NDT locations* equal to five did the $Abs.Err_{95}$ become lower than 14%, meaning that five testing locations with the Nitto hammer would be equivalent to three rebound testing locations to obtain similar expected strength errors.

Finally, in the pullout test, the $Abs.Err_{95}$ dropped abruptly from 20% to 13% at *# NDT locations*, and then reached 11% error at *# NDT locations* equal to three. It also did not appear to have become constant, which indicated that additional testing measurements could reduce the expected error significantly.

To summarize: From this analysis, it can be observed that when carrying out an NDT method at one single testing location, the method that yielded the lowest expected error was the rebound hammer. Carrying out pullout test at two testing locations reached an expected error $Abs.Err_{95}$ similar to carrying out rebound hammer at three or more testing locations, or Nitto hammer at five or more testing locations. The total lowest expected error was yielded by pullout; at 3 NDT locations the pullout expected error became 11%, which was around 4% lower than the other NDT methods.

5.12.6 Section Conclusions

On the basis of the results presented and discussed in this section, the following can be concluded:

- The OLS method yielded more-accurate correlation curves than logOLS for the rebound hammer and pullout tests; for the Nitto hammer method, the logOLS method yielded more-accurate results than the OLS.
- Based on RSD to assess correlation curve uncertainties, the pullout test (OLS) was the least uncertain, and the Nitto hammer was the most uncertain (both OLS and logOLS curves).
- The pullout test had significantly higher NDT variability (within-test coupled with within-structure variability) than the other two methods, which, in turn, had similar NDT variability between them.
- The pullout test was the most sensitive technique, having an OLS NDT vs. strength slope (normalized) around half of that of the rebound hammer, and a third of that of the Nitto hammer.
- When considering only one NDT location, the rebound hammer (OLS) was the method that yielded the lowest expected error (using percentile 95th), with 18%. This error dropped to 14% at three NDT locations and did not change significantly for additional testing locations (i.e., it became constant at three NDT locations). The pullout test (OLS) started with a higher expected error than the rebound hammer when considering one NDT location, but it achieved a 13% expected error with two NDT locations, similar to the rebound hammer at three or more testing locations. Carrying out the pullout test at three locations reduced the expected

error to 11%. The Nitto hammer (logOLS) yielded higher expected errors than the rebound hammer and pullout tests at lower *# NDT locations*, but after five *# NDT locations*, the expected error became very similar to the other two NDT, reaching expected errors between 11% and 12%.

5.13 ANALYSIS OF NDT VS. IN-PLACE CYLINDER COMPRESSIVE STRENGTH OF PV/SI, PS, AND PV/SI-LOW MIXTURES

5.13.1 NDT vs. Compressive Strength Relationships

Figure 47, Figure 48, and Figure 49 present the NDT vs. strength relationships (correlation curves) for the rebound hammer, Nitto hammer and pullout tests, respectively. Each blue dot corresponds to the average NDT values (average of testing location values) plotted against the average in-place compressive strength values, for every slab. The horizontal error bars mark the minimum and maximum NDT location values for each slab. The ordinary least squares and logOLS best-fit lines have been computed and are also shown in the figures.

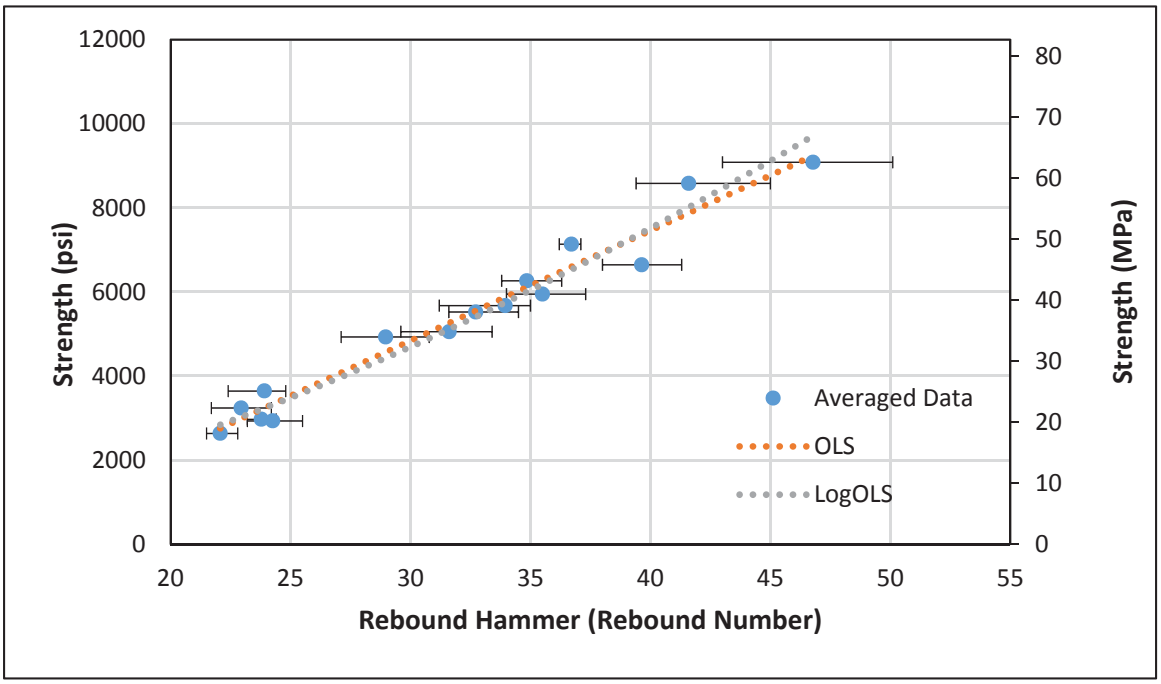

Figure 47: Rebound hammer NDT vs. strength correlation curves for PV/SI, PS, and PV/SI-low mixtures. Blue dots indicate average NDT and strength results of each slab. Horizontal error bars indicate data range (testing location results) for every slab. Red dotted lines are the best-fit OLS correlation curves. Gray dotted lines are best-fit logOLS correlation curves.

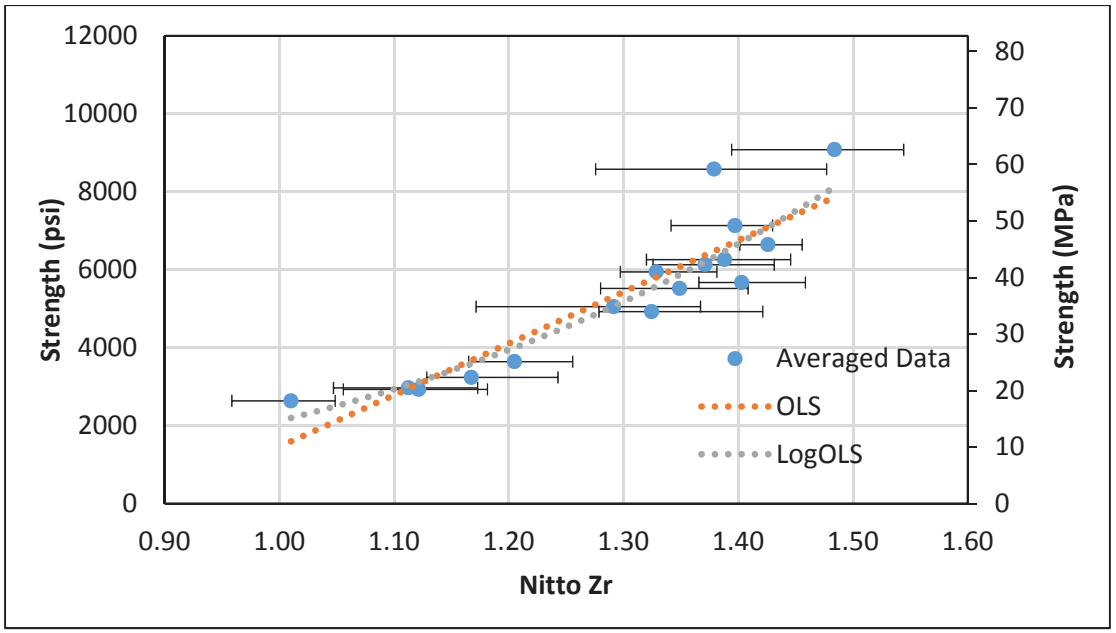

Figure 48: Nitto hammer NDT vs. strength correlation curves for PV/SI, PS, and PV/SI-low mixtures. Blue dots indicate average NDT and strength results of each slab. Horizontal error bars indicate data range (testing location results) for every slab. Red dotted lines are the best-fit OLS correlation curves. Gray dotted lines are best-fit logOLS correlation curves.

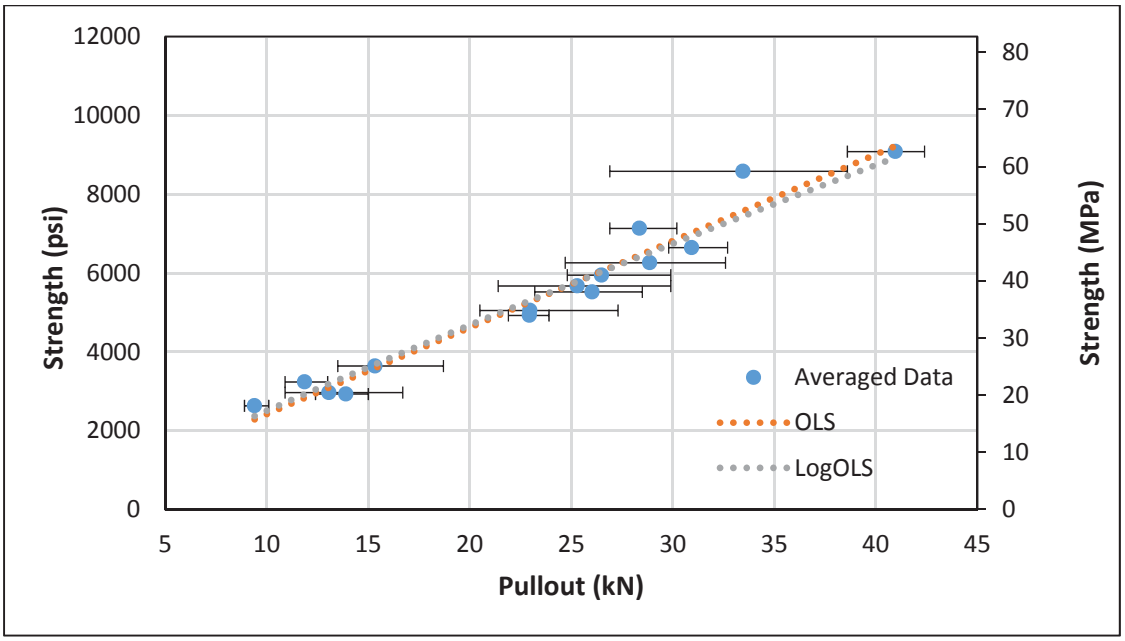

Figure 49: Pullout test NDT vs. strength correlation curves for PV/SI, PS, and PV/SI-low mixtures. Blue dots indicate average NDT and strength results of each slab. Horizontal error bars indicate data range (testing location results) for every slab. Red dotted lines are the best-fit OLS correlation curves. Gray dotted lines are best-fit logOLS correlation curves.

It can be seen in Figures 46 and 48 that for the rebound hammer and pullout tests, the OLS and logOLS best-fit lines almost overlap, except for edges of the curves. For the Nitto hammer, shown in Figure 48, there are larger differences between the best-fit lines. The same observations were presented in Section 5.13.1 for the analysis of PV/SI and PV/SI-low.

Table 11 contains the parameters of the computed OLS and logOLS NDT vs. strength relationships.

Table 11: Computed Parameters of OLS and LogOLS NDT vs. Compressive Strength Relationships for PV/SI, PS, and PV/SI-Low Mixtures

	Parameter	Rebound, rebound number	Pullout, kN	Nitto, Zr
OLS	Slope, psi/NDT (MPa/NDT)	263 (1.81)	13229 (91.21)	220 (1.51)
	Y-intercept, psi (MPa)	–3041 (–20.97)	–11769 (–81.14)	225 (1.55)
LogOLS	Factor A	17.83*	2121.82*	315.16*
	Exponent B	1.64*	3.40*	0.90*

* Values calculated and valid only for strengths in units of psi.

5.13.2 NDT Variability

The NDT variability can be qualitatively assessed by observing the horizontal error bars in Figure 47 through Figure 49. Those bars indicate the data dispersion of each slab, where each bar extends from the minimum testing location value to the maximum testing location value of each slab (i.e., each error bar is a graphical representation of the range of testing locations for each slab).

Figure 50 contains the normalized average NDT location ranges among slabs for each NDT method. In other words, each bar shown in Figure 50 represents the average of all the error bar widths shown in Figures 47, 48, and 49 for each NDT method, and normalized with regard to the value of R5.

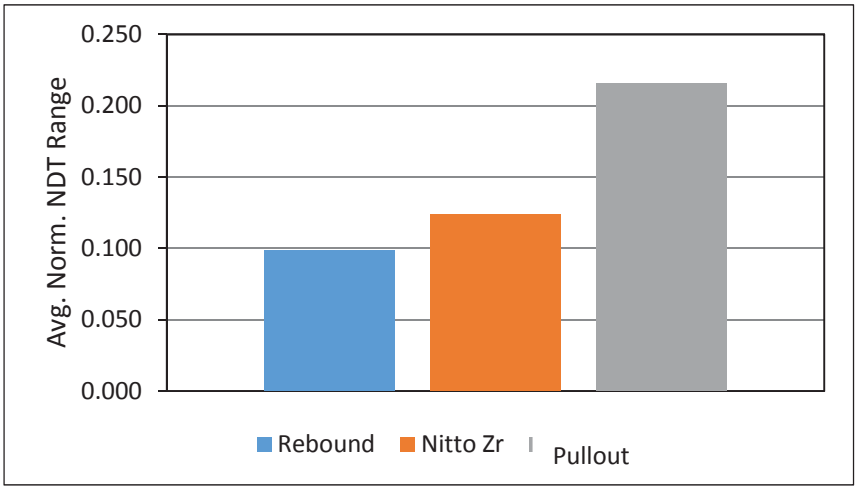

Figure 50: Average NDT location ranges (error bar width) of each NDT method normalized with regard to the average NDT location value of slab R5 (mixtures PV/SI, PS, and PV/SI-low).

Figure 50 clearly shows that the pullout's variability (normalized range) is more than double that of the other two NDT methods. The same observation was made in Section 5.12.2 (shown in Figure 43), for the analysis that excluded the PS mixtures.

By comparing Figure 50 with Figure 43, it can be seen that only the Nitto hammer increased its average variability when the PS mixtures were included in the analysis, but the other two NDT methods did not significantly change their average variability.

5.13.3 Correlation Curve Uncertainty

The uncertainty of the computed correlation curves can be assessed using the RSD parameter, as defined in Section 4.5.3 and by ACI 228 1.R (2003). Figure 51 shows the RSD computed for each NDT method using both the OLS and the logOLS methods.

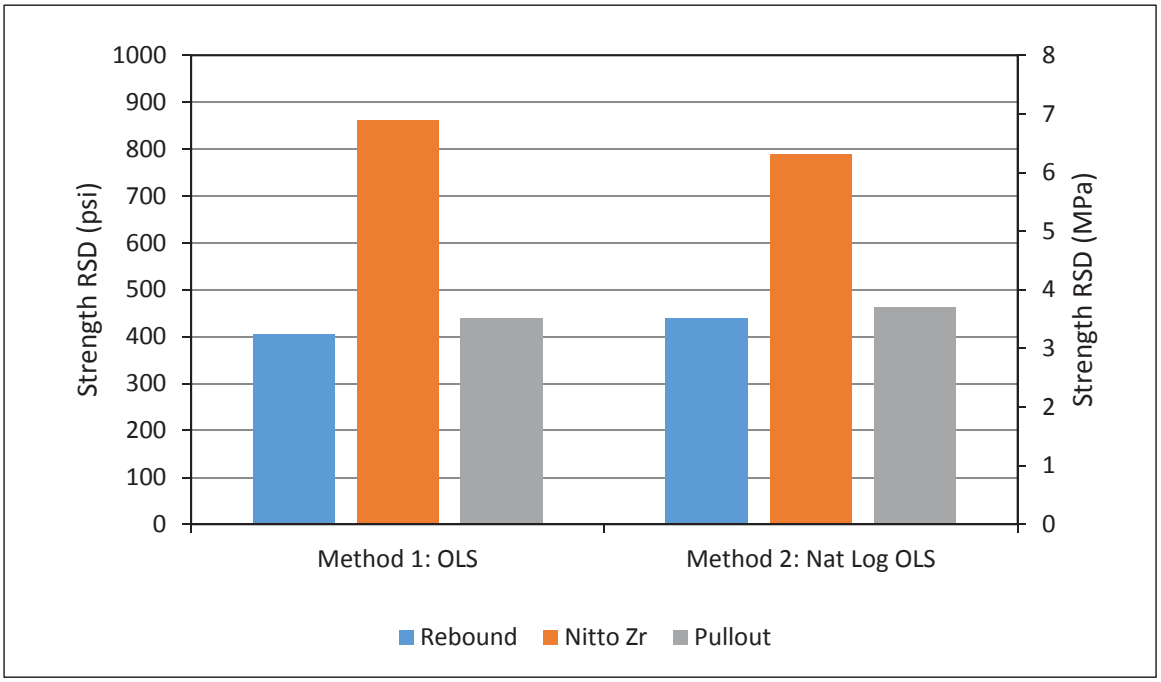

Figure 51: Residual standard deviation of OLS and logOLS correlation curves relating NDT vs.in-place cylinder compressive strength data (mixtures PV/SI, PS, and PV/SI-low).

Figure 51 shows that for both correlation curves, the pullout and rebound hammer had the lowest RSD (similar to each other) and the Nitto had the highest. In the RSD results obtained with the logOLS method compared with those obtained using the OLS method, the RSD of the Nitto was reduced, whereas it increased for the rebound hammer and pullout tests. This trend was also noted in Section 5.13.3, where the PS mixture slabs were excluded from the analysis. This fact confirms that using OLS is better for approximating the relationship of the rebound hammer and pullout test vs. compressive strength, but it is more accurate to use logOLS with the Nitto hammer.

5.13.4 NDT Sensitivity

Figure 52 shows the normalized OLS and logOLS NDT vs. strength relationships for the rebound hammer, Nitto hammer, and pullout tests. It can clearly be seen that the pullout test had the lowest slope (or range of slopes in the case of logOLS), followed by the rebound hammer and then the Nitto hammer. This means that, when considering PS mixture slabs, the pullout test is again the most sensitive and the Nitto is the least sensitive of the NDT methods.

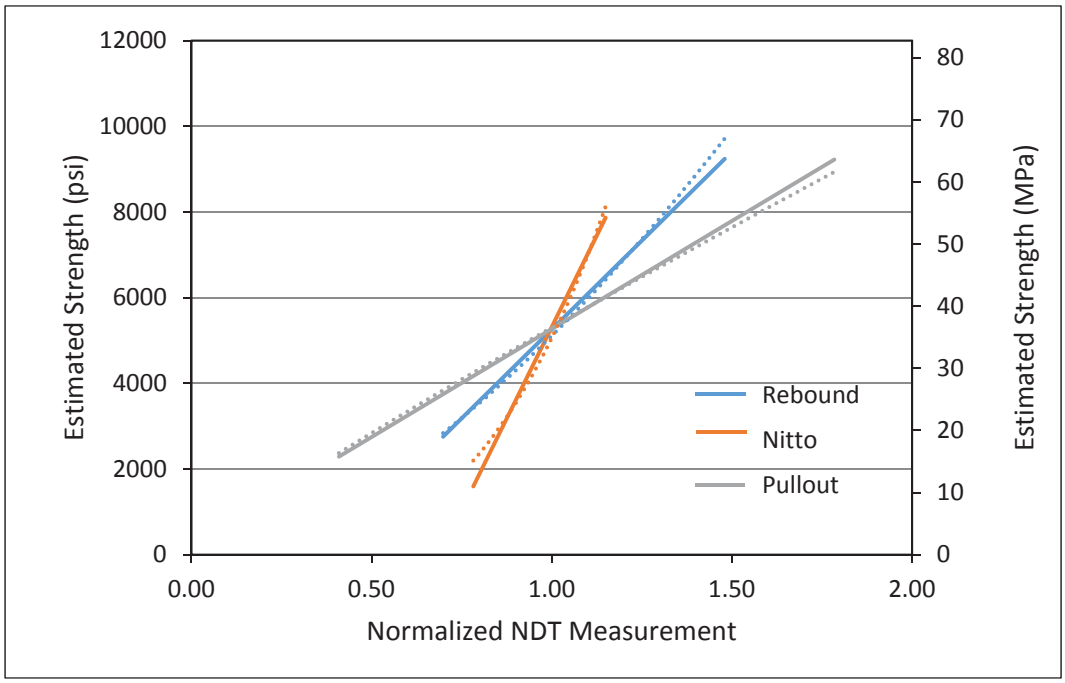

Figure 52: Analysis of sensitivity showing estimated strength vs. NDT location data normalized with regard to slab R5. Solid lines and dotted lines correspond to OLS and logOLS methods, respectively (mixtures PV/SI, PS, and PV/SI-low).

As it was discussed in Section 5.13.4, the use of OLS or logOLS does not significantly affect the overall sensitivity of each method of strength determination. Thus, to simplify the analysis, sensitivity can be quantified by observing only the slopes of the OLS correlation curves of each NDT method. With the OLS best-fit lines, a lower slope indicates higher sensitivity than a higher slope.

Table 12 summarizes the normalized slopes of the OLS correlation curves. The pullout test had a normalized slope of 4447 psi (31 MPa) per normalized NDT unit; the normalized slopes of the rebound hammer and Nitto hammer OLS correlation curves were 80% and 200% higher, respectively, than those of the pullout test. This analysis clearly shows that pullout test is the most sensitive of the three studied NDT methods.

Table 12: Normalized OLS Slopes and Slopes' Relative Differences for Mixtures PV/SI, PS, and PV/SI-Low Analyzed Together

	Rebound, rebound number	Nitto, Zr	Pullout, kN
Slope, psi/normalized unit (MPa/normalized unit)	8298 (57)	17087 (118)	5043 (35)
Relative difference (%)	65	239	0

5.13.5 Random Sampling Analysis

This analysis is analogous to the one explained in Section 5.13.5. Figure 53 contains the results of the random sampling analysis when using both types of correlation curves (OLS and logOLS). The *Abs.Err*$_{95}$ metric is the value of error between the estimated strength that leaves 95% of the population below it (see Section 4.4 for details on this metric).

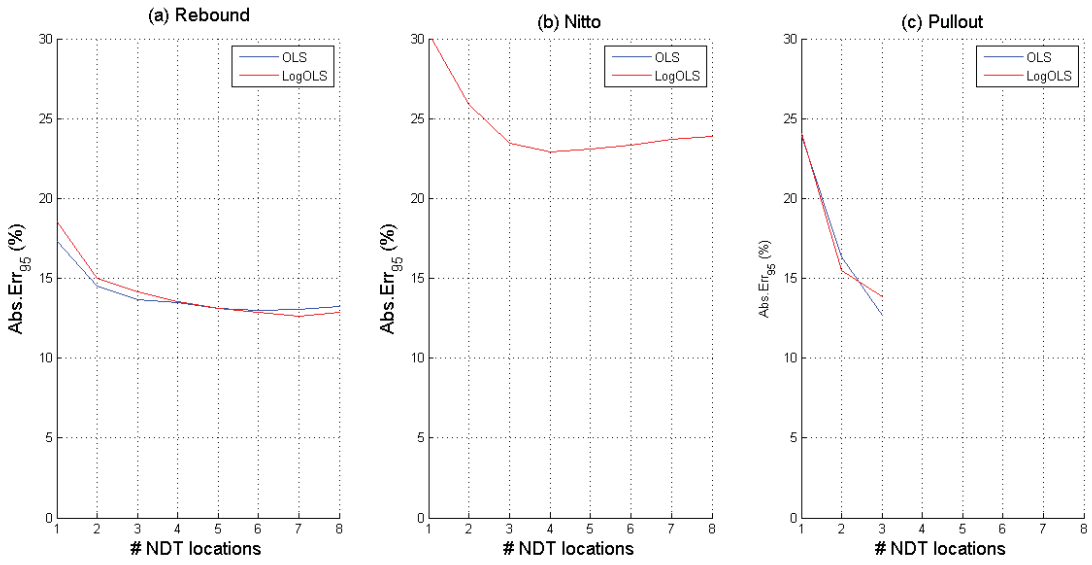

Figure 53: Random sampling analysis of (a) rebound hammer, (b) Nitto hammer, and (c) pullout, showing the behavior of the *Abs.Err*$_{95}$ metric vs. *# NDT locations* (mixtures PV/SI, PS, and PV/SI-low).

Figure 53 shows the same trends as the ones observed in Figure 46 for the PV/SI and PV/SI-low analysis that excluded the PS mixture. However, when the PS mixture slabs were included in the analysis, the *Abs.Err*$_{95}$ parameter tended to shift around 5% to higher values; this fact is graphically depicted by observing that in Figure 53, the *Abs.Err*$_{95}$ curves tend to be displaced around 5%, to higher values than the corresponding *Abs.Err*$_{95}$ curves in Figure 46. This means that using the PS

mixture with the other mixtures increased the expected strength errors given by the correlation curves.

It can be seen in Figure 53 that at three testing locations, both the rebound hammer and pullout tests had the same $Abs.Err_{95}$. However, the Nitto hammer yielded poor $Abs.Err_{95}$ results, even for seven and eight testing locations. The OLS $Abs.Err_{95}$ curve is not shown because it had values higher than 30%, indicating very high inaccuracy in estimating strength.

5.13.6 Section Conclusions

The same conclusions can be drawn as those in Section 5.13.6, with the following differences/additions:

- Including the PS mixture slabs tended to increase the $Abs.Err_{95}$ by approximately 5% more than when it was not included. This was not an unexpected result given that the PS mixture was a nominally different mixture design with different aggregate sizes and proportions. In addition, it was seen that PS mixture slabs had more variable fresh and hardened concrete properties than the other two mixtures.
- The use of the Nitto hammer for strength estimations when the PS mixture is included was inaccurate, yielding expected error results higher than 23%.
- The rebound hammer had a slightly better performance than the pullout test, reaching expected strength errors of less than 15% for two or more testing locations, whereas the pullout test reached the 15% expected error at two testing locations and 12% at three testing locations.

CHAPTER 6: CONCLUSIONS

The objectives of this research were to evaluate core strength correction factors considering a range of pertinent factors that are encountered in the field, and to investigate more practical core field curing practices that provide acceptable estimates of in-place concrete strength. The in-place strength was established by testing in-place cylinders at day 16 after casting. It should be noted that this approach is different to the factors given elsewhere, for example in ACI 214.4R (2010), which are provided to estimate f'_c obtained using conditioned cores after extraction.

The following conclusions can be drawn from the results and discussion presented in the report.

- Regarding the number of core samples to use to estimate in-place strength, the results confirm that increasing number of core samples extracted from a given mixture improves the in-place strength estimate of that mixture where the average of core sample strengths are used in the estimation.
- Assuming that 1-day-dry core treatment is used along with the 1.05 correction factor for core samples from PV-SI and PV-SI-low mixtures that do not contain embedded rebar (based on analysis A with data from slab samples R1, R2, R13 and R14), the average of two cores is needed to provide at least a 95% likelihood of having an absolute error of 5% or lower with respect to the actual in-place strength.
- Assuming that 1-day-dry core treatment is used along with the 1.05 correction factor for core samples from PV-SI and PV-SI-low mixtures that both do and do not contain embedded rebar (based on analysis B with data from slab samples R1, R2, R5, R6, R8, R13 and R14), the average of three cores is needed to provide at least an 85% likelihood of having an absolute error of 5% or lower with respect to the actual in-place strength.
- Now considering all three mixture types together for the case of slabs with and without embedded rebar (based on analysis J with data from slab samples R1, R2, R5, R6, R8, R9, R10, R13, and R14), assuming that 1-day-dry core treatment is used along with the 1.05 correction factor for core samples from PV-SI and PV-SI-low mixtures, a 1.08 correction factor for core samples from PV-SI mixture with embedded rebar and 1.03 correction factor for core samples from PS mixtures without rebar, the average of three cores is needed to provide at least a 90% likelihood of having an absolute error of 5% or lower with respect to the actual in-place strength.
- The position of the rebar within the cross-section did not have a significant effect on the results.
- NDT conclusions:
    - All NDT methods showed positive correlation with in-place strength. Linear correlation curves (OLS) were found to be more appropriate than the power correlation curve (LogOLS) for the rebound hammer and pullout test data, and the opposite was found for Nitto hammer data.

- For each NDT method, correlations curves established using only PV/SI and PV/SI-low mixtures were more certain than when including the PS mixture in the analysis.
- Each NDT method exhibited benefits and drawbacks. The Nitto hammer and rebound hammer were easier and faster to carry out as compared with the pullout test in in terms of collecting data from a single testing location. On the other hand, pullout was the most sensitive to in-place strength and Nitto the least.
- The confidence in the strength estimation from NDT increased with data from increasing number of testing locations. Random sampling analysis showed that, for the same number of testing locations, pullout and rebound tests had similar expected error in the estimated strengths ($Abs.Err._{95}$), whereas Nitto hammer had higher expected errors. For one single testing location, rebound yielded the lowest expected error and Nitto the highest; for two or more testing locations pullout yielded the lowest expected error and Nitto hammer the highest.
- For rebound hammer, in the analysis excluding the PS mixture, carrying out more than four testing locations did not reduce the expected error any further; i.e., carrying out a fifth test location with rebound hammer did not reduce the expected error of the estimated strength. At four or more testing locations, the rebound hammer expected error was equivalent to the expected error of pullout at two testing locations. Carrying out pullout at three testing locations yielded the least expected error.

CHAPTER 7: RECOMMENDATIONS

On the basis of the experimental results and analysis of this investigation, which consider cores and in-place cylinders tested 16 days after casting, the following recommendations are offered:

- It is beneficial to employ the fan dry core treatment described here as an option to the AASHTO T 24 standard in order to obtain core test samples more rapidly. Furthermore, it is beneficial to the State Agency to apply correction factors described in this report to obtain reliable in-place compressive strength estimates obtained from those core samples.
- It is possible and beneficial to use the rebound hammer, and/or pullout NDT methods to reduce the number of cores to be drawn from a concrete structure. Correlation curves can be constructed according to ACI 228.1R (2003) to correlate NDT measurements to in-place strength yielding estimates with expected errors of less than 15% at a 95% confidence level. Using a well-established correlation curve, either the rebound hammer or pullout can be carried out in one testing location to obtain fairly accurate strength estimation. Three testing locations per batch are enough to achieve good accuracy.
- Further research is needed to establish the behavior of concrete with higher strength, greater age after casting, and larger aggregate sizes and core samples exposed to different treatments.

REFERENCES

ACI 214.4R, "Guide for obtaining cores and interpreting compressive strength results." American Concrete Institute, Farmington Hills, MI, 2010.

ACI 228.1R, "In-place methods to estimate concrete strength." American Concrete Institute, Farmington Hills, MI, 2003.

ACI 318, "Building code requirements for structural concrete." American Concrete Institute, Farmington Hills, MI, 2010.

Arıöz, M., Tuncan, M., Ramyar, K. and Tuncan, A., "A comparative study on the interpretation of concrete core strength results." *Magazine of Concrete Research*, Vol. 58, No. 2, pp. 117-122, 2006

ASTM C 39/C 39M-12a. "Standard test method for compressive strength of cylindrical concrete specimens." ASTM International, West Conshohocken, PA, 2012.

ASTM C 143/C 143M-15a. "Standard test method for slump of hydraulic-cement concrete." ASTM International, West Conshohocken, PA, 2015.

ASTM C 192/C 192M-13a. "Standard practice for making and curing concrete test specimens in the laboratory." ASTM International, West Conshohocken, PA, 2013.

ASTM C 215-02. "Standard test method for fundamental transverse, longitudinal, and torsional resonant frequencies of concrete specimens." ASTM International, West Conshohocken, PA, 2002.

ASTM C 231/C 231M-16. "Standard test method for air content of freshly mixed concrete by the pressure method." ASTM International, West Conshohocken, PA, 2016.

ASTM C 805. "Standard test method for rebound number of hardened concrete." ASTM International, West Conshohocken, PA, 2002.

ASTM C 873. "Standard test method for compressive strength of concrete cylinders cast in place in cylindrical molds." ASTM International, West Conshohocken, PA, 2002.

ASTM C 900. "Standard test method for pullout strength of hardened concrete." ASTM International, West Conshohocken, PA, 2013.

Gaynor, R.D. "Effect of horizontal reinforcing steel on the strength of molded cylinders." *Journal of the American Concrete Institute*, Vol. 62, No. 7, pp. 837-840, 1965.

Mindess, S., Young, J.F., and Darwin, D. *Concrete*. Pearson Education, Inc., 2nd edition, 2003.

Nikbin, I.M., Eslami, M. and Rezvani, S.M.D. "An experimental comparative survey on the interpretation of concrete core strength results." *European Journal of Scientific Research*, Vol. 37, No. 3, pp. 445-456, 2009.

APPENDIX A: TABLES OF RESULTS

Table A.1: Full Fresh Concrete Experimental Results, Part 1

Slab Name	Casting Day	Slump (in)	Uncorrected Air (%)	Corrected Air (%)	Measured Weight (lb)	Unit weight (lb/ft^3)
R1	Jul-29-2014	4.5	8.4	8	41	134
R2	Aug-05-2014	4.25	5.3	4.9	43.5	144
R3	Aug-12-2014	4.25	6.2	5.8	43	142
R4	Aug-19-2014	4	6.2	5.8	44	146
R5	Sep-02-2014	4.75	7	6.6	43	142
R6	Sep-16-2014	4.5	6.2	5.8	43.5	144
R7	Sep-23-2014	3.25	8	7.6	43	142
R8	Sep-30-2014	3.5	6	5.6	43.5	144
R9	Oct-07-2014	4.75	7	6.6	42.5	140
R10	Oct-21-2014	4	5.5	5.1	44	146
R11	Oct-28-2014	3.75	6.5	6.1	-	-
R12	Nov-5-2014	7	8.3	7.9	-	-
R13	Nov-4-2014	8–9	9.5	9.1	42	138
R14	Nov-10-2014	8.75	10	9.6	41	134
R15	Nov-19-2014	8	8.5	8.1	-	-
R16	Nov-24-2014	8	9.5	9.1	41.5	136
R15B	Jan-21-2015	7.75	8.4	8	43	142

Table A.2: Full Fresh Concrete Experimental Results, Part 2

Slab Name	Observations
R1	First slump test gave 5.5 in. Second slump test performed after 10 minutes gave 4.5 in.
R2	Air is 0.1 % out of spec (spec 5 to 8 %).
R3	First slump test gave 3.75 in. Super was added and gave 6.5 in. 5 minutes after slump was 5. Finally 10 minutes after the last test the slump was 4.25 in.
R4	
R5	
R6	
R7	
R8	
R9	
R10	Upon arrival, half gallon of super was added and tests yielded 0.25 in slump and 2.5 % uncorrected air. Then 1 additional gal. of super and 20 oz of AEA were added, and tests yielded the final results. The resulting concrete had very high slump loss. Thus, the vibration was harsh and finishing was tough too; the resulting surface had to be wetted to enable steel troweling and still was not smooth.
R11	
R12	Upon arrival, at 1:20pm tests gave: slump 7 in, UW + bucket = 41.5 lb and uncorrected air 11%. Concrete was submitted to 40 rev and the uncorrected air was reduced to 10.5 %. Then the concrete was let to sit for 10 minutes and the new (final) uncorrected air was obtained.
R13	Slump measurement was not registered but it was between 8 and 9 in
R14	Slab was kept with the burlap bags on for three days more than it was supposed to (a weekend).
R15	Curing done for 2.5 days instead of 3 days—**WRONG CORING. Cores were drawn one day before they were supposed to and in-place were also drawn one day before. Tests were done in the correct day. This slab was not used to in the discussion nor to draw final conclusions.**
R16	
R15B	Moist curing done for 4 days instead of 3 days.

TABLE A.3 (MULTI-PART)

In the tables on the following pages, cells colored with blue are direct measurements, and cells not colored are calculated results. Cells colored in yellow indicate the existence of comments, sometimes unimportant. “Range dif.” is the range of the corresponding dataset (cores or in-place cylinders’ strength datasets) divided by its mean, expressed in %, “L/D” is the aspect ratio and, in the column titled Type of Break, “exp” indicates that the specimen exploded during compressive strength testing

Table A.3: Companion, Core, and In-Place Cylinders' Compressive Strength Test Results, Part 1

			COMPRESSIVE STRENGTH TESTING (ASTM C 39 / AASHTO T 22)																		
			DATE	Age of Conc at testing	GROUP/SAMPLE ID NUMBER	Roughness		Perpendicularity		HEIGHT				DIAMETER				CROSS-SECTIONAL AREA	LOAD	STRENGTH
						mm	mm	mm	mm	inch				inch				in^2	lbs.	psi
			-	day	-	Top	Bot	Top	Bot	1	2	3	Ave	1	2	Ave	L/D	Ave	-	-
SLAB R1	Companion	1	Aug-12-14	14	Comp_1	2	1	1	1	8.0313	8	8	8.01	4.047	4.007	4.027	1.989	12.74	54975	4316
		2	Aug-12-14	14	Comp_2	1	1	1	0	8	8.0313	8.0313	8.02	4.04	4.003	4.022	1.994	12.70	53875	4242
		3	Aug-12-14	14	Comp_3	1	2	1	0	7.9688	8.0313	8.0313	8.01	4.029	4.029	4.029	1.988	12.75	53755	4216
		4	Aug-12-14	14	Comp_4	0	2	0	0	12.063	12.063	12.063	12.06	6.021	6.003	6.012	2.006	28.39	119060	4194
		5	Aug-12-14	14	Comp_5	2	2	0	0	12.031	12.063	12.023	12.04	5.948	5.993	5.971	2.016	28.00	119020	4251
	Cores	6	Aug-14-14	16	Core_1	2	0	1	2	8.125	8.0938	8.0938	8.10	3.976	3.976	3.976	2.038	12.42	55650	4482
		7	Aug-14-14	16	Core_2	0	1	0	0	8.0938	8.125	8.0938	8.10	3.98	3.98	3.980	2.036	12.44	59580	4789
		8	Aug-14-14	16	Core_3	1	0	1	1	8.0938	8.0938	8.125	8.10	3.975	3.977	3.976	2.038	12.42	58120	4681
		9	Aug-14-14	16	Core_4	0	0	0	0	8.0938	8	8	8.03	3.972	3.977	3.975	2.021	12.41	62685	5053
		10	Aug-14-14	16	Core_5	0	0	0	2	8.0313	8.125	8.0938	8.08	3.981	3.977	3.979	2.031	12.43	56705	4560
		11	Aug-14-14	16	Core_6	0	0	0	0	8.0938	8.125	8.0938	8.10	3.977	3.977	3.977	2.038	12.42	60375	4860
		12	Aug-14-14	16	Core_7	0	0	0	0	8.1563	8.0625	8.125	8.11	3.972	3.973	3.973	2.043	12.39	54020	4358
		13	Aug-14-14	16	Core_8	0	1	0	0	8	8.0625	8.0938	8.05	3.976	3.975	3.976	2.025	12.41	59050	4757
	In-Place Cylinders	14	Aug-14-14	16	InCyl_1	0	0	3	0	8.0625	8.0625	8.0938	8.07	4.072	3.987	4.030	2.003	12.75	66585	5221
		15	Aug-14-14	16	InCyl_2	0	0	2	1	8	8.0625	8.0313	8.03	4.023	4.025	4.024	1.996	12.72	61160	4809
		16	Aug-14-14	16	InCyl_3	0	0	1	1	8.0625	8.0625	8.0938	8.07	4.028	4.013	4.021	2.008	12.70	65715	5176
		17	Aug-14-14	16	InCyl_4	0	0	0	0	8	8.0625	8.0625	8.04	4.023	4.028	4.026	1.998	12.73	57560	4523
		18	Aug-14-14	16	InCyl_5	0	0	4	1	8	8	8	8.00	4.014	4.058	4.036	1.982	12.79	61965	4843
		19	Aug-14-14	16	InCyl_6	0	0	1	1	8	8	8.0313	8.01	4.002	4.049	4.026	1.990	12.73	61205	4809
		20	Aug-14-14	16	InCyl_7	0	0	2	0	8	8.0313	8.0313	8.02	4.027	4.01	4.019	1.996	12.68	64470	5083
		21	Aug-14-14	16	InCyl_8	0	0	0	0	8	8	8.0313	8.01	4.014	4.047	4.031	1.987	12.76	62890	4929
SLAB R2	Companion	22	Aug-21-14	14	Comp_1	1	1	3	0	8.25	8.0625	8.0313	8.11	4.055	4.023	4.039	2.009	12.81	64155	5007
		23	Aug-21-14	14	Comp_2	2	2	0	0	8	8.0938	8.0313	8.04	4.024	4.03	4.027	1.997	12.74	65630	5153
		24	Aug-21-14	14	Comp_3	4	3	0	0	8.0625	8.0313	8.25	8.11	4.087	3.948	4.018	2.020	12.68	NaN	NaN
		25	Aug-21-14	14	Comp_4	1	1	2	1	12.063	12.063	12	12.04	5.972	6.008	5.990	2.010	28.18	134070	4758
		26	Aug-21-14	14	Comp_5	5	1	3	0	12.125	12.063	12.063	12.08	6.007	5.995	6.001	2.014	28.28	135140	4778
	Cores	27	Aug-21-14	16	Core_1	3	0	0	0	8	7.9688	7.9688	7.98	3.982	3.981	3.982	2.004	12.45	62840	5047
		28	Aug-21-14	16	Core_2	5	1	0	0	8.0625	8.0938	7.9375	8.03	3.981	3.982	3.982	2.017	12.45	65075	5227
		29	Aug-21-14	16	Core_3	2	0	0	0	8.0313	8	8	8.01	3.983	3.982	3.983	2.011	12.46	65095	5226
		30	Aug-21-14	16	Core_4	3	0	0	0	7.9688	7.9688	7.9375	7.96	3.983	3.982	3.983	1.998	12.46	64655	5190
		31	Aug-21-14	16	Core_5	1	1	0	0	8	8	8.0313	8.01	3.983	3.984	3.984	2.011	12.46	62905	5047
		32	Aug-21-14	16	Core_6	3	0	0	0	7.9688	7.9375	7.9375	7.95	3.982	3.982	3.982	1.996	12.45	69420	5574
		33	Aug-21-14	16	Core_7	2	1	0	0	8	8.0313	8.0625	8.03	3.983	3.982	3.983	2.017	12.46	62405	5010
		34	Aug-21-14	16	Core_8	1	0	0	0	7.9688	8	7.9688	7.98	3.984	3.984	3.984	2.003	12.47	68135	5466
	In-Place Cylinders	35	Aug-21-14	16	InCyl_1	0	0	1	0	8.0313	8.0938	8.0625	8.06	4.025	4.023	4.024	2.004	12.72	69530	5467
		36	Aug-21-14	16	InCyl_2	3	1	2	0	8.0938	8.1563	8.0938	8.11	3.994	4.067	4.031	2.013	12.76	73975	5798
		37	Aug-21-14	16	InCyl_3	3	0	1	1	8.125	8.0625	8.125	8.10	4.043	4.017	4.030	2.011	12.76	67840	5318
		38	Aug-21-14	16	InCyl_4	3	0	0	0	8.125	8.1875	8.0938	8.14	4.042	4.025	4.034	2.017	12.78	69930	5473
		39	Aug-21-14	16	InCyl_5	2	0	0	1	8.0313	8	8.0313	8.02	4.043	4.021	4.032	1.989	12.77	74655	5847
		40	Aug-21-14	16	InCyl_6	0	0	2	1	8.125	8.0938	8.1563	8.13	4.044	4.046	4.045	2.009	12.85	69590	5415
		41	Aug-21-14	16	InCyl_7	1	0	0	0	8.0625	8.0938	8.0625	8.07	4.045	4.022	4.034	2.001	12.78	71915	5628
		42	Aug-21-14	16	InCyl_8	1	0	0	1	7.9375	7.9688	7.9688	7.96	4.012	4.001	4.007	1.986	12.61	65705	5212

Table A.3: Companion, Core, and In-Place Cylinders' Compressive Strength Test Results, Part 2

			COMPRESSIVE STRENGTH TESTING (ASTM C 39 / AASHTO T 22)																	
			DATE	Age of Conc at testing	GROUP/SAMPLE ID NUMBER	Roughness		Perpendicularity		HEIGHT				DIAMETER				CROSS-SECTIONAL AREA	LOAD	STRENGTH
						mm	mm	mm	mm	inch				inch				in^2	lbs.	psi
			-	day	-	Top	Bot	Top	Bot	1	2	3	Ave	1	2	Ave	L/D	Ave	-	-
SLAB R3	Companion	43	Aug-12-14	14	Comp_1	2	1	0	0	8.07	8.06	8.05	8.06	4.04	4.004	4.022	2.004	12.70	69455	5467
		44	Aug-12-14	14	Comp_2	2	1	0	0	8.022	8.044	8.003	8.02	4.024	4.018	4.021	1.995	12.70	66560	5241
		45	Aug-12-14	14	Comp_3	2	2	0	0	8.039	8.058	8.076	8.06	4.031	4.011	4.021	2.004	12.70	69880	5503
		46	Aug-12-14	14	Comp_4	2	1	2	1	12.094	12.063	12.031	12.06	5.959	5.998	5.979	2.018	28.07	154400	5500
		47	Aug-12-14	14	Comp_5	2	0	0	1	12.125	12.063	12.063	12.08	5.995	5.969	5.982	2.020	28.10	159315	5669
	Cores	48	Aug-12-14	16	Core_1	1	0	4	0	7.875	7.9688	7.9688	7.94	3.981	3.979	3.980	1.994	12.44	63855	5133
		49	Aug-12-14	16	Core_2	0	0	2	0	7.875	7.9063	7.9375	7.91	3.981	3.972	3.977	1.988	12.42	63300	5097
		50	Aug-12-14	16	Core_3	0	1	3	1	8	7.9375	7.9375	7.96	3.979	3.979	3.979	2.000	12.43	64375	5177
		51	Aug-12-14	16	Core_4	1	1	2	1	7.9688	7.9688	8	7.98	3.978	3.981	3.980	2.005	12.44	67375	5417
		52	Aug-12-14	16	Core_5	1	1	5	2	7.9375	7.875	8	7.94	3.979	3.977	3.978	1.995	12.43	70860	5701
		53	Aug-12-14	16	Core_6	0	0	2	0	8.0313	8	8.0313	8.02	3.979	3.981	3.980	2.015	12.44	67445	5421
		54	Aug-12-14	16	Core_7	2	0	4	0	7.9688	8.0313	8.0313	8.01	3.98	3.981	3.981	2.012	12.44	73560	5911
		55	Aug-12-14	16	Core_8	0	1	1	0	7.9688	7.9688	8	7.98	3.98	3.978	3.979	2.005	12.43	67085	5395
	In-Place Cylinders	56	Aug-12-14	16	InCyl_1	2	1	3	0	8.162	8.102	8.123	8.13	4.002	4.039	4.021	2.022	12.70	80760	6361
		57	Aug-12-14	16	InCyl_2	1	2	2	0	8.154	8.197	8.153	8.17	4.023	4.027	4.025	2.029	12.72	81020	6368
		58	Aug-12-14	16	InCyl_3	3	1	1	1	8.198	8.204	8.178	8.19	4.002	4.035	4.019	2.039	12.68	81455	6422
		59	Aug-12-14	16	InCyl_4	1	1	2	0	8.174	8.17	8.175	8.17	4.019	4.007	4.013	2.037	12.65	78845	6234
		60	Aug-12-14	16	InCyl_5	1	0	3	0	8.19	8.212	8.222	8.21	4.014	4.014	4.014	2.045	12.65	77415	6118
		61	Aug-12-14	16	InCyl_6	2	0	4	0	8.148	8.169	8.189	8.17	3.996	4.056	4.026	2.029	12.73	77505	6088
		62	Aug-12-14	16	InCyl_7	0	1	0	0	7.986	7.986	7.985	7.99	4.013	4.038	4.026	1.984	12.73	80440	6320
		63	Aug-12-14	16	InCyl_8	0	0	1	1	7.921	7.927	7.966	7.94	4.004	4.042	4.023	1.973	12.71	78465	6173
SLAB R4	Companion	64	Sep-02-14	14	Comp_1	1	2	1	0	8.058	8.023	8.045	8.04	4.031	4.015	4.023	1.999	12.71	69975	5505
		65	Sep-02-14	14	Comp_2	2	1	1	1	8.068	8.073	8.096	8.08	4.044	4.027	4.036	2.002	12.79	73550	5750
		66	Sep-02-14	14	Comp_3	2	2	1	0	8.073	8.081	8.086	8.08	4.037	4.021	4.029	2.005	12.75	67315	5280
		67	Sep-02-14	14	Comp_4	-	-	-	-	-	-	-	NaN	-	-	NaN	NaN	NaN	NaN	NaN
		68	Sep-02-14	14	Comp_5	1	1	0	0	12.063	12.031	12.031	12.04	5.953	5.986	5.970	2.017	27.99	153610	5489
	Cores	69	Sep-04-14	16	Core_1	1	0	4	0	7.904	7.921	7.954	7.93	3.984	3.884	3.934	2.015	12.16	67585	5560
		70	Sep-04-14	16	Core_2	1	0	3	0	7.978	7.952	7.954	7.96	3.979	3.981	3.980	2.000	12.44	68955	5543
		71	Sep-04-14	16	Core_3	2	0	3	1	7.985	8.008	7.985	7.99	3.984	3.962	3.973	2.012	12.40	64028	5165
		72	Sep-04-14	16	Core_4	0	0	1	1	7.981	7.975	8.009	7.99	3.966	3.988	3.977	2.009	12.42	68530	5517
		73	Sep-04-14	16	Core_5	1	0	3	0	7.987	7.957	7.986	7.98	3.967	3.973	3.970	2.009	12.38	61405	4961
		74	Sep-04-14	16	Core_6	1	0	4	1	8.067	8.005	8.042	8.04	3.966	3.976	3.971	2.024	12.38	68535	5534
		75	Sep-04-14	16	Core_7	1	0	3	1	7.98	7.987	7.967	7.98	3.983	3.936	3.960	2.015	12.31	67130	5452
		76	Sep-04-14	16	Core_8	1	0	4	1	8.006	7.992	8.011	8.00	3.99	3.976	3.983	2.009	12.46	66815	5362
	In-Place Cylinders	77	Sep-04-14	16	InCyl_1	-	-	-	-	8.191	8.149	8.117	8.15	4.036	4.017	4.027	2.025	12.73	69435	5453
		78	Sep-04-14	16	InCyl_2	1	1	1	0	8.095	8.091	8.107	8.10	4.026	4.043	4.035	2.007	12.78	71665	5606
		79	Sep-04-14	16	InCyl_3	1	0	1	0	8.115	8.111	8.101	8.11	4.018	4.046	4.032	2.011	12.77	73860	5785
		80	Sep-04-14	16	InCyl_4	3	0	2	0	8.126	8.12	8.107	8.12	4.023	4.046	4.035	2.012	12.78	71615	5602
		81	Sep-04-14	16	InCyl_5	-	-	-	-	8.132	8.078	8.115	8.11	4.049	4.011	4.030	2.012	12.76	76295	5981
		82	Sep-04-14	16	InCyl_6	2	1	1	2	8.132	8.107	8.113	8.12	4.04	4.018	4.029	2.015	12.75	73930	5799
		83	Sep-04-14	16	InCyl_7	1	0	1	0	8.124	8.109	8.113	8.12	4.009	4.035	4.022	2.018	12.70	70775	5571
		84	Sep-04-14	16	InCyl_8	-	-	-	-	8.093	8.116	8.137	8.12	4.019	4.029	4.024	2.017	12.72	70880	5573

Table A.3: Companion, Core, and In-Place Cylinders' Compressive Strength Test Results, Part 3

			COMPRESSIVE STRENGTH TESTING (ASTM C 39 / AASHTO T 22)																		
			DATE	Age of Conc at testing	GROUP/SAMPLE ID NUMBER	Roughness		Perpendicularity		HEIGHT				DIAMETER				CROSS-SECTIONAL AREA	LOAD	STRENGTH
						mm	mm	mm	mm	inch				inch				in^2	lbs.	psi
			-	day	-	Top	Bot	Top	Bot	1	2	3	Ave	1	2	Ave	L/D	Ave	-	-
SLAB R5	Companion	85	Sep-16-14	14	Comp_1	2	1	2	1	8.0313	8.0313	8.0938	8.05	4.043	4.017	4.030	1.998	12.76	60375	4733
		86	Sep-16-14	14	Comp_2	2	0	2	1	8	8.0625	8.0313	8.03	4	3.9375	3.969	2.024	12.37	59350	4798
		87	Sep-16-14	14	Comp_3	1	0	4	1	7.9375	8.0625	8.25	8.08	3.9375	4	3.969	2.037	12.37	61205	4948
		88	Sep-16-14	14	Comp_4	1	1	1	1	12.063	12.25	12.25	12.19	6.0313	5.9688	6.000	2.031	28.27	130235	4606
		89	Sep-16-14	14	Comp_5	2	1	2	1	12.188	12.063	12.25	12.17	5.9375	6	5.969	2.038	27.98	129040	4612
	Cores	90	Sep-18-14	16	Core_1	2	1	3	2	7.846	7.767	7.798	7.80	3.993	3.987	3.990	1.956	12.50	60950	4875
		91	Sep-18-14	16	Core_2	2	3	3	1	7.878	8.004	8.007	7.96	3.974	3.994	3.984	1.999	12.47	57760	4633
		92	Sep-18-14	16	Core_3	2	2	3	2	8.11	8.039	8.079	8.08	3.978	3.979	3.979	2.030	12.43	56420	4538
		93	Sep-18-14	16	Core_4	3	2	4	3	8.093	8.087	7.993	8.06	3.978	3.976	3.977	2.026	12.42	55835	4495
		94	Sep-18-14	16	Core_5	1	2	4	1	8.031	7.986	8.107	8.04	3.981	3.983	3.982	2.019	12.45	56380	4527
		95	Sep-18-14	16	Core_6	0	0	1	1	8.05	8.049	8.04	8.05	3.977	3.979	3.978	2.023	12.43	54160	4358
		96	Sep-18-14	16	Core_7	1	1	3	2	8.088	8.039	8.036	8.05	3.979	3.986	3.983	2.022	12.46	56210	4512
		97	Sep-18-14	16	Core_8	2	1	3	2	7.945	7.983	7.975	7.97	3.987	3.991	3.989	1.997	12.50	57795	4625
	In-Place Cylinders	98	Sep-18-14	16	InCyl_1	0	2	0	3	8.16	8.202	8.109	8.16	4.023	4.012	4.018	2.030	12.68	66470	5244
		99	Sep-18-14	16	InCyl_2	1	2	2	3	8.137	8.13	8.152	8.14	4.034	4.033	4.034	2.018	12.78	64140	5020
		100	Sep-18-14	16	InCyl_3	2	0	1	3	8.056	8.025	8.072	8.05	4.03	4.036	4.033	1.996	12.77	63535	4974
		101	Sep-18-14	16	InCyl_4	1	3	2	3	8.105	8.118	8.112	8.11	4.014	4.008	4.011	2.022	12.64	64275	5087
		102	Sep-18-14	16	InCyl_5	2	0	2	1	7.98	8.004	8.034	8.01	4.042	4.039	4.041	1.981	12.82	63395	4944
		103	Sep-18-14	16	InCyl_6	1	3	2	3	8.079	8.071	8.106	8.09	3.994	4.065	4.030	2.007	12.75	62620	4910
		104	Sep-18-14	16	InCyl_7	0	3	1	2	8.182	8.161	8.156	8.17	4.018	4.019	4.019	2.032	12.68	65400	5157
		105	Sep-18-14	16	InCyl_8	2	0	1	3	8.058	8.044	8.028	8.04	4.045	3.976	4.011	2.006	12.63	64040	5069
SLAB R6	Companion	106	Oct-21-14	14	Comp_1	3	2	1	0	8	8.0313	8.0313	8.02	4.03	4.004	4.017	1.997	12.67	74760	5899
		107	Oct-21-14	14	Comp_2	2	1	2	0	8	7.9688	8	7.99	3.989	4.004	3.997	1.999	12.54	75455	6015
		108	Oct-21-14	14	Comp_3	4	2	1	0	8.25	8.125	8.0938	8.16	3.967	3.962	3.965	2.057	12.34	74930	6070
		109	Oct-21-14	14	Comp_4	3	1	2	1	11.969	12.125	12	12.03	5.948	5.893	5.921	2.032	27.53	167640	6089
		110	Oct-21-14	14	Comp_5	1	1	4	1	12.125	12.063	12.063	12.08	5.959	5.933	5.946	2.032	27.77	161465	5815
	Cores	111	Oct-23-14	16	Core_1	1	0	2	1	8.0313	8	8.0313	8.02	3.982	3.984	3.983	2.014	12.46	77120	6190
		112	Oct-23-14	16	Core_2	0	0	3	0	7.9688	8	7.9688	7.98	3.986	3.987	3.987	2.002	12.48	76200	6105
		113	Oct-23-14	16	Core_3	1	0	3	0	7.875	7.875	7.9375	7.90	3.987	3.988	3.988	1.980	12.49	70255	5626
		114	Oct-23-14	16	Core_4	1	0	2	1	7.9688	8.0313	7.9375	7.98	3.984	3.989	3.987	2.002	12.48	70450	5644
		115	Oct-23-14	16	Core_5	2	0	2	1	8.0625	7.9688	8.0313	8.02	3.984	3.985	3.985	2.013	12.47	70880	5684
		116	Oct-23-14	16	Core_6	0	0	3	1	8	8	8	8.00	3.985	3.988	3.987	2.007	12.48	73670	5902
		117	Oct-23-14	16	Core_7	0	0	1	0	8.0313	8	8.0313	8.02	3.989	3.989	3.989	2.011	12.50	75610	6050
		118	Oct-23-14	16	Core_8	0	0	3	0	7.9688	8.0313	8.0625	8.02	3.987	3.989	3.988	2.011	12.49	74530	5967
	In-Place Cylinders	119	Oct-23-14	16	InCyl_1	2	0	1.5	0.1	8.0625	8.0938	8.125	8.09	4.023	4.036	4.030	2.009	12.75	75605	5929
		120	Oct-23-14	16	InCyl_2	0.5	0	1.5	0	8.0313	8.0625	8.0625	8.05	4	4	4.000	2.013	12.57	77435	6162
		121	Oct-23-14	16	InCyl_3	1.5	0	2.5	0	8	8.0313	8.0313	8.02	4.057	3.985	4.021	1.995	12.70	81660	6431
		122	Oct-23-14	16	InCyl_4	2	0	2.5	0	8.0938	8.125	8.125	8.11	4.041	4.014	4.028	2.015	12.74	80035	6282
		123	Oct-23-14	16	InCyl_5	3	0	3	0	8.1563	8.1563	8.1563	8.16	4	4	4.000	2.039	12.57	75575	6014
		124	Oct-23-14	16	InCyl_6	1.5	0	1	0	8.0625	8.0625	8.0938	8.07	4.023	4.036	4.030	2.003	12.75	78760	6176
		125	Oct-23-14	16	InCyl_7	1.5	1	3	0	8.125	8.0625	8.125	8.10	4.051	4.007	4.029	2.011	12.75	76130	5971
		126	Oct-23-14	16	InCyl_8	0.5	0	0	0	8	8	8	8.00	4.008	4.018	4.013	1.994	12.65	76625	6058

Table A.3: Companion, Core, and In-Place Cylinders' Compressive Strength Test Results, Part 4

			COMPRESSIVE STRENGTH TESTING (ASTM C 39 / AASHTO T 22)																		
			DATE	Age of Conc at testing	GROUP/SAMPLE ID NUMBER	Roughness		Perpendicularity		HEIGHT				DIAMETER				CROSS-SECTIONAL AREA	LOAD	STRENGTH
						mm	mm	mm	mm	inch				inch				in^2	lbs.	psi
			-	day	-	Top	Bot	Top	Bot	1	2	3	Ave	1	2	Ave	L/D	Ave	-	-
SLAB R7	Companion	127	Oct-7-14	14	Comp_1	1	0	2	1	8.09	8.092	8.082	8.09	4.02	4.034	4.027	2.008	12.74	70910	5567
		128	Oct-7-14	14	Comp_2	1	0	1	2	8.083	8.11	8.13	8.11	3.999	4.065	4.032	2.011	12.77	70720	5539
		129	Oct-7-14	14	Comp_3	1	0	2	0	8.07	8.088	8.093	8.08	4.054	4.042	4.048	1.997	12.87	65225	5068
		130	Oct-7-14	14	Comp_4	1	0	1	0	12.125	12.188	12.125	12.15	5.97	5.984	5.977	2.032	28.06	167290	5962
		131	Oct-7-14	14	Comp_5	2	0	3	1	12.125	12.125	12.125	12.13	5.966	5.946	5.956	2.036	27.86	165120	5927
	Cores	132	Oct-9-14	16	Core_1	0	0	0	0	7.984	8	8.004	8.00	3.989	3.987	3.988	2.005	12.49	79370	6354
		133	Oct-9-14	16	Core_2	0	0	1	0	7.941	7.938	7.97	7.95	3.991	3.987	3.989	1.993	12.50	71970	5759
		134	Oct-9-14	16	Core_3	0	3	2	1	8.038	8.065	8.003	8.04	3.99	3.986	3.988	2.015	12.49	75015	6005
		135	Oct-9-14	16	Core_4	0	1	1	2	7.991	7.999	7.991	7.99	3.985	3.985	3.985	2.006	12.47	78195	6269
		136	Oct-9-14	16	Core_5	0	1	0	0	8.007	8.006	7.983	8.00	3.989	3.985	3.987	2.006	12.48	77825	6234
		137	Oct-9-14	16	Core_6	1	0	0	0	8.013	8.02	8.106	8.05	3.99	3.989	3.990	2.017	12.50	75785	6063
		138											NaN				NaN	NaN		NaN
		139	Oct-9-14	16	Core_8	0	1	2	2	8.01	8.069	8.03	8.04	3.984	3.987	3.986	2.016	12.48	72990	5851
	In-Place Cylinders	140	Oct-9-14	16	InCyl_1	0	0	0	1	8.008	8.01	7.946	7.99	4	4	4.000	1.997	12.57	70155	5583
		141	Oct-9-14	16	InCyl_2	1	0	0	2	8.065	8.086	8.008	8.05	4	4	4.000	2.013	12.57	66105	5260
		142	Oct-9-14	16	InCyl_3	1	1	1	2	8.112	8.096	8.095	8.10	4	4	4.000	2.025	12.57	68455	5447
		143	Oct-9-14	16	InCyl_4	1	0	1	1	7.942	7.962	7.954	7.95	4	4	4.000	1.988	12.57	67895	5403
		144	Oct-9-14	16	InCyl_5	1	0	1	1	7.975	7.986	7.962	7.97	4	4	4.000	1.994	12.57	70165	5584
		145	Oct-9-14	16	InCyl_6	2	0	0	2	8.052	8.266	7.843	8.05	4	4	4.000	2.013	12.57	67655	5384
		146	Oct-9-14	16	InCyl_7	3	0	0	2	7.975	7.986	7.962	7.97	4	4	4.000	1.994	12.57	72695	5785
		147	Oct-9-14	16	InCyl_8	1	3	0	3	7.919	7.951	7.917	7.93	4	4	4.000	1.982	12.57	61380	4884
SLAB R8	Companion	148	Oct-14-14	14	Comp_1	2	0	1	0	8.1	8.056	8.129	8.10	4.049	4.062	4.056	1.996	12.92	75095	5813
		149	Oct-14-14	14	Comp_2	2	0	4	0	8.059	8.099	8.152	8.10	4.016	4.032	4.024	2.014	12.72	74765	5879
		150	Oct-14-14	14	Comp_3	3	0	1	1	8.129	8.119	8.142	8.13	4.064	4.054	4.059	2.003	12.94	74810	5781
		151	Oct-14-14	14	Comp_4	3	1	3	0	12.125	12.063	12.125	12.10	5.963	6.002	5.983	2.023	28.11	153200	5450
		152	Oct-14-14	14	Comp_5	2	0	4	1	11.938	12.125	12.125	12.06	5.959	6.035	5.997	2.011	28.25	156850	5553
	Cores	153	Oct-16-14	16	Core_1	0	2	0	0	8.052	8.036	8.053	8.05	3.997	3.994	3.996	2.014	12.54	73470	5860
		154	Oct-16-14	16	Core_2	0	2	0	0	8.005	8.08	8.062	8.05	3.985	3.986	3.986	2.020	12.48	59220	4747
		155	Oct-16-14	16	Core_3	0	1	0	0	8.024	7.986	8.042	8.02	3.992	3.993	3.993	2.008	12.52	68465	5469
		156	Oct-16-14	16	Core_4	0	1	0	0	8.086	8.053	8.116	8.09	3.982	3.986	3.984	2.029	12.47	65430	5249
		157	Oct-16-14	16	Core_5	0	3	0	0	8.05	8.025	8.026	8.03	3.992	3.994	3.993	2.012	12.52	66875	5340
		158	Oct-16-14	16	Core_6	0	0	0	2	8.043	8.026	8.009	8.03	3.994	3.992	3.993	2.010	12.52	69330	5536
		159	Oct-16-14	16	Core_7	0	0	0	0	8.132	8.041	8.066	8.08	3.992	3.987	3.990	2.025	12.50	67220	5377
		160	Oct-16-14	16	Core_8	0	2	0	0	8.012	8.013	7.994	8.01	3.989	3.985	3.987	2.008	12.48	70790	5670
	In-Place Cylinders	161	Oct-16-14	16	InCyl_1	0	1	0	2	8.096	8.063	8.044	8.07	4.022	4.033	4.028	2.003	12.74	71235	5592
		162	Oct-16-14	16	InCyl_2	0	1	0	2	8.117	8.142	8.179	8.15	4.027	4.036	4.032	2.021	12.77	73660	5770
		163	Oct-16-14	16	InCyl_3	0	2	0	3	8.189	8.139	8.176	8.17	4.012	4.035	4.024	2.030	12.71	78015	6136
		164	Oct-16-14	16	InCyl_4	0	1	0	2	8.033	8.087	8.061	8.06	4.052	3.994	4.023	2.004	12.71	77350	6085
		165	Oct-16-14	16	InCyl_5	0	2	1	2	8.124	8.202	8.168	8.16	4.047	4.014	4.031	2.026	12.76	73475	5759
		166	Oct-16-14	16	InCyl_6	0	2	0	3	8.038	8.063	8.139	8.08	4.04	4.013	4.027	2.007	12.73	75190	5905
		167	Oct-16-14	16	InCyl_7	0	1	0	2	8.109	8.052	8.11	8.09	4.034	4.023	4.029	2.008	12.75	77700	6096
		168	Oct-16-14	16	InCyl_8	0	1	0	2	8.165	8.136	8.11	8.14	4.009	4.065	4.037	2.016	12.80	79540	6214

Table A.3: Companion, Core, and In-Place Cylinders' Compressive Strength Test Results, Part 5

			COMPRESSIVE STRENGTH TESTING (ASTM C 39 / AASHTO T 22)																		
			DATE	Age of Conc at testing	GROUP/SAMPLE ID NUMBER	Roughness		Perpendicularity		HEIGHT				DIAMETER				CROSS-SECTIONAL AREA	LOAD	STRENGTH
						mm	mm	mm	mm	inch				inch				in^2	lbs.	psi
			-	day	-	Top	Bot	Top	Bot	1	2	3	Ave	1	2	Ave	L/D	Ave	-	-
SLAB R9	Companion	169	Oct-21-14	14	Comp_1	2	1	0	0	8.086	8.023	8.055	8.05	4.007	4.023	4.015	2.006	12.66	84225	6652
		170	Oct-21-14	14	Comp_2	1	1	0	0	8.086	8.082	8.092	8.09	4.0034	4.015	4.009	2.017	12.62	86580	6858
		171	Oct-21-14	14	Comp_3	2	0	0	0	8.034	8.039	8.048	8.04	4.012	4.015	4.014	2.003	12.65	85290	6742
		172	Oct-21-14	14	Comp_4	2	0	1	0	12	12.063	12.063	12.04	5.981	5.984	5.983	2.013	28.11	172715	6144
		173	Oct-21-14	14	Comp_5	2	0	1	1	12.063	12	12.031	12.03	5.977	5.985	5.981	2.012	28.10	169520	6034
	Cores	174	Oct-23-14	16	Core_1	0	1	0	0	8.079	8.057	7.999	8.05	4	4.005	4.003	2.010	12.58	81805	6502
		175	Oct-23-14	16	Core_2	0	0	0	0	8.044	8.063	8.011	8.04	4.003	4.015	4.009	2.005	12.62	87595	6939
		176	Oct-23-14	16	Core_3	0	1	0	0	8.002	8.011	7.982	8.00	4	4.005	4.003	1.998	12.58	82880	6587
		177	Oct-23-14	16	Core_4	0	0	0	0	7.899	7.942	7.91	7.92	4.008	3.999	4.004	1.978	12.59	86715	6889
		178	Oct-23-14	16	Core_5	0	0	0	0	8.006	8.06	8.033	8.03	4.002	4.002	4.002	2.007	12.58	78790	6264
		179	Oct-23-14	16	Core_6	0	1	0	0	8.013	8.071	8.036	8.04	4.012	4.004	4.008	2.006	12.62	85205	6753
		180	Oct-23-14	16	Core_7	0	2	0	0	7.946	7.934	7.998	7.96	4.016	4.021	4.019	1.981	12.68	82870	6534
		181	Oct-23-14	16	Core_8	2	1	0	0	7.913	7.937	7.97	7.94	3.999	3.998	3.999	1.986	12.56	84045	6693
	In-Place Cylinders	182	Oct-23-14	16	InCyl_1	3	0	2	0	8.234	8.208	8.268	8.24	4.042	4.044	4.043	2.037	12.84	88305	6878
		183	Oct-23-14	16	InCyl_2	1	1	2	1	8.153	8.107	8.126	8.13	4.025	4.06	4.043	2.011	12.83	86485	6738
		184	Oct-23-14	16	InCyl_3	1	0	1	1	8.121	8.116	8.1	8.11	4.013	4.056	4.035	2.011	12.78	85505	6688
		185	Oct-23-14	16	InCyl_4	2	1	3	1	8.148	8.144	8.102	8.13	4.022	4.015	4.019	2.023	12.68	82470	6502
		186	Oct-23-14	16	InCyl_5	1	0	2	0	8.122	8.109	8.1	8.11	4.034	4.029	4.032	2.012	12.77	87300	6839
		187	Oct-23-14	16	InCyl_6	2	0	0	1	8.146	8.167	8.121	8.14	4.001	4.029	4.015	2.029	12.66	80005	6319
		188	Oct-23-14	16	InCyl_7	1	0	1	0	8.103	8.145	8.094	8.11	3.999	4.03	4.015	2.021	12.66	84725	6694
		189	Oct-23-14	16	InCyl_8	3	1	2	0	8.078	8.075	8.099	8.08	4.043	3.999	4.021	2.010	12.70	82305	6481
SLAB R10	Companion	190	Nov-4-14	14	Comp_1	1	0	1	0	8.042	8.065	8.104	8.07	4.04	4.001	4.021	2.007	12.70	120285	9475
		191	Nov-4-14	14	Comp_2	2	0	1	1	8.04	8.06	8.032	8.04	4.042	4.019	4.031	1.996	12.76	117905	9241
		192	Nov-4-14	14	Comp_3	1	2	1	2	8.137	8.114	8.114	8.12	4.034	4.014	4.024	2.018	12.72	121585	9560
		193	Nov-4-14	14	Comp_4	1	1	1	1	12.125	12.188	12.125	12.15	6.011	6.021	6.016	2.019	28.43	263195	9259
		194	Nov-4-14	14	Comp_5	2	2	1	1	12.25	12.188	12.125	12.19	5.997	5.963	5.980	2.038	28.09	253965	9042
	Cores	195	Nov-6-14	16	Core_1	0	0	0	0	7.992	8.026	8.06	8.03	3.988	3.987	3.988	2.013	12.49	115795	9273
		196	Nov-6-14	16	Core_2	0	2	1	0	8.008	7.977	8.006	8.00	3.988	3.987	3.988	2.006	12.49	115760	9270
		197	Nov-6-14	16	Core_3	0	1	1	0	7.946	7.919	7.924	7.93	3.987	3.989	3.988	1.988	12.49	107175	8580
		198	Nov-6-14	16	Core_4	0	2	2	0	7.982	7.971	8.04	8.00	3.988	3.988	3.988	2.005	12.49	95015	7607
		199	Nov-6-14	16	Core_5	1	2	1	0	7.965	7.956	7.969	7.96	3.987	3.988	3.988	1.997	12.49	105925	8482
		200	Nov-6-14	16	Core_6	0	0	2	0	7.964	7.979	8.007	7.98	3.987	3.998	3.993	2.000	12.52	Unplugged	NaN
		201	Nov-6-14	16	Core_7	0	2	1	0	8.013	8.027	8.008	8.02	3.988	3.99	3.989	2.010	12.50	81990	6561
		202	Nov-6-14	16	Core_8	1	0	0	0	8.059	8.037	8.105	8.07	3.989	3.989	3.989	2.022	12.50	113650	9094
	In-Place Cylinders	203	Nov-6-14	16	InCyl_1	1	2	2	1	8.143	8.15	8.152	8.15	4.025	4.011	4.018	2.028	12.68	113670	8965
		204	Nov-6-14	16	InCyl_2	3	0	2	1	8.239	8.255	8.234	8.24	4.024	4.044	4.034	2.043	12.78	117145	9166
		205	Nov-6-14	16	InCyl_3	2	1	2	1	8.124	8.155	8.156	8.15	4.06	4.033	4.047	2.013	12.86	112610	8756
		206	Nov-6-14	16	InCyl_4	0	2	0	1	8.172	8.181	8.191	8.18	4.017	4.025	4.021	2.035	12.70	50000	3937
		207	Nov-6-14	16	InCyl_5	1	2	0	1	8.241	8.282	8.281	8.27	4.084	3.989	4.037	2.048	12.80	121380	9485
		208	Nov-6-14	16	InCyl_6	0	1	0	1	8.262	8.273	8.271	8.27	4.035	4.027	4.031	2.051	12.76	No reading	NaN
		209	Nov-6-14	16	InCyl_7	0	2	0	0	8.08	8.124	8.118	8.11	4.007	4.05	4.029	2.012	12.75	114200	8960
		210	Nov-6-14	16	InCyl_8	0	1	0	1	8.147	8.202	8.163	8.17	4.043	3.998	4.021	2.032	12.70	116275	9159

Table A.3: Companion, Core, and In-Place Cylinders' Compressive Strength Test Results, Part 6

			COMPRESSIVE STRENGTH TESTING (ASTM C 39 / AASHTO T 22)																	
			DATE	Age of Conc at testing	GROUP/SAMPLE ID NUMBER	Roughness		Perpendicularity		HEIGHT				DIAMETER				CROSS-SECTIONAL AREA	LOAD	STRENGTH
						mm	mm	mm	mm	inch				inch				in^2	lbs.	psi
			-	day	-	Top	Bot	Top	Bot	1	2	3	Ave	1	2	Ave	L/D	Ave	-	-
SLAB R11	Companion	211	Nov-11-14	14	Comp_1	2	0	1	0	8.151	8.212	8.212	8.19	4.029	4.053	4.041	2.027	12.83	112670	8785
		212	Nov-11-14	14	Comp_2	1	0	0	0	8.091	8.054	8.114	8.09	4.032	4.041	4.037	2.003	12.80	113825	8895
		213	Nov-11-14	14	Comp_3	2	1	3	0	8.121	8.134	8.151	8.14	4.072	4.05	4.061	2.003	12.95	106140	8195
		214	Nov-11-14	14	Comp_4	2	1	1	0	12.031	12.062	12.062	12.05	6.007	6.004	6.006	2.007	28.33	225165	7949
		215	Nov-11-14	14	Comp_5	3	2	2	0	12.062	12.062	12	12.04	5.98	5.987	5.984	2.012	28.12	228230	8117
	Cores	216	Nov-13-14	16	Core_1	0	0	0	0	8.03	8.093	8.071	8.06	3.997	3.994	3.996	2.018	12.54	83620	6669
		217	Nov-13-14	16	Core_2	0	0	0	1	8.051	8.112	8.125	8.10	3.994	3.994	3.994	2.027	12.53	89295	7127
		218	Nov-13-14	16	Core_3	0	3	2	0	8.047	8.072	8.114	8.08	3.991	3.994	3.993	2.023	12.52	90115	7198
		219	Nov-13-14	16	Core_4	0	0	0	0	8.029	8.075	8.072	8.06	3.994	3.993	3.994	2.018	12.53	84600	6754
		220	Nov-13-14	16	Core_5	1	0	1	0	8.054	8.042	8.006	8.03	3.996	3.996	3.996	2.011	12.54	90450	7212
		221	Nov-13-14	16	Core_6	0	0	0	0	8.008	7.987	8.025	8.01	3.997	3.997	3.997	2.003	12.55	85760	6835
		222	Nov-13-14	16	Core_7	0	0	3	0	8.07	8.131	8.086	8.10	3.995	3.995	3.995	2.026	12.53	87835	7007
		223	Nov-13-14	16	Core_8	0	0	2	1	8.088	8.049	8.074	8.07	3.994	3.993	3.994	2.021	12.53	93310	7450
	In-Place Cylinders	224	Nov-13-14	16	InCyl_1	3	0	3	0	8.073	8.081	8.077	8.08	4.026	4.099	4.063	1.988	12.96	110785	8547
		225	Nov-13-14	16	InCyl_2	0	1	0	0	8.063	8.071	8.085	8.07	4.025	4.005	4.015	2.011	12.66	109795	8672
		226	Nov-13-14	16	InCyl_3	1	1	1	0	8.193	8.168	8.189	8.18	4.002	4.046	4.024	2.034	12.72	111250	8748
		227	Nov-13-14	16	InCyl_4	1	0	1	1	8.144	8.142	8.133	8.14	4.011	4.019	4.015	2.027	12.66	107510	8492
		228	Nov-13-14	16	InCyl_5	1	0	0	1	8.141	8.132	8.103	8.13	4.012	4.037	4.025	2.019	12.72	107900	8482
		229	Nov-13-14	16	InCyl_6	0	1	0	1	8.083	8.135	8.176	8.13	4.022	4.057	4.040	2.013	12.82	112340	8766
		230	Nov-13-14	16	InCyl_7	0	0	0	1	8.111	8.112	8.158	8.13	4.026	4.03	4.028	2.018	12.74	110100	8640
		231	Nov-13-14	16	InCyl_8	0	0	0	1	8.168	8.158	8.165	8.16	4.024	4.062	4.043	2.019	12.84	106470	8293
SLAB R12	Companion	232	Nov-19-14	14	Comp_1	3	1	2	0	7.988	8.047	8.045	8.03	3.968	4.034	4.001	2.006	12.57	90300	7182
		233	Nov-19-14	14	Comp_2	2	1	2	1	7.987	8.027	8.033	8.02	4.02	3.987	4.004	2.002	12.59	89085	7077
		234	Nov-19-14	14	Comp_3	2	0	0	0	7.997	8.02	8.014	8.01	3.96	4.032	3.996	2.005	12.54	91340	7283
		235	Nov-19-14	14	Comp_4	3	1	1	0	12	12	12.094	12.03	6.02	6.028	6.024	1.997	28.50	213335	7485
		236	Nov-19-14	14	Comp_5	3	0	2	0	12.125	12.063	12.063	12.08	6.03	5.996	6.013	2.010	28.40	211715	7456
	Cores	237	Nov-21-14	16	Core_1	0	0	1	0	7.995	7.992	8.004	8.00	3.996	3.997	3.997	2.001	12.54	67115	5350
		238	Nov-21-14	16	Core_2	0	0	0	0	7.992	8.014	8.041	8.02	3.996	3.994	3.995	2.006	12.53	73960	5900
		239	Nov-21-14	16	Core_3	0	0	0	0	8.089	8.096	8.014	8.07	3.993	4	3.997	2.018	12.54	78520	6259
		240	Nov-21-14	16	Core_4	0	1	0	1	8.015	7.997	8.006	8.01	3.995	3.995	3.995	2.004	12.53	82145	6553
		241	Nov-21-14	16	Core_5	1	1	0	1	8.023	8.006	7.998	8.01	3.994	3.998	3.996	2.004	12.54	70530	5624
		242	Nov-21-14	16	Core_6	0	2	0	2	8.005	7.983	7.994	7.99	3.998	3.997	3.998	2.000	12.55	77790	6198
		243	Nov-21-14	16	Core_7	0	2	0	2	8.1	8.08	8.079	8.09	3.993	3.996	3.995	2.024	12.53	73210	5842
		244	Nov-21-14	16	Core_8	0	1	0	1	7.992	7.996	8.005	8.00	4.001	3.998	4.000	2.000	12.56	78815	6273
	In-Place Cylinders	245	Nov-21-14	16	InCyl_1	0	0	3	0	8.049	8.069	8.09	8.07	4.009	3.992	4.001	2.017	12.57	87300	6945
		246	Nov-21-14	16	InCyl_2	2	0	0	0	8.005	8.005	8.004	8.00	4.007	4.006	4.007	1.998	12.61	88480	7018
		247	Nov-21-14	16	InCyl_3	0	0	2	0	8.057	8.072	8.067	8.07	3.967	4.039	4.003	2.015	12.59	93670	7443
		248	Nov-21-14	16	InCyl_4	0	0	0	0	8.03	8.055	8.034	8.04	4.009	3.995	4.002	2.009	12.58	95820	7617
		249	Nov-21-14	16	InCyl_5	1	0	1	0	7.996	8.033	8.04	8.02	3.987	4.02	4.004	2.004	12.59	93840	7454
		250	Nov-21-14	16	InCyl_6	0	0	0	0	8.005	8.062	8.081	8.05	4.007	4.006	4.007	2.009	12.61	87930	6975
		251	Nov-21-14	16	InCyl_7	1	0	0	0	8.046	8.062	8.038	8.05	4.029	3.987	4.008	2.008	12.62	87100	6904
		252	Nov-21-14	16	InCyl_8	1	1	0	1	8.004	8.004	8.022	8.01	4.005	4.007	4.006	2.000	12.60	84530	6707

Table A.3: Companion, Core, and In-Place Cylinders' Compressive Strength Test Results, Part 7

			COMPRESSIVE STRENGTH TESTING (ASTM C 39 / AASHTO T 22)																		PAD USE	PAD DUROMETER
			DATE	Age of Conc at testing	GROUP/SAMPLE ID NUMBER	Roughness		Perpendicularity		HEIGHT				DIAMETER				CROSS-SECTIONAL AREA	LOAD	STRENGTH		
						mm	mm	mm	mm	inch				inch				in^2	lbs.	psi		
			-	day	-	Top	Bot	Top	Bot	1	2	3	Ave	1	2	Ave	L/D	Ave	-	-	-	-
SLAB R13	Companion	253	Nov-18-14	14	Comp_1	1	4	2	2	8.073	8.032	8.071	8.06	4.029	4.021	4.025	2.002	12.72	39535	3107	36	60
		254	Nov-18-14	14	Comp_2	2	1	3	1	8.088	8.057	8.097	8.08	4.022	4.023	4.023	2.009	12.71	39595	3116	37	60
		255	Nov-18-14	14	Comp_3	2	2	0	0	8.025	8.041	8.02	8.03	4.036	4.014	4.025	1.995	12.72	37400	2939	38	60
		256	Nov-18-14	14	Comp_4	1	3	0	1	12.063	12.125	12.125	12.10	5.973	6.001	5.987	2.022	28.15	77760	2762	25	60
		257	Nov-18-14	14	Comp_5	2	2	0	2	12.031	12.031	12.063	12.04	6.015	6.012	6.014	2.002	28.40	83840	2952	26	60
	Cores	258	Nov-20-14	16	Core_1	1	0	2	0	8.046	8.027	8.007	8.03	3.992	3.99	3.991	2.011	12.51	37485	2996	42	60
		259	Nov-20-14	16	Core_2	1	0	3	0	8.002	8.066	8.038	8.04	3.991	3.996	3.994	2.012	12.53	36520	2916	43	60
		260	Nov-20-14	16	Core_3	1	0	2	0	7.985	8.013	8.022	8.01	3.998	3.989	3.994	2.005	12.53	33640	2686	44	60
		261	Nov-20-14	16	Core_4	0	0	0	3	7.975	8.052	8.038	8.02	3.989	3.989	3.989	2.011	12.50	35210	2817	45	60
		262	Nov-20-14	16	Core_5	0	0	3	0	8.019	7.95	7.945	7.97	3.993	3.99	3.992	1.997	12.51	36545	2921	46	60
		263	Nov-20-14	16	Core_6	0	0	2	0	8	8.046	8.045	8.03	3.998	3.991	3.995	2.010	12.53	36755	2933	47	60
		264	Nov-20-14	16	Core_7	1	0	1	0	7.98	7.982	7.989	7.98	3.991	3.998	3.995	1.999	12.53	33435	2668	48	60
		265	Nov-20-14	16	Core_8	0	0	2	0	8.055	8.058	8.02	8.04	3.99	3.988	3.989	2.017	12.50	35885	2871	49	60
	In-Place Cylinders	266	Nov-20-14	16	InCyl_1	1	0	0	0	8	8	7.982	7.99	4.004	3.991	3.998	2.000	12.55	37215	2965	50	60
		267	Nov-20-14	16	InCyl_2	0	0	0	0	7.905	7.912	7.907	7.91	4.004	3.984	3.994	1.980	12.53	35330	2820	51	60
		268	Nov-20-14	16	InCyl_3	2	0	0	0	8.02	8.039	8.059	8.04	3.985	4.008	3.997	2.012	12.54	35300	2814	52	60
		269	Nov-20-14	16	InCyl_4	0	0	0	0	7.959	7.966	7.963	7.96	4.006	4.012	4.009	1.986	12.62	39610	3138	53	60
		270	Nov-20-14	16	InCyl_5	0	0	1	0	8.009	8.07	8.063	8.05	4	3.999	4.000	2.012	12.56	36320	2891	54	60
		271	Nov-20-14	16	InCyl_6	1	0	0	0	8.028	8.001	7.997	8.01	4.003	3.992	3.998	2.003	12.55	37640	2999	55	60
		272	Nov-20-14	16	InCyl_7	1	0	1	1	8.021	8.036	8.025	8.03	4.017	4.002	4.010	2.002	12.63	39235	3107	56	60
		273	Nov-20-14	16	InCyl_8	2	0	1	1	8.006	7.999	7.996	8.00	4.009	3.993	4.001	2.000	12.57	37635	2993	57	60
SLAB R14	Companion	274	Nov-24-14	14	Comp_1	2	1	0	0	8.052	8.042	8.082	8.06	4.146	4.03	4.088	1.971	13.13	38880	2962	75	60
		275	Nov-24-14	14	Comp_2	3	1	2	0	8.007	8.089	8.11	8.07	4.029	4.015	4.022	2.006	12.70	37995	2991	76	60
		276	Nov-24-14	14	Comp_3	2	1	1	0	8.096	8.132	8.106	8.11	4.044	4.03	4.037	2.009	12.80	38140	2980	77	60
		277	Nov-24-14	14	Comp_4	2	0	1	1	12.125	12	12	12.04	6.005	5.996	6.001	2.007	28.28	85855	3036	29	60
		278	Nov-24-14	14	Comp_5	2	1	1	0	12.063	12.125	12.094	12.09	6.009	6.008	6.009	2.013	28.35	83225	2935	30	60
	Cores	279	Nov-26-14	16	Core_1	0	0	1	1	7.965	7.972	7.977	7.97	3.993	3.984	3.989	1.999	12.49	36420	2915	1	60
		280	Nov-26-14	16	Core_2	0	0	1	0	8.001	7.992	7.992	8.00	3.996	3.984	3.990	2.004	12.50	39445	3155	2	60
		281	Nov-26-14	16	Core_3	0	0	0	0	7.918	7.919	7.932	7.92	3.994	3.996	3.995	1.983	12.53	39295	3135	3	60
		282	Nov-26-14	16	Core_4	0	0	0	0	7.929	7.925	7.94	7.93	3.993	3.993	3.993	1.986	12.52	37505	2995	4	60
		283	Nov-26-14	16	Core_5	0	0	0	1	7.954	7.933	7.943	7.94	3.996	3.996	3.996	1.988	12.54	36005	2871	5	60
		284	Nov-26-14	16	Core_6	0	0	1	1	7.92	7.918	7.924	7.92	3.996	3.997	3.997	1.982	12.54	39805	3173	6	60
		285	Nov-26-14	16	Core_7	0	0	1	1	7.953	7.945	7.954	7.95	3.995	3.995	3.995	1.990	12.53	38275	3053	7	60
		286	Nov-26-14	16	Core_8	0	0	2	0	7.951	7.962	7.97	7.96	3.996	3.997	3.997	1.992	12.54	39410	3142	8	60
	In-Place Cylinders	287	Nov-26-14	16	InCyl_1	1	0	3	0	8.1	8.05	8.048	8.07	3.986	4.017	4.002	2.016	12.58	40220	3198	9	60
		288	Nov-26-14	16	InCyl_2	2	0	3	0	8.093	8.158	8.111	8.12	3.995	4.012	4.004	2.028	12.59	39160	3111	10	60
		289	Nov-26-14	16	InCyl_3	1	0	2	0	8.077	8.094	8.128	8.10	4.05	3.989	4.020	2.015	12.69	43165	3402	11	60
		290	Nov-26-14	16	InCyl_4	3	2	2	0	8.121	8.145	8.103	8.12	4.016	4.05	4.033	2.014	12.77	40230	3149	12	60
		291	Nov-26-14	16	InCyl_5	1	0	2	1	8.026	8.039	8.023	8.03	4.002	3.994	3.998	2.008	12.55	41095	3274	13	60
		292	Nov-26-14	16	InCyl_6	2	0	1	0	8.072	8.055	8.065	8.06	4.033	3.975	4.004	2.014	12.59	41770	3317	14	60
		293	Nov-26-14	16	InCyl_7	2	0	0	1	8.073	8.039	8.117	8.08	4.009	4	4.005	2.017	12.59	40720	3233	15	60
		294	Nov-26-14	16	InCyl_8	0	0	0	0	8.0625	8.0938	-	8.08	3.966	4.033	4.000	2.020	12.56	40205	3200	16	60

Table A.3: Companion, Core, and In-Place Cylinders' Compressive Strength Test Results, Part 8

			COMPRESSIVE STRENGTH TESTING (ASTM C 39 / AASHTO T 22)																		
			DATE	Age of Conc at testing	GROUP/SAMPLE ID NUMBER	Roughness		Perpendicularity		HEIGHT				DIAMETER				CROSS-SECTIONAL AREA	LOAD	STRENGTH
						mm	mm	mm	mm	inch				inch				in^2	lbs.	psi
			-	day	-	Top	Bot	Top	Bot	1	2	3	Ave	1	2	Ave	L/D	Ave	-	-
SLAB R16	Companion	316	Dec-08-14	14	Comp_1	1	2	0	1	8.03	8.008	8.025	8.02	4.014	3.989	4.002	2.004	12.58	34020	2705
		317	Dec-08-14	14	Comp_2	2	2	1	1	8.044	8.039	8.043	8.04	4.001	4.006	4.004	2.009	12.59	33405	2654
		318	Dec-08-14	14	Comp_3	1	1	0	1	8.005	8.033	8.06	8.03	4.028	4	4.014	2.001	12.65	33890	2678
		319	Dec-08-14	14	Comp_4	1	2	1	2	12.125	12.094	12.063	12.09	5.99	5.964	5.977	2.023	28.06	74860	2668
		320	Dec-08-14	14	Comp_5	-	-	-	-	12.031	11.969	11.969	11.99	5.996	5.968	5.982	2.004	28.10	67230	2392
	Cores	321	Dec-08-14	16	Core_1	1	0	1	1	8.019	8.01	8.022	8.02	4.005	4	4.003	2.003	12.58	25775	2049
		322	Dec-08-14	16	Core_2	3	0	1	2	8.02	8.018	8.002	8.01	3.995	3.998	3.997	2.005	12.54	26320	2098
		323	Dec-08-14	16	Core_3	0	0	0	1	8.073	8.074	8.073	8.07	3.995	3.994	3.995	2.021	12.53	25370	2024
		324	Dec-08-14	16	Core_4	3	0	0	0	7.996	8.004	7.99	8.00	4.001	3.996	3.999	2.000	12.56	23685	1886
		325	Dec-08-14	16	Core_5	0	0	3	1	7.984	7.994	7.988	7.99	3.994	3.997	3.996	1.999	12.54	26430	2108
		326	Dec-08-14	16	Core_6	1	0	3	0	8.016	8.004	8.015	8.01	3.999	3.999	3.999	2.003	12.56	27675	2203
		327	Dec-08-14	16	Core_7	0	0	1	1	8.081	8.06	8.067	8.07	3.997	4	3.999	2.018	12.56	26795	2134
		328	Dec-08-14	16	Core_8	0	1	1	2	8.041	8.032	8.04	8.04	3.999	4.004	4.002	2.009	12.58	27465	2184
	In-Place Cylinders	329	Dec-08-14	16	InCyl_1	2	0	2	0	8.059	8.008	8.038	8.04	4.002	4.005	4.004	2.007	12.59	31055	2467
		330	Dec-08-14	16	InCyl_2	1	2	2	0	8.013	8.04	8.041	8.03	3.977	4.029	4.003	2.006	12.59	32910	2615
		331	Dec-08-14	16	InCyl_3	3	0	1	0	8.013	8.017	8.019	8.02	3.993	4.011	4.002	2.003	12.58	31560	2509
		332	Dec-08-14	16	InCyl_4	2	0	1	0	8.1	8.093	8.091	8.09	3.991	4.016	4.004	2.022	12.59	33195	2637
		333	Dec-08-14	16	InCyl_5	2	0	1	0	8.013	8.029	8.055	8.03	4.002	4.024	4.013	2.002	12.65	32650	2581
		334	Dec-08-14	16	InCyl_6	2	0	1	1	8.022	8.011	8.028	8.02	3.987	4.018	4.003	2.004	12.58	33670	2676
		335	Dec-08-14	16	InCyl_7	1	0	1	0	8.043	8.108	8.06	8.07	3.997	4.024	4.011	2.012	12.63	35375	2800
		336	Dec-08-14	16	InCyl_8	1	0	2	0	8.044	8.069	8.115	8.08	4.035	4.017	4.026	2.006	12.73	35235	2768
SLAB R15B	Companion	337	Feb-04-15	14	Comp_1	1	0	0	0	8	8	8	8.00	3.9688	3.9375	3.953	2.024	12.27	44245	3605
		338	Feb-04-15	14	Comp_2	1	1	1	0	8	7.9688	7.9375	7.97	3.9375	3.9375	3.938	2.024	12.18	43430	3567
		339	Feb-04-15	14	Comp_3	1	0	1	1	8	7.9688	8	7.99	4	3.9375	3.969	2.013	12.37	40820	3300
		340	Feb-04-15	14	Comp_4	2	0	0	1	12.125	12.125	12.094	12.11	5.9688	6	5.984	2.024	28.13	95890	3409
		341	Feb-04-15	14	Comp_5	2	0	2	0	12.25	12.125	12	12.13	6	5.9688	5.984	2.026	28.13	93770	3334
	Cores	342	Feb-06-15	16	Core_1	1	0	0	0	8	7.9688	7.9688	7.98	4	4	4.000	1.995	12.57	34610	2754
		343	Feb-06-15	16	Core_2	1	0	1	0	7.9688	8	8	7.99	3.9688	3.9688	3.969	2.013	12.37	39415	3186
		344	Feb-06-15	16	Core_3	1	0	1	0	8	8	7.9688	7.99	4	4	4.000	1.997	12.57	38440	3059
		345	Feb-06-15	16	Core_4	1	0	2	0	8	7.9375	7.9375	7.96	3.969	3.9688	3.969	2.005	12.37	38340	3099
		346	Feb-06-15	16	Core_5	1	0	1	0	7.9375	8	7.9688	7.97	3.969	3.9688	3.969	2.008	12.37	36460	2947
		347	Feb-06-15	16	Core_6	1	0	0	0	7.9375	7.9375	7.9375	7.94	4	3.9688	3.984	1.992	12.47	36580	2934
		348	Feb-06-15	16	Core_7	1	0	1	0	8.125	8.125	7.9688	8.07	3.969	3.9688	3.969	2.034	12.37	33565	2713
		349	Feb-06-15	16	Core_8	1	0	1	0	7.9688	7.9688	8	7.98	4	3.9688	3.984	2.003	12.47	37675	3022
	In-Place Cylinders	350	Feb-06-15	16	InCyl_1	1	0	0	0	8.0625	8.0313	8.0625	8.05	4	4	4.000	2.013	12.57	46170	3674
		351	Feb-06-15	16	InCyl_2	1	0	0	0	8.0313	8.0313	8	8.02	4	4	4.000	2.005	12.57	45580	3627
		352	Feb-06-15	16	InCyl_3	2	0	1	0	8.0313	8.0625	8.0313	8.04	4	4	4.000	2.010	12.57	47440	3775
		353	Feb-06-15	16	InCyl_4	2	0	2	0	8.0313	8.0313	8.0625	8.04	4.0313	3.9688	4.000	2.010	12.57	44670	3555
		354	Feb-06-15	16	InCyl_5	1	0	1	0	8.0313	7.9688	8.0625	8.02	4	3.9688	3.984	2.013	12.47	46110	3698
		355	Feb-06-15	16	InCyl_6	1	0	2	0	8	8.0313	8.0625	8.03	4	4	4.000	2.008	12.57	45900	3653
		356	Feb-06-15	16	InCyl_7	2	0	2	0	8.0625	8.0313	8.0625	8.05	3.9688	4	3.984	2.021	12.47	45065	3614
		357	Feb-06-15	16	InCyl_8	0	0	0	1	8	8	8	8.00	4	4	4.000	2.000	12.57	44240	3521

Table A.3: Companion, Core, and In-Place Cylinders' Other Test Results, Part 1

			PAD USE	PAD DUROMETER	TYPE OF BREAK	WEIGHT OF CYLINDER (grams)	DENSITY (lbs/ft³)	Frequency (Hz)	$E_{d,long}$ (ksi)	Visual Inspection before compressive strength test	General Observations
			-	-	-	-					
SLAB R1	Companion	1	20	60	5	3829.2	143.0				
		2	21	60	3	3833.2	143.3				
		3	22	60	3	3820.2	142.5				
		4	4	60	2	12768.6	142.1				
		5	5	60	5	12810.1	144.8				
	Cores	6	23	60	2	3651.3	138.2	8.96E+03	4368.6	Some of the cores had the upper edge (0.75") slightly distorted to one side, up to 5 mm. This is due to the movement of the drill at the beginning of the coring.	
		7	24	60	1	3674.8	138.9	9.09E+03	4514.5		
		8	25	60	4	3636.3	137.7	8888.3722	4282.9		
		9	26	60	2	3634.4	139.0	9045.0202	4396.3		
		10	27	60	1	3645	138.1	8929.1863	4315.0		
		11	28	60	3	3657.7	138.4	9043.3536	4457.4		
		12	29	60	1	3627.2	137.4	8852.5193	4250.7		
		13	30	60	3	3618.1	137.9	9065.8537	4406.0		
	In-Place Cylinders	14	31	60	3	3766.8	139.4	9.27E+03	4679.2		
		15	32	60	3	3758	140.2	9275.0214	4663.1		
		16	33	60	3	3758.1	139.7	9306.6882	4727.7		
		17	34	60	2	3716.6	138.3	9232.5212	4572.1		
		18	35	60	5	3741.2	139.3	9278.3547	4600.0		
		19	36	60	5	3759	140.5	9160.0208	4534.2		
		20	37	60	3	3739.3	140.0	9215.0211	4586.6		
		21	38	60	1	3745.9	139.6	9200.8543	4547.5		
SLAB R2	Companion	22	39	60	3	3915.7	143.47726		0		
		23	40	60	1	3919	145.8		0		
		24	41	60	NaN	3940	145.9		0		Cylinder deformed and was not tested.
		25	6	60	5	13108.4	147.2		0		
		26	7	60	5	13132.5	146.4		0		
	Cores	27	42	60	1	3710.4	142.3	9.20E+03	4593.8		
		28	43	60	2	3739.6	142.5	9.11E+03	4572.7		
		29	44	60	2	3718.1	142.0	9070.0407	4492.7		
		30	45	60	5	3703.7	142.3	9166.7083	4541.4		
		31	46	60	2	3724.7	142.1	9146.7081	4574.8		
		32	47	60	3	3710.5	142.8	9230.0423	4608.0		
		33	48	60	2	3729.4	142.0	9270.0427	4719.5		
		34	49	60	2	3737.4	143.1	9280.0428	4705.5		
	In-Place Cylinders	35	50	60	2	3864.5	143.6	9.26E+03	4798.4		
		36	51	60	1	3860.6	142.1	9240.0424	4788.2		
		37	52	60	1	3882.3	143.1	9210.0421	4778.9		
		38	53	60	1	3926.7	143.9	9180.0418	4812.3		
		39	54	60	4	3851.5	143.3	9330.0433	4810.6		
		40	55	60	3	3921.6	143.1	9250.0425	4845.7		
		41	56	60	3	3876.7	143.2	9280.0428	4817.8		
		42	57	60	5	3864.9	146.7	9440.0444	4965.9		

Table A.3: Companion, Core, and In-Place Cylinders' Other Test Results, Part 2

			PAD USE	PAD DUROMETER	TYPE OF BREAK	WEIGHT OF CYLINDER (grams)	DENSITY (lbs/ft³)	Frequency (Hz)	$E_{d,long}$ (ksi)	Visual Inspection before compressive strength test	General Observations
			-	-	-	-					
SLAB R3	Companion	43	58	60	2	3947.2	146.8		0		
		44	59	60	1	3925	146.8		0		
		45	60	60	2	3927.8	146.2		0		
		46	8	60	2	13232.8	148.9		0		
		47	9	60	5	13156.2	147.6		0		
	Cores	48	61	60	5	3696.2	142.6	9.39E+03	4749.3		
		49	62	60	1	3762.1	146.0	9.31E+03	4741.6		
		50	63	60	4	3732.9	143.7	9290.0429	4709.5		
		51	64	60	1	3726.6	143.0	9280.0428	4702.6		
		52	65	60	3	3705.5	143.1	9280.0428	4655.0		
		53	66	60	4	3759.8	143.5	9240.0424	4727.0		
		54	67	60	4	3792.3	144.9	9330.0433	4853.7		
		55	68	60	2	3735.4	143.4	9270.0427	4704.7		
	In-Place Cylinders	56	69	60	2	3910.3	144.3	9.43E+03	5085.5		
		57	70	60	2	3934.4	144.2	9390.0439	5086.5		
		58	71	60	1	3917.2	143.6	9373.3771	5078.3		
		59	72	60	4	3998.8	147.4	9326.7099	5133.9		
		60	73	60	1	3903.9	143.2	9370.0437	5077.9		
		61	74	60	3	3915.6	143.4	9310.0431	4974.2		
		62	75	60	1	3855.9	144.5	9606.7127	5100.0		
		63	76	60	1	3826.3	144.5	9590.0459	5019.4		
SLAB R4	Companion	64	77	60	5	3941.3	146.8801		0		
		65	78	60	3	3966	146.2		0		
		66	79	60	5	3963.1	146.6		0		
		67	-	-	-	-	NaN		NaN		
		68	10	60	5	13194.8	149.2		0		
	Cores	69	80	60	3	3735.7	147.7	9.59E+03	5117.3		
		70	81	60	3	3742.9	144.0	9.50E+03	4937.4		
		71	82	60	2	3754.4	144.3	9473.3781	4961.6		
		72	83	60	3	3751.8	144.0	9450.0445	4921.2		
		73	84	60	2	3727.5	143.8	9386.7105	4834.0		
		74	85	60	2	3806.8	145.7	9416.7108	5004.1		
		75	86	60	1	3748	145.3	9496.7116	5002.4		
		76	87	60	2	3767.4	143.9	9460.0446	4946.3		
	In-Place Cylinders	77	88	60	1	3867.1	141.9	9.44E+03	5039.4		
		78	89	60	2	3855.4	141.9	9443.3778	4974.2		
		79	90	60	2	3842.6	141.4	9370.0437	4893.9		
		80	91	60	1	3879.8	142.4	9360.0436	4929.9		
		81	92	60	1	3899.6	143.6	9610.0461	5228.9		
		82	93	60	1	3892.7	143.3	9470.0447	5076.9		
		83	94	60	3	3854.2	142.4	9473.3781	5046.5		
		84	95	60	1	3870.2	142.9	9400.044	4984.3		

Table A.3: Companion, Core, and In-Place Cylinders' Other Test Results, Part 3

			PAD USE	PAD DUROMETER	TYPE OF BREAK	WEIGHT OF CYLINDER (grams)	DENSITY (lbs/ft³)	Frequency (Hz)	$E_{d,long}$ (ksi)	Visual Inspection before compressive strength test	General Observations
			-	-	-	-					
SLAB R5	Companion	85	1	60	3	3885.6	144.12072		0	Cracked in middle of test	
		86	2	60	4	3863.1	148.1		0		
		87	3	60	4	3882.6	147.9		0		
		88	11	60	5	12953	143.2		0		
		89	12	60	5	13003.64	145.5		0		
	Cores	90	4	60	1	3659.3	142.9	9.22E+03	4437.6	d = rebar location top surface to top of rebar = 1.92 in	
		91	5	60	5	3731.4	143.2	9.04E+03	4449.1	d = 2.16	
		92	6	60	5	3756.8	142.6	8890.0389	4405.6	d=2.08	
		93	7	60	5	3745.4	142.5	8886.7055	4382.3	d=2.15	
		94	8	60	3	3769.6	143.4	8990.0399	4493.3	d=2.19	
		95	9	60	2	3756	143.1	8773.3711	4275.1	d=2.31	
		96	10	60	5	3756.7	142.6	8926.7059	4421.1	d=2.34	
		97	11	60	2	3725.5	142.5	8986.7065	4381.4	d=2.04	
	In-Place Cylinders	98	12	60	2	3871.1	142.6	9.20E+03	4815.6		
		99	13	60	3	3874.4	141.9	9140.0414	4709.4	Required grinding on one face to fit into end cap	
		100	14	60	2	3821.4	141.5	9290.0429	4747.6		
		101	15	60	5	3872.4	143.9	9260.0426	4868.9		
		102	16	60	2	3841.8	142.6	9450.0445	4892.9		
		103	17	60	2	3842.7	142.0	9260.0426	4771.8		
		104	18	60	1	3916	144.0	9290.0429	4970.5		
		105	19	60	2	3812.3	142.9	9340.0434	4836.7		
SLAB R6	Companion	106	20	60	3	3906.4	146.40003		0		
		107	21	60	5	3926.3	149.2		0		
		108	22	60	5	3933.3	148.8		0		
		109	13	60	Exp	13142.1	151.2		0		
		110	14	60	5	13054.5	148.2		0		
	Cores	111	23	60	2	3849.1	146.7	9.25E+03	4846.0		
		112	24	60	2	3752	143.5	9.43E+03	4871.8		
		113	25	60	3	3795.8	146.7	9220.0422	4660.0		
		114	26	60	3	3838	146.8	9303.3764	4850.4		
		115	27	60	2	3869.4	147.4	9166.7083	4777.1		
		116	28	60	2	3839.9	146.5	9193.3753	4751.1		
		117	29	60	2	3860.3	146.7	9286.7095	4880.4		
		118	30	60	2	3865.3	147.0	9383.3772	4991.5		
	In-Place Cylinders	119	31	60	3	3912.6	144.4	9.49E+03	5108.2		
		120	32	60	2	3867	145.6	9620.0462	5237.7		
		121	33	60	2	3859.9	144.4	9550.0455	5078.8		
		122	34	60	3	3947.8	145.5	9450.0445	5129.1		
		123	35	60	3	3941	146.5	9420.0442	5184.5		
		124	36	60	2	3907.2	144.6	9490.0449	5088.0		
		125	37	60	4	3956.4	145.9	9480.0448	5162.4		
		126	38	60	2	3869.5	145.7	9500.045	5045.2		

Table A.3: Companion, Core, and In-Place Cylinders' Other Test Results, Part 4

			PAD USE	PAD DUROMETER	TYPE OF BREAK	WEIGHT OF CYLINDER (grams)	DENSITY (lbs/ft³)	Frequency (Hz)	$E_{d,long}$ (ksi)	Visual Inspection before compressive strength test	General Observations
			-	-	-	-					
SLAB R7	Companion	127	39	60	4	3898.1	144.15715		0		
		128	40	60	5	3888.4	143.1		0		
		129	41	60		3904.8	143.0		0		
		130	15	60	5	13353.4	149.3		0		
		131	16	60	4	13266.4	149.6		0		
	Cores	132	42	60	2	3876.4	147.9	9.60E+03	5223.5		
		133	43	60	2	3867.2	148.3	9.49E+03	5060.3		
		134	44	60	3	3879.4	147.2	9500.045	5144.3		
		135	45	60	2	3862	147.6	9613.3795	5224.9		
		136	46	60	1	3859.9	147.2	9426.7109	5019.3		
		137	47	60	2	3894.4	147.5	9506.7117	5174.7	Elongated void by rebar	
		138	48				NaN		NaN	Not used	
		139	49	60	2	3890.8	147.8	9390.0439	5047.6		
	In-Place Cylinders	140	50	60	2	3940.8	149.6	9.35E+03	4996.7		measured diameters: 3.853 and 3.797
		141	51	60	2	3926.1	147.8	9260.0426	4927.7		measured diameters: 3.829 and 3.836
		142	52	60	2	3878.5	145.1	9440.0444	5089.2		measured diameters: 4.017 and 4.015
		143	53	60	2	3920.8	149.5	9390.0439	4997.2		measured diameters: 3.857 and 3.822
		144	54	60	3	3873.1	147.2	9440.0444	5002.7		measured diameters: 3.827 and 3.833
		145	55	60	2	3814.5	143.6	9450.0445	4986.5		measured diameters: 4.037 and 4.005
		146	56	60	3	3929.6	149.4	9360.0436	4990.0		measured diameters: 3.686 and 3.827
		147	57	60	2	3880.3	148.4	9380.0438	4920.3	Bottom surface wire exposed	measured diameters: 3.835 and 3.795
SLAB R8	Companion	148	58	60	3	3951.2	143.9		0		
		149	59	60	5	3936.6	145.5		0		
		150	60	60	2	3945.2	142.9		0		
		151	17	60	1	13132.9	147.0		0	Fractured twice during compression test	*Fractured twice during compression test
		152	18	60	3	13190.1	147.5		0		
	Cores	153	61	60	5	3868.5	146.1	9.40E+03	5014.4		
		154	62	60	5	3813.7	144.7	8.92E+03	4468.4	Did not completely fracture	Did not completely fracture, machine stopped
		155	63	60	5	3840.6	145.8	9300.043	4858.8		
		156	64	60	3	3834	144.9	9000.04	4600.5		
		157	65	60	3	3827.2	144.9	9163.375	4709.0		
		158	66	60	3	3838.1	145.5	9210.0421	4766.1		
		159	67	60	3	3852.2	145.3	9150.0415	4761.4		
		160	68	60	3	3819.6	145.6	9350.0435	4891.1		
	In-Place Cylinders	161	69	60	2	3882.1	143.9	9.44E+03	5003.9		
		162	70	60	2	3957.5	145.0	9400.044	5097.0		
		163	71	60	3	3923.5	143.9	9510.0451	5206.8		
		164	72	60	2	3889.4	144.6	9590	5180.8		
		165	73	60	2	3945.9	144.3	9430.0443	5128.8		
		166	74	60	5	3887.6	143.9	9460.0446	5042.5		
		167	75	60	2	3898.8	144.0	9530.0453	5133.6		
		168	76	60	2	3976.7	145.5	9480.0448	5189.3		

Table A.3: Companion, Core, and In-Place Cylinders' Other Test Results, Part 5

			PAD USE	PAD DUROMETER	TYPE OF BREAK	WEIGHT OF CYLINDER (grams)	DENSITY (lbs/ft³)	Frequency (Hz)	$E_{d,long}$ (ksi)	Visual Inspection before compressive strength test	General Observations
			-	-	-	-					
SLAB R9	Companion	169	77	60	1	3875.7	144.8		0	Some companion cylinders with visible porosity	
		170	78	60	3	3861.1	144.1		0		
		171	79	60	5	3788.1	141.9		0		
		172	19	60	5	12760.1	143.6		0		
		173	20	60	5	12760.7	143.8		0		
	Cores	174	80	60	5	3781.6	142.3	9.38E+03	4859.3		
		175	81	60	Exp	3797.1	142.5	9.51E+03	4995.6		
		176	82	60	2	3755.5	142.2	9460.0446	4879.9		
		177	83	60	3	3737.8	142.9	9600.046	4948.4		
		178	84	60	4	3781.9	142.6	9380.0438	4853.6		
		179	85	60	Exp	3773.5	141.7	9380.0438	4832.5		
		180	86	60	3	3753.6	141.7	9530.0453	4886.6		
		181	87	60	4	3757.2	143.6	9560.0456	4959.4		
	In-Place Cylinders	182	88	60	4	3899.8	140.5	9.22E+03	4858.2		
		183	89	60	5	3835.3	140.0	9250.0425	4747.1		
		184	90	60	2	3847.6	141.3	9300.043	4823.3		
		185	91	60	5	3837.3	141.8	9250.0425	4808.0		
		186	92	60	4	3829	140.9	9380.0438	4889.0		
		187	93	60	2	3851.1	142.3	9230.0423	4820.8		
		188	94	60	2	3843.6	142.6	9320.0432	4888.4		
		189	95	60	5	3807.3	141.3	9430.0443	4922.9		
SLAB R10	Companion	190	96	60	4	3940.5	146.5		0		
		191	97	60	5	3911.8	145.2		0		
		192	98	60	1	3962.9	146.2		0		
		193	21	60	Exp	13159.6	145.2		0		Specimen exploded.
		194	22	60	5	13183.2	146.7		0		
	Cores	195	1	60	2	3866.1	146.9	9.80E+03	5450.6		
		196	2	60	Exp	3844.5	146.7	9.77E+03	5371.3		
		197	3	60	Exp	3799.9	146.1	9850.0485	5345.8		Core 2 started the new pads; specimen exploded
		198	4	60	1	3823	145.8	9676.7134	5235.2	At 1.5" a 1/2" void	
		199	5	60	3	3821.1	146.4	9750.0475	5290.7	At 1.25" a 1/4" void; At 1.9" a 1/2" void	
		200	6	60	5	3825.1	145.8	9710.0471	5252.9	At 3" a 1.5" void	Unplugged Forney power supply
		201	7	60	5	3810.1	144.9	9590.0459	5133.7	At 1.1" a 1/2" void; at 2.5" a 1" void	
		202	8	60	5	3919.5	148.1	9780.0478	5527.4	At 3" a 1" void; at 3.25" a 1" void	The side with voids failed quickly
	In-Place Cylinders	203	9	60	Exp	3977	146.6	9.71E+03	5503.9	At 7" a 1/2" void	Specimen exploded.
		204	10	60	2	4039.3	146.1	9630.0463	5518.0		
		205	11	60	3	4027.6	146.5	9700.047	5482.1		
		206	12	60	3	4001.2	146.7	9690.0469	5528.6	At 7" a 3/4" void	Load did not hold
		207	13	60	3	4062.7	146.3	9530.0453	5445.2	Oblong deformation from mold	
		208	14	60	Exp	4062.3	146.7	9580.0458	5517.4		Specimen exploded.
		209	15	60	3	3952	145.7	9770.0477	5480.5	At 5.25" a 1/2" void	
		210	16	60	2	3975	146.0	9680.0468	5475.3		

Table A.3: Companion, Core, and In-Place Cylinders' Other Test Results, Part 6

			PAD USE	PAD DUROMETER	TYPE OF BREAK	WEIGHT OF CYLINDER (grams)	DENSITY (lbs/ft³)	Frequency (Hz)	$E_{d,long}$ (ksi)	Visual Inspection before compressive strength test	General Observations
			-	-	-	-					
SLAB R11	Companion	211	17	60	1	4024.2	145.92079		0		
		212	18	60	3	3970.7	146.2		0		
		213	19	60	1	4033.2	145.8		0		
		214	23	60	5	13114.8	146.4		0		
		215	24	60	5	13117.6	147.6		0		
	Cores	216	20	60	3	3830.8	144.3	9.54E+03	5122.2		
		217	21	60	2	3835.7	144.1	9.56E+03	5174.2		
		218	22	60	2	3842	144.7	9500.045	5110.1		
		219	23	60	5	3844.7	145.1	9560.0456	5163.7		
		220	24	60	3	3852.6	145.7	9730.0473	5336.9		
		221	25	60	2	3810.5	144.5	9630.0463	5150.4		
		222	26	60	2	3841.1	144.2	9540.0454	5157.0		
		223	27	60	2	3842.9	144.8	9610.0461	5222.9		
	In-Place Cylinders	224	28	60	5	3911.1	142.3	9.90E+03	5455.8		
		225	29	60	3	3927.1	146.4	9830.0483	5526.7		
		226	30	60	Exp	4015.1	147.0	9790.0479	5655.9		
		227	31	60	2	3955.3	146.2	9710.0471	5476.2		
		228	32	60	5	3970.4	146.3	9780.0478	5540.6		
		229	33	60	3	3993.8	146.0	9800.048	5558.7		
		230	34	60	3	4002.9	147.2	9830.0483	5634.5		
		231	35	60	2	3994.8	145.2	9690.0469	5448.1		
SLAB R12	Companion	232	39	60	1	3747	141.4487		0		
		233	40	60	Exp	3756.3	141.8		0		
		234	41	60	Exp	3746.6	142.1		0		
		235	27	60	Exp	12905.9	143.4		0		
		236	28	60	5	12890.2	143.1		0		
	Cores	237	58	60	2	3645.9	138.5	9.20E+03	4493.4		
		238	59	60	5	3652	138.5	9.23E+03	4547.6	1/2 inch void 2 inches down the top	
		239	60	60	5	3671.7	138.2	9340.0434	4704.4		
		240	61	60	3	3663.2	139.1	9293.3763	4615.4		
		241	62	60	5	3572.6	135.5	9340.0434	4546.0		
		242	63	60	5	3619.7	137.4	9310.0431	4564.4		
		243	64	60	5	3632.7	136.6	9263.376	4594.3		
		244	65	60	5	3656.1	138.6	9240.0424	4538.8		
	In-Place Cylinders	245	66	60	Exp	3696.6	138.8	9.38E+03	4765.8		
		246	67	60	Exp	3704.2	139.8	9360.0436	4706.3		
		247	68	60	Exp	3723.7	139.8	9360.0436	4775.3		
		248	69	60	Exp	3697.5	139.3	9410.0441	4779.7		
		249	70	60	5	3706	139.8	9390.0439	4756.8		
		250	71	60	5	3740.2	140.4	9370.0437	4788.8		
		251	72	60	5	3742	140.4	9453.3779	4872.7		
		252	73	60	5	3666.1	138.3	9420.0442	4722.2		

Table A.3: Companion, Core, and In-Place Cylinders' Other Test Results, Part 7

			PAD USE	PAD DUROMETER	TYPE OF BREAK	WEIGHT OF CYLINDER (grams)	DENSITY (lbs/ft³)	Frequency (Hz)	$E_{d,long}$ (ksi)	Visual Inspection before compressive strength test	General Observations
			-	-	-	-					
SLAB R13	Companion	253	36	60	3	3658.5	135.92386		0	Edge on bottom is worn down a bit	
		254	37	60	5	3713.4	137.8		0		
		255	38	60	2	3693.8	137.7		0		
		256	25	60	5	12583.1	140.7		0		
		257	26	60	5	12540	139.7		0		
	Cores	258	42	60	2	3534.2	134.1	8.42E+03	3669.2	1/2 inch void at 1 inch from top	
		259	43	60	2	3567.4	135.0	8.40E+03	3688.3		
		260	44	60	5	3551.6	134.9	8516.7018	3761.3		
		261	45	60	5	3550.7	134.9	8470.0347	3734.6		
		262	46	60	5	3483.5	133.0	8366.7003	3548.2		
		263	47	60	5	3487.3	132.0	8236.699	3462.8		
		264	48	60	5	3487.2	132.8	8376.7004	3560.6		
		265	49	60	5	3516	133.2	8160	3442.0		
	In-Place Cylinders	266	50	60	5	3648.4	138.5	8.76E+03	4073.1		
		267	51	60	5	3558.8	136.8	8680.0368	3865.6		
		268	52	60	5	3568	134.8	8603.3694	3865.8		
		269	53	60	5	3661.3	138.8	8790.0379	4075.9		
		270	54	60	5	3633.4	136.9	8590.0359	3922.5		
		271	55	60	5	3622.2	137.3	8636.703	3938.0		
		272	56	60	5	3657.2	137.5	8656.7032	3979.8		
		273	57	60	3	3600.4	136.4	8700.037	3960.8		
SLAB R14	Companion	274	75	60	2	3680.7	132.56628		0		
		275	76	60	3	3678.6	136.7		0		
		276	77	60	5	3701.9	135.8		0		
		277	29	60	3	12234.7	136.9		0		
		278	30	60	3	12297.6	136.6		0		
	Cores	279	1	60	3	3451	132.0	8.40E+03	3548.5		
		280	2	60	3	3489.2	133.0	8.44E+03	3630.0		
		281	3	60	3	3401.3	130.5	8660.0366	3682.7		
		282	4	60	3	3494	134.0	8396.7006	3563.8		
		283	5	60	3	3470	132.7	8326.6999	3480.6		
		284	6	60	3	3486.8	133.7	8660.0366	3771.3		
		285	7	60	3	3501.1	133.8	8410.0341	3587.5	chipped in bottom edge because of coring	
		286	8	60	3	3491.6	133.2	8313.3665	3497.9		
	In-Place Cylinders	287	9	60	5	3640	136.7	8.46E+03	3816.6		
		288	10	60	2	3653.7	136.2	8400.034	3798.6		
		289	11	60	5	3676.4	136.3	8440.0344	3818.2		
		290	12	60	2	3703.9	136.0	8370.0337	3768.7		
		291	13	60	3	3604.9	136.2	8510.0351	3813.9		
		292	14	60	3	3606.2	135.3	8400.034	3722.2		
		293	15	60	3	3653.5	136.8	8476.7014	3845.0		
		294	16	60	5	3639.8	136.6	8440.0344	3807.9		

Table A.3: Companion, Core, and In-Place Cylinders' Other Test Results, Part 8

			PAD USE	PAD DUROMETER	TYPE OF BREAK	WEIGHT OF CYLINDER (grams)	DENSITY (lbs/ft³)	Frequency (Hz)	$E_{d,long}$ (ksi)	Visual Inspection before compressive strength test	General Observations
			-	-	-	-					
SLAB R16	Companion	316	37	60	4	3616	136.56577		0		
		317	38	60	4	3593	135.2		0		
		318	39	60	5	3586.6	134.4		0		
		319	33	60	5	12242.6	137.4		0		
		320	34	60	5	12220.9	138.2		0		
	Cores	321	40	60	5	3583.1	135.3	8.20E+03	3506.4		
		322	41	60	5	3563.6	135.1	8.25E+03	3539.0		
		323	42	60	5	3566.7	134.3	8036.697	3389.8		
		324	43	60	5	3506.8	133.0	8103.3644	3349.5		
		325	44	60	5	3574.3	135.9	8300.033	3583.5		
		326	45	60	5	3544.9	134.2	8190.0319	3464.3		
		327	46	60	5	3568.4	134.2	8026.6969	3374.5		
		328	47	60	5	3592.8	135.4	8260.0326	3578.5		
	In-Place Cylinders	329	48	60	5	3634.9	136.9	8.36E+03	3700.7		
		330	49	60	5	3616.3	136.3	8410.0341	3728.2		
		331	50	60	5	3638.5	137.5	8400.034	3737.0		
		332	51	60	5	3668.6	137.2	8310.0331	3720.9		
		333	52	60	5	3639.7	136.5	-	#VALUE!		
		334	53	60	5	3654.4	138.0	8523.3686	3865.4		
		335	54	60	5	3648.6	136.3	8466.7013	3816.5		
		336	55	60	3	3648	135.2	-	#VALUE!		
SLAB R15B	Companion	337	56	60	5	3654.2	141.778		0		
		338	57	60	5	3660.9	143.7		0		
		339	58	60	5	3650.3	140.7		0		
		340	35	60	5	12515	139.9		0		
		341	36	60	5	12509	139.7		0		
	Cores	342	59	60	5	3603	136.9	8.57E+03	3834.9		
		343	60	60	5	3638.9	140.3	8.65E+03	4016.5		
		344	61	60	5	3583	136.0	8536.702	3791.9		
		345	62	60	5	3623.3	140.2	8613.3695	3949.9		
		346	63	60	5	3567.8	137.9	8380.0338	3686.3		
		347	64	60	5	3635.9	140.0	8533.3687	3849.8		
		348	65	60	5	3630.4	138.5	8416.7008	3833.4		
		349	66	60	3	3658.6	140.1	8516.7018	3879.0		
	In-Place Cylinders	350	67	60	3	3655.4	137.6	8.64E+03	3993.7		
		351	68	60	2	3647	137.8	8690.0369	4015.1		
		352	69	60	5	3689.3	139.1	8770.0377	4147.6		
		353	70	60	5	3677.5	138.6	8696.7036	4065.5		
		354	71	60	4	3691.6	140.6	8750.0375	4152.9		
		355	72	60	4	3684.6	139.1	8690.0369	4061.8		
		356	73	60	3	3656.6	138.8	8740.0374	4120.1		
		357	74	60	5	3662.8	138.8	8653.3699	3988.2		

APPENDIX B: TEMPERATURE RESULTS

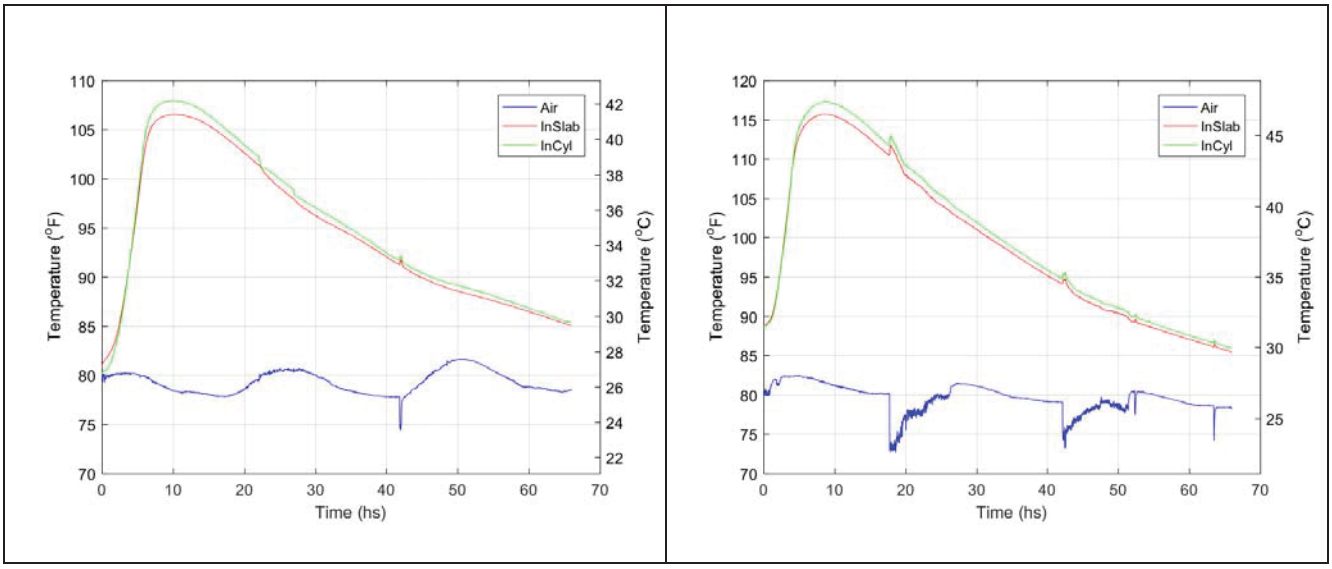

Figure B.1: Temperature monitoring of slab (a) R1 and (b) R2. "Air" corresponds to air temperature. "InSlab" represents slab temperature at mid depth measured by an embedded thermocouple. "InCylinder" represents temperature of an in-place cylinder at mid depth measured by an embedded thermocouple.

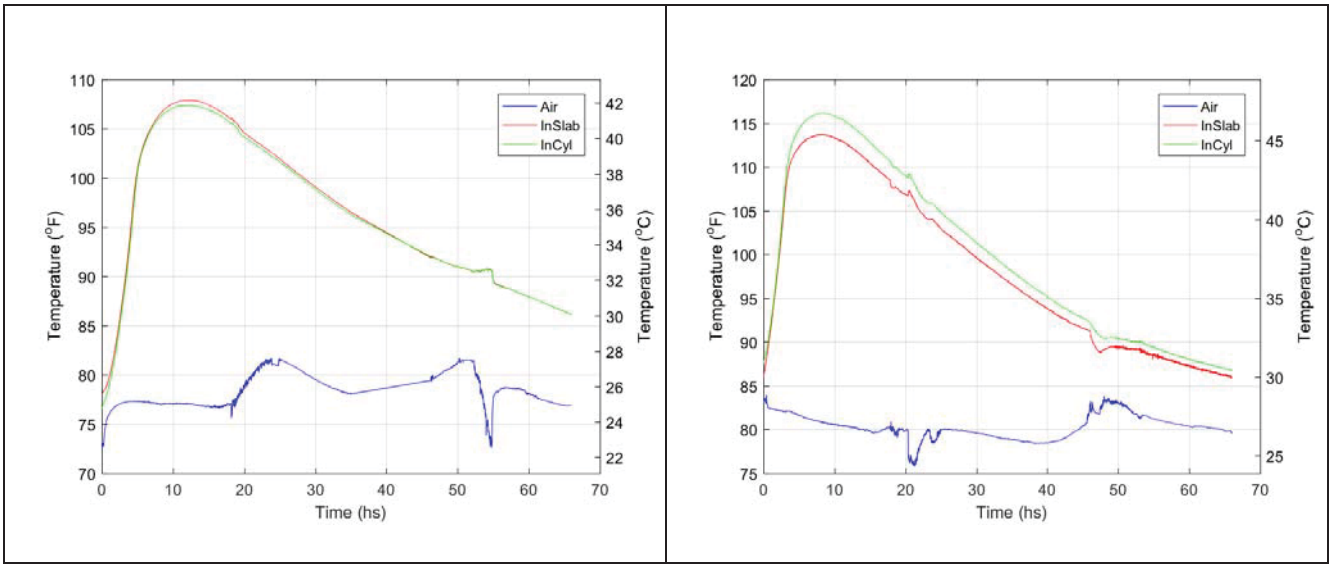

Figure B.2: Temperature monitoring of slab (a) R3 and (b) R4. "Air" corresponds to air temperature. "InSlab" represents slab temperature at mid depth measured by an embedded thermocouple. "InCylinder" represents temperature of an in-place cylinder at mid depth measured by an embedded thermocouple.

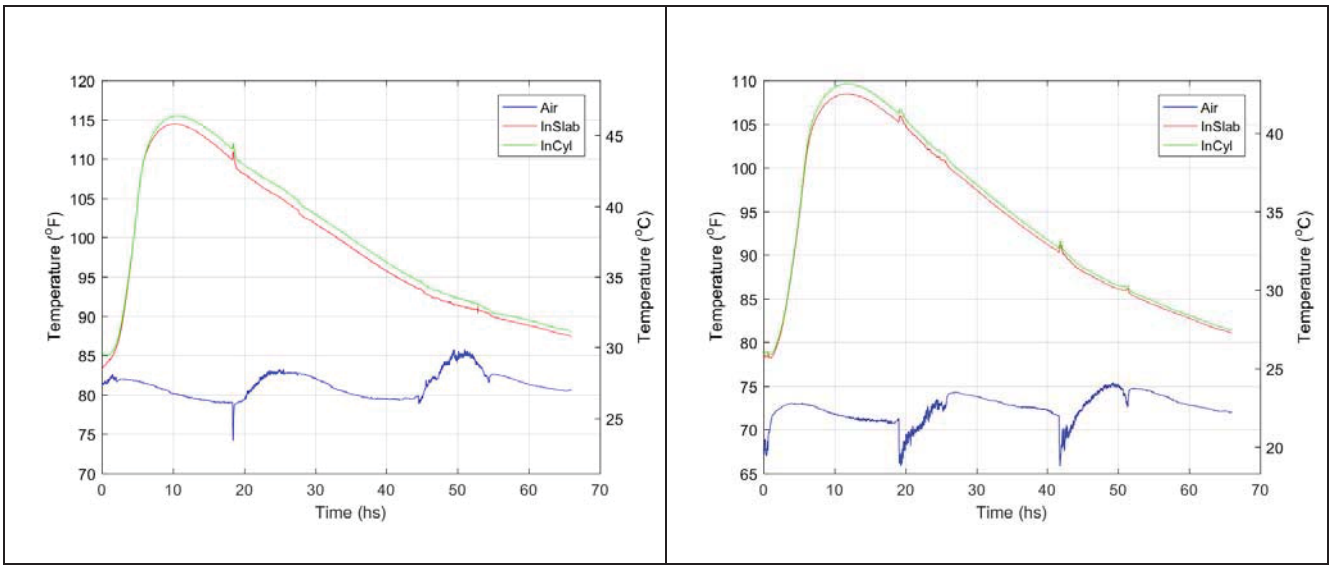

Figure B.3: Temperature monitoring of slab (a) R5 and (b) R6. "Air" corresponds to air temperature. "InSlab" represents slab temperature at mid depth measured by an embedded thermocouple. "InCylinder" represents temperature of an in-place cylinder at mid depth measured by an embedded thermocouple.

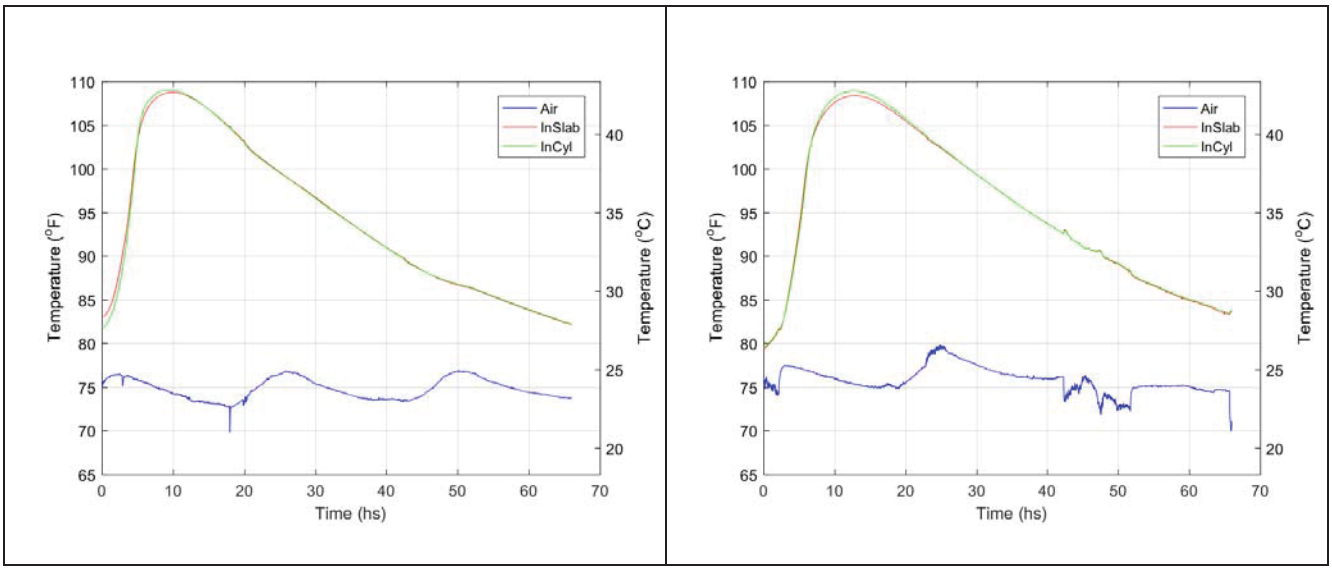

Figure B.4: Temperature monitoring of slab (a) R7 and (b) R8. "Air" corresponds to air temperature. "InSlab" represents slab temperature at mid depth measured by an embedded thermocouple. "InCylinder" represents temperature of an in-place cylinder at mid depth measured by an embedded thermocouple.

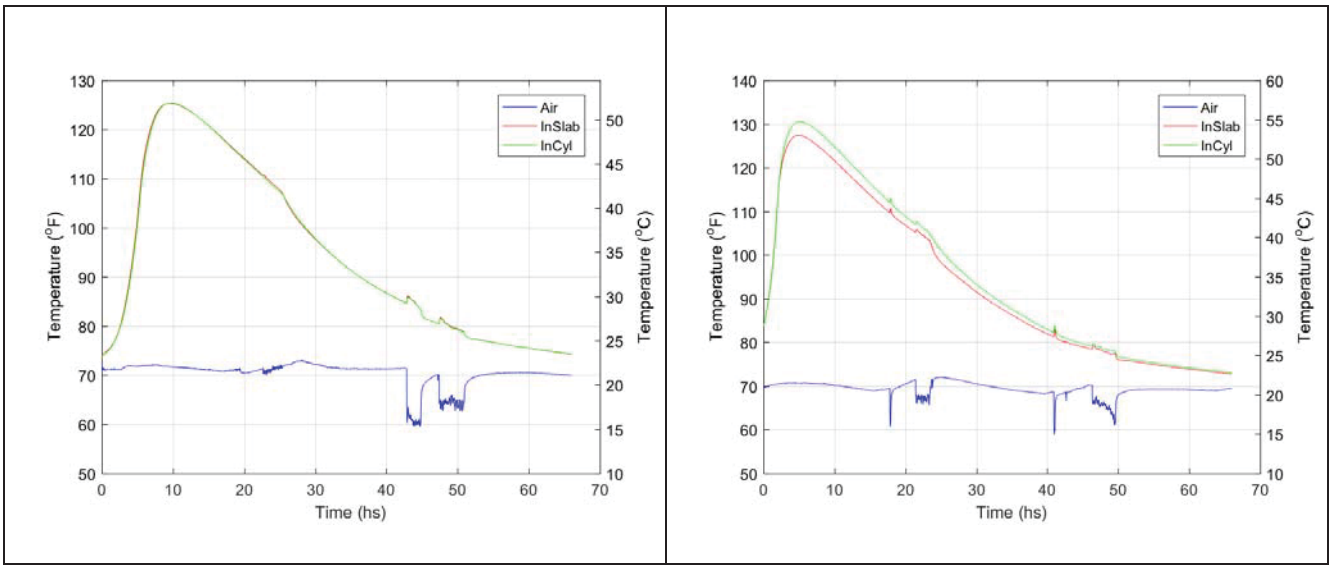

Figure B.5: Temperature monitoring of slab (a) R9 and (b) R10. "Air" corresponds to air temperature. "InSlab" represents slab temperature at mid depth measured by an embedded thermocouple. "InCylinder" represents temperature of an in-place cylinder at mid depth measured by an embedded thermocouple.

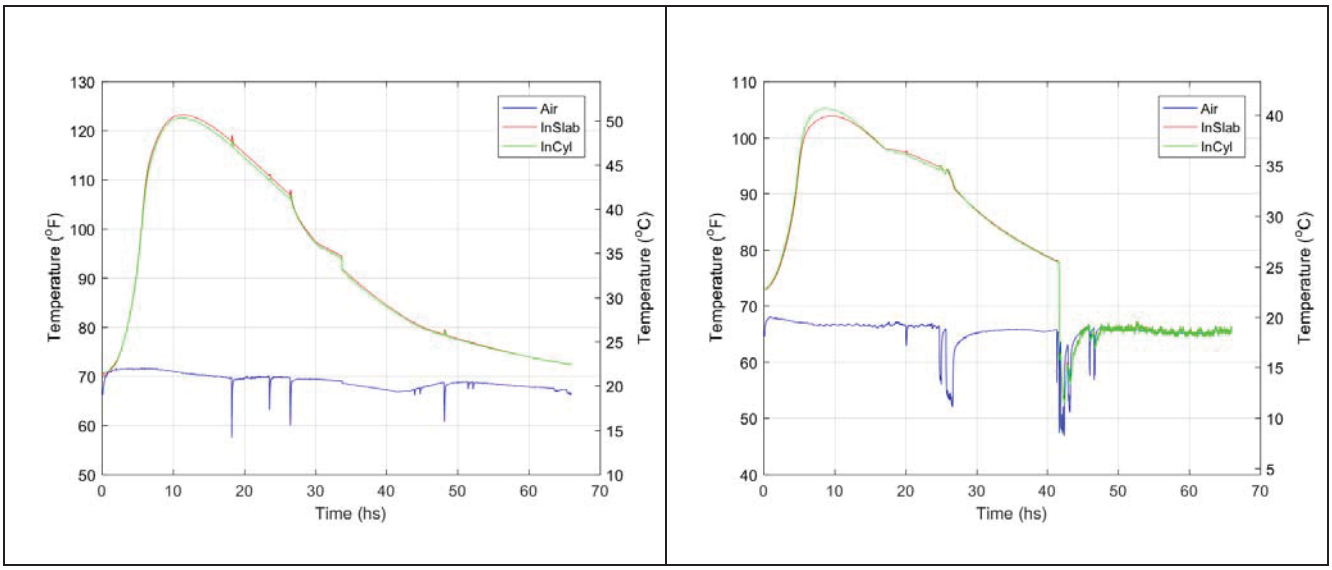

Figure B.6: Temperature monitoring of slab (a) R11 and (b) R12. "Air" corresponds to air temperature. "InSlab" represents slab temperature at mid depth measured by an embedded thermocouple. "InCylinder" represents temperature of an in-place cylinder at mid depth measured by an embedded thermocouple.

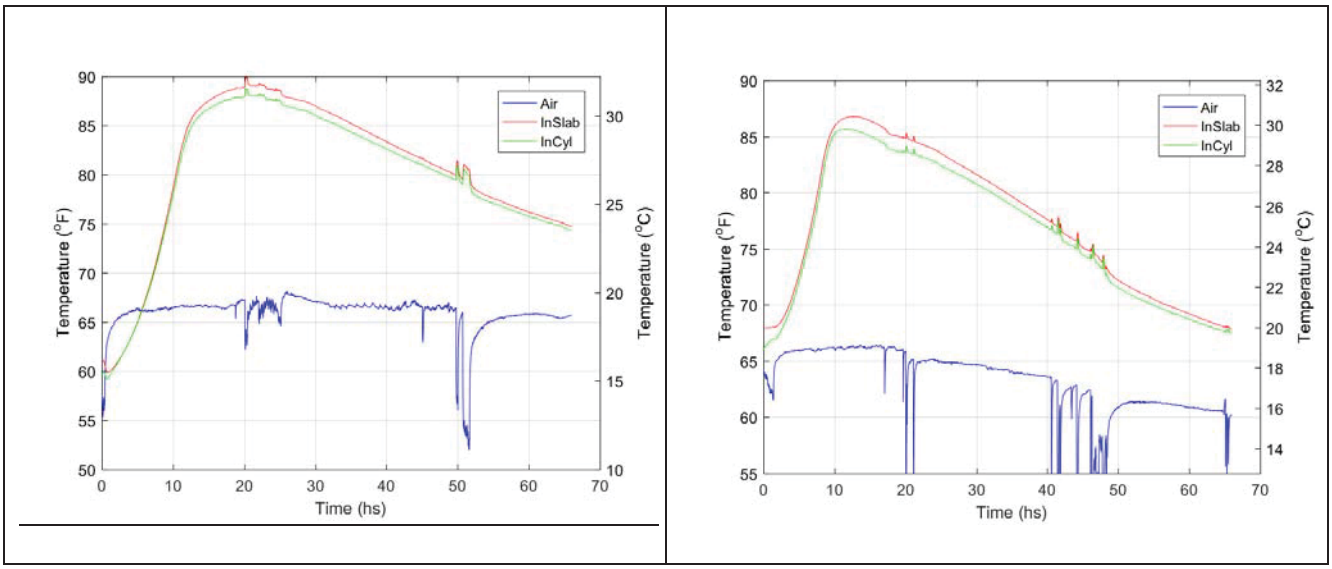

Figure B.7: Temperature monitoring of slab (a) R13 and (b) R14. "Air" corresponds to air temperature. "InSlab" represents slab temperature at mid depth measured by an embedded thermocouple. "InCylinder" represents temperature of an in-place cylinder at mid depth measured by an embedded thermocouple.

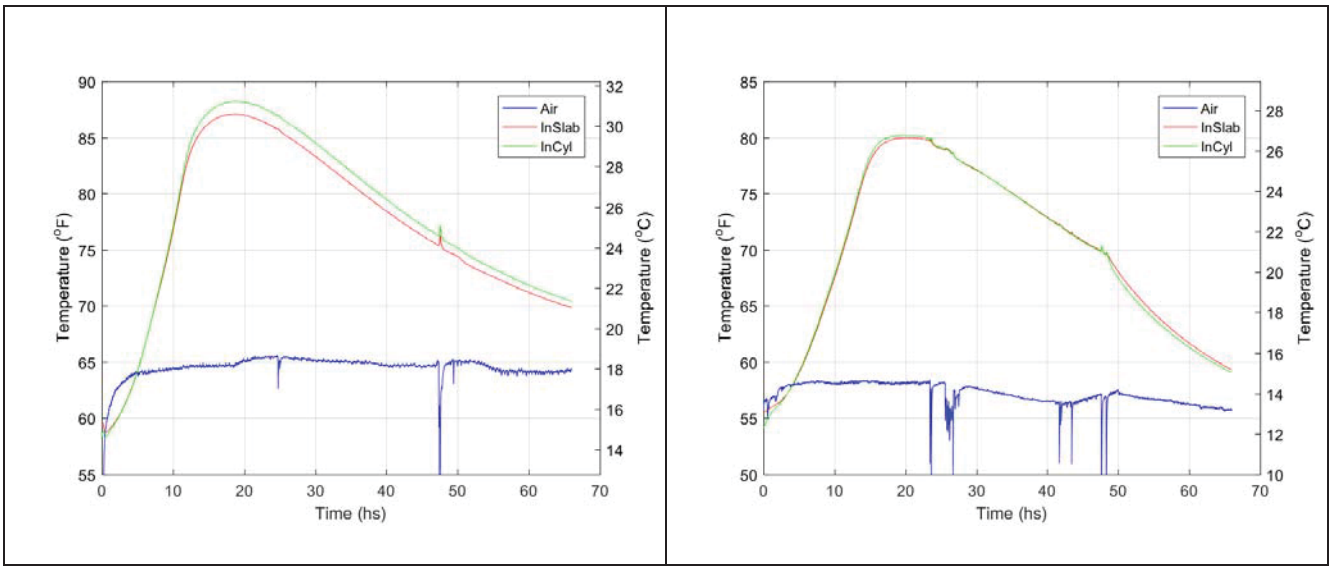

Figure B.8: Temperature monitoring of slab (a) R15B and (b) R16. "Air" corresponds to air temperature. "InSlab" represents slab temperature at mid depth measured by an embedded thermocouple. "InCylinder" represents temperature of an in-place cylinder at mid depth measured by an embedded thermocouple.

APPENDIX C: DENSITY STUDY FOR CONSOLIDATION PROCEDURE ASSESSEMENT

C.1 INTRODUCTION

IDOT's research project "Evaluation of PCC Pavement and Structure Coring and In Situ Testing Alternatives" consists of comparing the strength of cores to in-place cylinders at a certain age in order to identify the inherent damage that coring does to concrete. For this purpose, both kinds of cylinders should have equal or very similar compaction so as to produce equally dense concrete. The objective of this set of experiments was to identify the best vibrating method among several options to ensure similar consolidation between cores and in-place cylinders.

C.2 APPROACH

C.2.1 General

Four compacting methods were tested:

- Rodding
- Internal vibration
- Plastic-mold (external) vibration
- Sleeve (external) vibration

Two slabs were cast, Slab 5 (S5) and Slab 6 (S6). Slab 5 produced eight cores, eight in-place cylinders, and three companion cylinders. Slab 6 produced seven cores, eight in-place cylinders, and three companion cylinders. Companion cylinders are not analyzed in this report. All cores were sawed at the bottom to obtain 4 x 8 in. (10 x 20 cm) cylinders.

Within Slab 5, four of its in-place cylinders were rodded and the rest internally vibrated. Within Slab 6, four of its cylinders were consolidated with the plastic-mold vibration method and the rest with the sleeve vibration method.

Both slabs were cured for 3 days. Cores and in-place cylinders were extracted on the 7th day after casting. After that, they were submerged in water at 73°F (23°C) for 24 hours to achieve saturation. Mass and volume measurements were then taken to calculate density. These measurements were done on the 8th day after casting (Trial 1), and another set of measurements was taken the 14th day after casting (Trial 2). During both trials, all cylinders were maintained submerged in water at 73°F (23°C). All of the following measurements, results, and conclusions refer to Trial 2.

In summary, four different groups of in-place cylinders were tested by comparing their densities to the densities of their corresponding cores.

C.2.2 Density Methods

Two different methods were followed to calculate density.

The first method (geometric) consisted of calculating the volume of the samples by measuring diameter (average of three measurements) and height (average of two measurements), as established in ASTM C39 and AASHTO T22, to obtain an average sample's volume. The mass of each sample was then obtained by weighing the samples in a saturated surface dry (SSD) condition, and densities were calculated by simple division of weight over volume. Diameter was measured by using a clamp-like tool to set the sample diameter at the mid height, and then using a caliper. Height was measured with metric tape.

The second method (submerged method) consisted of calculating the volume samples by weighing the samples submerged, as established in ASTM C39 and AASHTO T22. Thus, the following formula was used to compute the samples' volumes:

$$V = \frac{W - W_s}{\gamma_s} \qquad \text{(C1)}$$

where W is the air weight of the sample, W_s is the submerged weight, and γ_s is the water density. Density was calculated by simple division between W over V.

C.2.3 Rodding Compaction Details

Rodding compaction was done following ASTM C39 and AASHTO T22. All four rodded cylinders were cast and finished outside the formwork and then put inside the form and fixed to the metal bracers. There, each cylinder was filled in two layers. Each layer was rodded 25 times and tapped 10 times. Finishing was done with metal trowel.

C.2.4 Internal Vibration Details

This procedure was done by following the specifications in ASTM C31 and AASHTO T23. Internal vibration was performed with the plastic molds already in position held by the metal bracers. Each cylinder was filled in two layers. Each layer was vibrated by introducing the vibrator into the concrete and holding it for 4 to 5 seconds before slowly removing it. All cylinders´ sleeves were tapped with a rubber mallet 10 times after filling each layer. Finishing was done with metal trowel.

C.2.5 Plastic Mold (External) Vibration

Only one brief reference to external vibration was found in ASTM standards document ASTM C873, which says to "use the vibrator externally, briefly touching the exterior of the mold support member." All four plastic-mold vibrated cylinders were cast and finished outside the formwork and then put inside the formwork fixed to the metal bracers. They were filled in two layers. Each layer was compacted by touching the plastic mold at four equally distributed points of the plastic mold (outer surface of the mold at approximately mid height of the layer), for 4 to 5 seconds per touch. After the four touches were done, each mold was tapped 10 times (each layer).

C.2.6 Sleeve (External) Vibration

Sleeve vibration was performed with the plastic molds already in position held by the metal bracers. Each cylinder was filled in two layers. Each layer was externally vibrated by touching the outer sleeve in three locations equally distributed for 4 to 5 seconds (three rather than four locations were chosen in order to avoid over-vibrating the rest of the slab). In this case, half the slab´s height was filled with concrete, then the first layer of the cylinders was filled and compacted, then the rest of the slab was filled with concrete. Finally, the second layer of the cylinders was filled, vibrated, and finished (see the procedure for Slab 6 below). These cylinders were not tapped.

C.2.7 Vibration of Slab Concrete

The concrete was vibrated using the internal vibrator following recommended practice: the vibrating head was inserted vertically downward into the concrete at a rapid rate but without touching the bottom of the form, and then it was more slowly lifted vertically to the surface (Mindess et al. 2003). The vibrator used generated 14,000 rpm. Thus, its radius of action was estimated to be around 4 in. (10 cm). For 4 in. (10 cm) slump concrete with 6.5% entrained air, the estimated insertion time is 4 to 5 seconds. The vibrator was therefore inserted vertically, at a regular spacing, at 4 to 5 seconds. The insertion spacing was around 6 in. (15 cm), which is 1.5 times the radius of action (Mindess et al. 2003).

C3 PROCEDURE

C.3.1 Slab 5—Rodding and Internal Vibration

- Concrete specifications were checked (slump, air content, and mix design).
- Four cylinders were placed outside the formwork and filled following the rodding method (filled in two layers, rodded 25 times, tapped 10 times, finished, and placed in final position).
- The remaining four cylinders were filled following the internal vibration method (filled in two layers, vibrator introduced, tapped 10 times, and finished).
- The rest of the slab was filled with concrete, vibrated, and finished.

C.3.2 Slab 6—Plastic-Mold (External) Vibration and Sleeve (External) Vibration

- Concrete specifications were checked (slump, air content, and mix design).
- Four cylinders were placed outside the formwork and filled following the plastic-mold vibration method (filled in two layers, externally vibrated by touching the plastic mold at four locations for 5 seconds each, tapped 10 times, finished, and placed in final position).
- Half of the slab was filled.
- The remaining four cylinders were filled to half their height, and the sleeve vibration method was performed.
- The second half of the slab was poured.
- The second layer of the sleeve-vibrated cylinders was filled and vibrated.
- The rest of the slab was vibrated and finished.

C.4 RESULTS

Visual inspection was performed to account for external defects. It was found that two of the rodded cylinders presented poor compaction at the bottom edge. In addition, one of the internally vibrated cylinders presented several superficial air voids, with dimensions of 0.75 in. (2 cm) deep and 0.5 in. (1 cm) diameter; two other internally vibrated cylinders also presented visible voids of the order of 0.5 in. (1 cm) deep and 0.5 in. (1 cm) diameter in several locations.

The Table C.1 presents the density results of the second set of experiments (Trial 2).

Table C.1: Density Results*

	TRIAL 2							
	Geometric Volume Method				Submerged Volume Method			
	Average Density (lb/ft^3)	Relative Difference to Cores (%)	Standard Deviation (lb/ft^3)	CV (std/ave) (%)	Average Density (lb/ft^3)	Relative Difference to Cores (%)	Standard Deviation (lb/ft^3)	CV (std/ave) (%)
Rodded	145.2	0.2	1.0	0.7	145.1	0.2	0.4	0.3
Internally Vibrated	146.1	0.7	0.9	0.6	145.2	0.3	0.3	0.2
Cores_S5	145.0	—	0.6	0.4	144.7	—	0.3	0.2
Plastic Mold	147.9	0.6	1.7	1.1	145.2	0.5	0.3	0.2
Sleeve	147.7	0.5	0.6	0.4	145.1	0.4	0.3	0.2
Cores_S6	147.1	—	0.8	0.5	144.5	—	0.2	0.2

* 1 lb/ft^3 =17.36 kg/m^3

Note: The number of samples tested of each cylinder group were four rodded samples, four internally vibrated samples, eight slab 5 cores (Cores_S5), four plastic-mold vibrated samples, four sleeve-vibrated samples, and seven slab 6 cores (Core_S6).

In Table C.1, average density corresponds to the average density of each group of cylinders, and relative difference to cores corresponds to the relative difference with respect the corresponding cores of the same slab (i.e., rodded and internally vibrated in-place cylinders are compared to Cores_S5, whereas plastic-mold vibrated and sleeve vibrated cylinders are compared to Cores_S6), calculated with the following equation.

$$Rel.Dif = \frac{\rho_{In-Place} - \rho_{core}}{\rho_{core}} \qquad \text{(C2)}$$

Standard deviation corresponds to the standard deviation of each group of cylinders, and CV refers to the coefficient of variation calculated as follows:

$$CV\ (\%) = \frac{StdDev}{Average} \times 100 \qquad \text{(C3)}$$

C.5 SAW-CUTTING AND VISUAL INSPECTION

One cylinder from each group was sawed longitudinally to account for potential segregation. The following figures show these results.

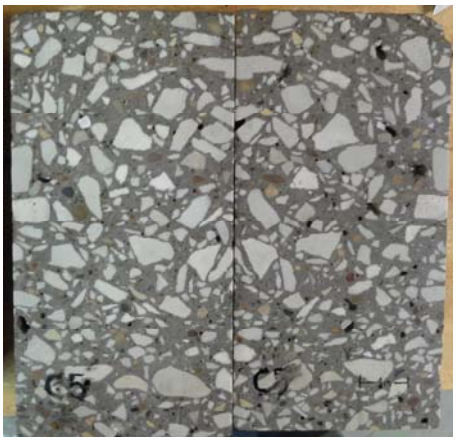

Figure C.1a: Core 5 (Slab 5) sawed

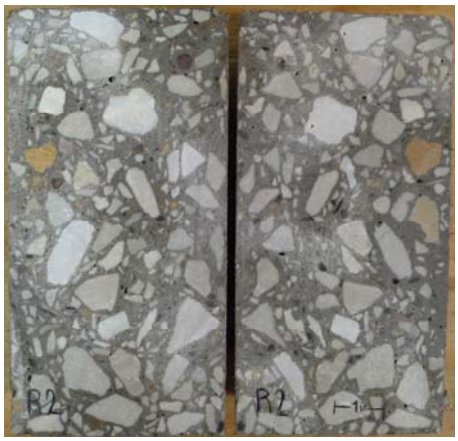

Figure C.1b: Rodded cylinder 2 sawed

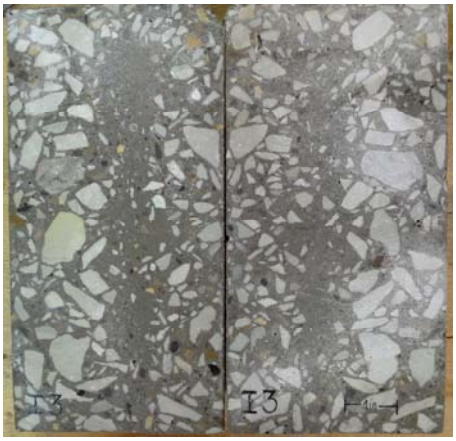

Figure C.1c: Internally vibrated cylinder 3 sawed

Figure C.1b: Core 1 (Slab 6) sawed

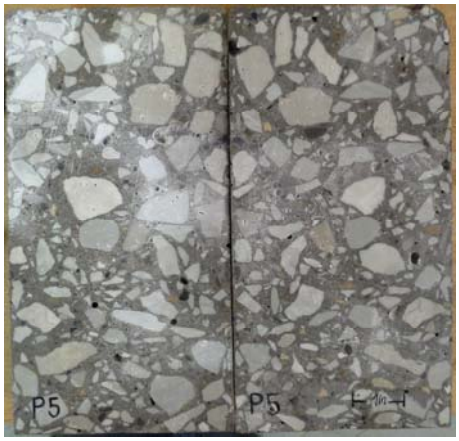

Figure C.1d: Plastic-mold vibrated cylinder 5 sawed

Figure C.1e: Sleeve vibrated cylinder 1 sawed

Figure C.1c shows the internally vibrated cylinder. It can be seen in that figure that the insertion of the vibrator generated segregation: the center of the cylinder did not have coarse aggregate, whereas the outer part of the cylinder had much more.

The other figures do not show clear segregation. Only the sleeve-vibrated cylinder, shown in Figure C.1e, had a 1 in. (2.5 cm) long by 0.1 in. (0.2 cm) wide void/crack. In addition, the transverse middle of that cylinder had a smaller amount of coarse aggregate than did the top and bottom edges.

C.6 ANALYSIS

It should be noted that the submerged volume method is more accurate than the geometric volume method because the former accounts for all superficial anomalies, such as external air voids, open pores, lack of perpendicularity and smoothness at the edges, and variation of diameter along the samples' height. On the other hand, the latter method assumes the cylinders to be perfectly cylindrical and computes the volume from the average of three heights and the average of three diameter measurements at mid height of the sample.

In looking at the submerged volume method section of Table C.1, it can be seen that all standard deviations were very small, yielding coefficients of variation of less than 0.5% in all cases. In addition, the relative difference of rodded and internally vibrated cylinders compared to Cores_S5 was less than 1%; the same relation was observed when comparing relative differences of plastic-mold and sleeve cylinders with respect to Cores_S6.

With the geometric volume method, it can be seen in Table C.1 that although the standard deviations increased a little, the coefficients of variation remained less than or around 1%. Furthermore, the corresponding relative differences of in-place cylinders to cores were also below 1%.

Figures C.2 and C.3 show the average densities of all cylinder groups measured with both methods.

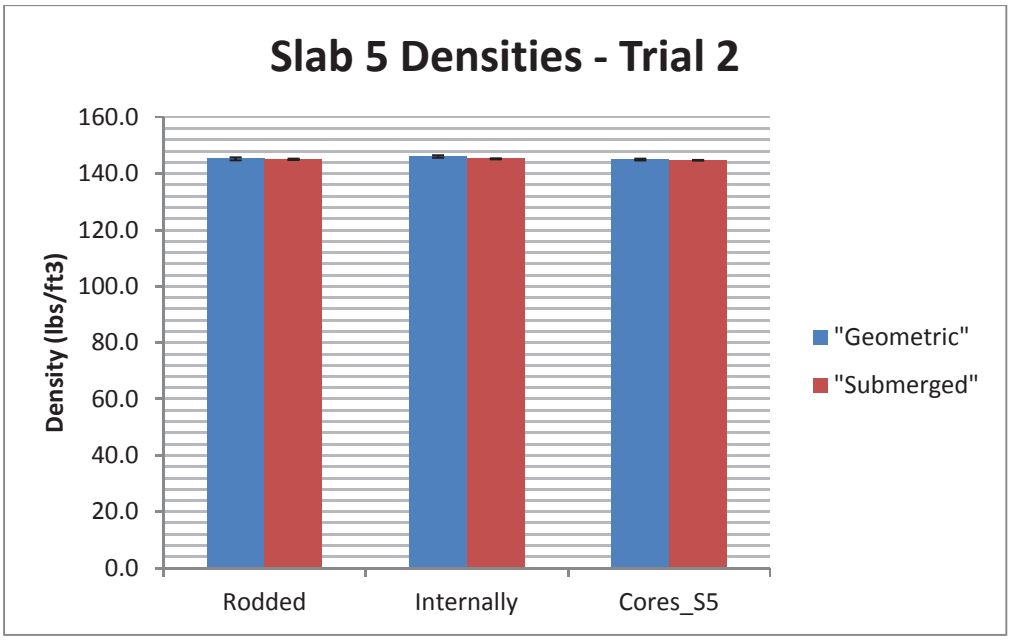

Figure C.2: Densities of Slab 5, Trial 2 (1 lb/ft^3 = 17.36 kg/m^3).

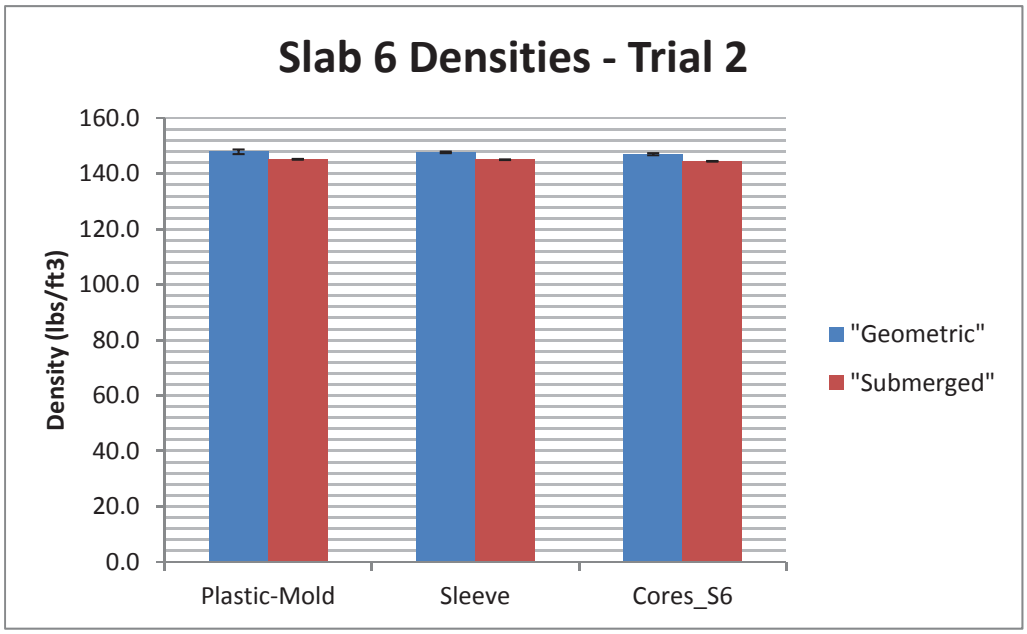

Figure C.3: Densities of Slab 6, Trial 2 (1 lb/ft^3 = 17.36 kg/m^3).

It can be seen in Figures C.2 and C.3 that the error bars were notably small compared to the density values. It can also be seen that densities calculated with the geometric method were larger than the corresponding ones calculated with the submerged method. Table C.2 provides a quantitative analysis of that observation.

Table C.2: Density Averages and Errors (1 ls/ft^3 = 17.36 kg/m^3)

	Geometric Volumetric Method (kg/m^3)	Submerged Volumetric Method (kg/m^3)	Relative Error to Submerged (%)
Rodded	145.2	145.1	0.1
Internal	146.1	145.2	0.6
Cores_S5	145.0	144.7	0.2
Plastic Mold	147.9	145.2	1.9
Sleeve	147.7	145.1	1.8
Cores_S6	147.1	144.5	1.8

where relative error to submerged is the relative error of the geometric method density with respect to the submerged method density, computed as follows:

$$Rel.Dif = \frac{\rho_{Geometric} - \rho_{Submerged}}{\rho_{Submerged}} \qquad \text{(C4)}.$$

It can be seen in Table C.2 that all relative differences are positive—that is, the geometric densities were always higher than the submerged densities. This trend was clearer for Slab 6, with values almost reaching 2%, whereas Slab 5 values were below 0.6% of relative difference. However, in both cases (Slab 5 and Slab 6), the relative difference of the geometric method densities with respect to the submerged method densities was significantly low (below 2% for all cases), which means that the geometric method is sufficiently accurate for this research project because density is not the most important concrete parameter.

However, the systematic density differences between the two methods were opposite the expected trend. The submerged method accounts for the open pores and small external air voids present in concrete; thus, the volume computed by the submerged method tends to be lower than the volume computed by the geometric method. Therefore, the former method tends to yield higher densities than the latter. The results are opposite because of the way volume is measured in the geometric method.

It was explained previously that in the geometric method the diameter was determined by using with a clamp-like tool and measuring the distance of the clamp with a caliper. It was seen that the clamp makes very small notches around 0.04 in. (1 mm) deep at the concrete surface when diameter is being measured. Thus, the diameter obtained tends to be around 0.08 in. (2 mm) smaller than the actual diameter. This systematic experimental error ends up yielding a theoretical difference of up to 4% between the geometric method and submerged method for calculating density.

C.7 CONCLUSIONS

Four consolidating methods were analyzed to identify the best way to compact slab concrete and in-place cylinders as similarly as possible. The analysis was done by comparing the cylinders' densities

using two methods: geometric and submerged. The cylinders comprised six groups, categorized by their nature (core or in-place cylinder) and compacting method (rodded, internally vibrated, plastic mold, sleeve).

When densities were compared by using the submerged method, all four compacting methods showed small relative differences between in-place cylinders and cores densities (less than 0.5%). In addition, all standard deviations for the six groups of cylinders were very small, yielding coefficients of variation less than or equal to 0.3%.

It was also observed that the experimental procedure conducted to measure volume with the geometric method yielded a systematic error that may go up to 4% of the actual density of each sample. The source of this error lay in the tools being used, and it will be changed in further experiments. In addition, the geometric method tended to yield more variable measurements because it did not account for open pores and external voids—nor did it account for variations in diameter and heights throughout the sample. Nevertheless, the geometric method was able to be performed much faster than the submerged method. Therefore, in the future, if measurements are taken with care and using proper tools, the geometric method could yield accurate results.

Visual inspection was done to each cylinder. It was observed that the rodded cylinders tended to be more porous and had fine honey-combing at their bottom edges. Internally vibrated cylinders showed large external air voids at their sides. Cores, plastic-mold vibrated cylinders, and sleeve-vibrated cylinders did not have significant external defects.

One sample cylinder per group was longitudinally sawed and visual inspection performed on the cut surface. It was found that the internally vibrated cylinder had segregation caused by insertion of the vibrator, which pushed the coarse aggregate far from the center and to the lateral surface of the cylinder. The sleeve-vibrated cylinder had a small elongated void and a zone with less aggregate in the middle cross-section; this light segregation could have been caused by the cylinders having been filled in two layers and not being tapped after each layer was vibrated.

Furthermore, it should be noted that the two slabs were vibrated following a systematic pattern of location and time of vibration. This pattern had not been followed with the previous slabs cast for this research project. This fact could have also contributed to the small standard deviations and small relative differences between cylinders and cores. This technique will be maintained for casting further slabs.

APPENDIX D: EXAMPLE OF RANDOM SAMPLING ANALYSIS

D.1 INTRODUCTION

The goal of this appendix is to provide a better explanation of the random sampling analysis. The analysis shows the trends and behavior of compressive strength estimates obtained from core samples with respect to in-place strength obtained from in-place cylinder samples using a statistical basis.

For the analysis described in this report, the 1.05 correction factor was applied to estimate in-place strength from air-dried core strength measurements. Eight cores were extracted from each test slab at day 15 after casting. The in-place strength of each slab was computed as the average of eight in-place cylinders tested at day 16.

The specific purpose of this analysis was to more closely evaluate the error in the estimated strength measurements from core samples using a statistical basis—for example, to understand how estimation error changes with the number of averaged core strength data considered. This appendix reports strength estimation errors using a subset of data—specifically, the cores that were air dried (1-day dry conditioned) and *did not* contain rebar. Those were the cores extracted from slabs R1, R2, R13, and R14. Slabs R1 and R2 had a PV/SI mixture type and R13 and R14 a PV/SI-low mixture type.

Notes:

- In this appendix, the concept of confidence refers to the percentile of a specific dataset and is not exactly the same as the commonly used confidence level defined elsewhere.
- The analysis is based on the absolute value of the strength errors. This means that the strength estimate error (*Str.Est.Err.*) was calculated as follows:

$$Str.Est.Err(\%) = 100 \times \left|\frac{Str.Est. - Avg.IP.Str.}{Avg.IP.Str.}\right| \qquad \text{(D.1)}$$

where *Str.Est.* is the strength estimate, which is computed from (averaged) core strength measurements times 1.05, and *Avg.IP.Str* is the average strength of eight in-place cylinders of a certain slab—here regarded as the actual in-place strength of that slab.

D.2 ANALYTICAL PROCEDURES

Calculations were carried out as explained in Section 4.4, “Random Sampling Analysis,” of the main report. In this case, the NDT method corresponds to core data rather than to NDT data.

D.3 RESULTS FROM CORE SAMPLES WITHOUT REBAR

Figure D.1 presents the expected strength error curves that show how the expected error of the strength prediction varies with an increasing number of tested cores at three confidence levels (75%, 85%, and 95%).

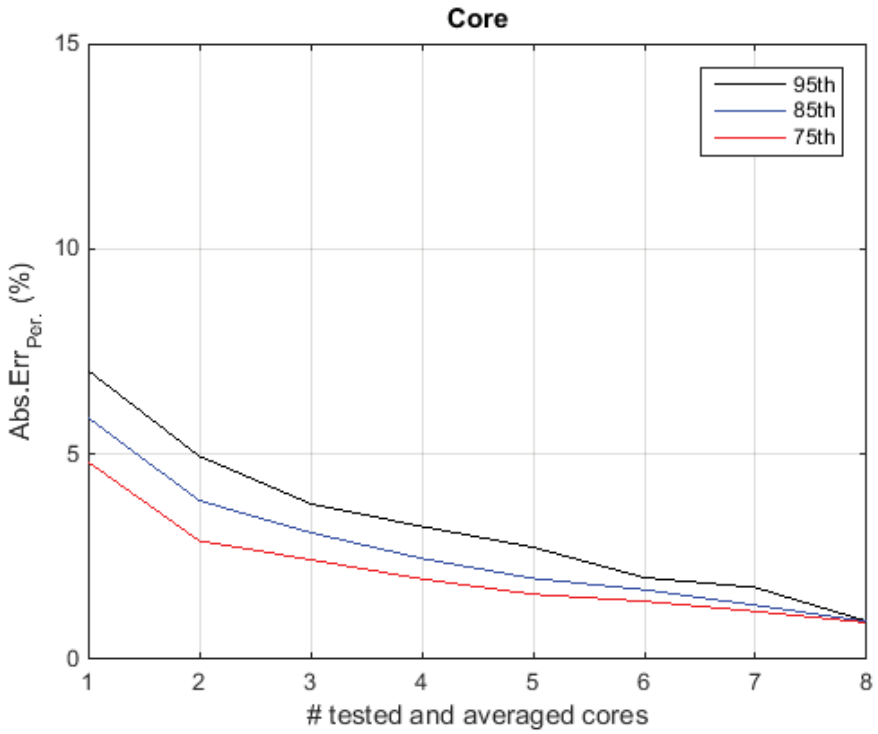

Figure D.1: Expected strength error curves using correction factor 1.05 for air-dried cores with no rebar from PV/SI and PV/SI mixtures (data from slabs R1, R2, R13, and R14).

The x-axis corresponds to the number of tested cores that are used to obtain a single strength measurement. This means that, for a given concrete element cast from a single batch (in this case, emulated with one specific slab), data from either one, two, three, or more cores are considered and averaged to obtain one single core strength value. The 1.05 correction factor is applied to the value to yield the strength estimate of the in-place concrete.

First consider only the black curve in Figure D.1. That line corresponds to the 95% confidence level, meaning that the y-axis corresponds to the 95th percentile expected strength error of the estimation in absolute value. Considering that the black line at x = 1 gives y ≈ 7% (meaning that if we were to estimate the in-place strength by using a single core and multiplying its strength by 1.05), there is a 95% chance that the strength estimation will have an error of 7% or lower with respect to the actual in-place strength of the selected slab.

If we now we consider the average of two random cores (see x = 2 in Figure D.1, which corresponds to y ≈ 5%), there is a ~95% chance that the calculated strength estimation would have a 5% error or

lower with respect to the actual in-place strength of the slab. A 95% confidence level is usually required for critical infrastructure (nuclear power plants, hospitals, etc.), but for other structures, such as pavements, lower confidence levels of 75% or 85% would be acceptable. At the 75% confidence level (red line), one random core results in an error of 5% or lower, and the average of three cores provides an error of 2.5% or lower—that is, we expect a 25% chance of having an error higher than 2.5%.

Clearly, the error of the strength estimation drops as more cores are extracted and averaged, assuming we maintain the same confidence level of the results. However, it should be noted that in these computations the concrete batches were clearly identified because each batch corresponds to one single slab. Therefore, when computing the strength average from different cores, only cores within the same batch were considered. In actual field application, this may not be so clear, and different cores could be drawn from different concrete batches, which would not represent the in-place strength of a specific concrete batch. To use these results as guidelines for other applications, strength estimates should come from cores drawn from a single concrete batch. Selection of the required confidence level of the strength estimations should be done by taking into consideration the consequences that may occur if the error in the prediction is higher than the tolerance. As previously noted, for pavements, a 75% to 85% confidence is usually acceptable.

Now consider a different approach to understand the effect of expected error of strength estimations. Figure D.2 presents the histograms created from all the strength estimation errors computed by considering every possible combination of averaged core strength values. These were computed using the same datasets and procedure as explained above. The data in Figure D.1 can be directly obtained by looking at the data shown in Figure D.2.

To understand Figure D.2, first look at the top left subfigure identified as ind = 1. This subfigure represents all the possible strength estimate errors, in absolute value, that are obtained from the experimental dataset. ind = 1 means that only one individual core strength value was used, then the 1.05 factor was applied to that one core to obtain the strength estimate. The percent errors of that estimate with regard to the real in-place strength value of the slab are shown. The other subfigures (ind = 2, ind = 3, etc.) correspond to the computed strength errors when all possible combinations of two, three, or more core strengths are averaged to obtain the strength estimation.

Note that a total of 32 cores were used in this analysis, corresponding to four different slabs with eight cores per slab. In subfigure ind = 1, N = 32 because there are 32 possible values of core strengths when only one core is used. In subfigure ind = 2, N = 112 because there are 112 possible combinations of cores (in all possible combinations of two) from which to take the average and obtain the strength estimate. This means that if we were to randomly select the strength values of two cores, there are 112 possibilities—thus, there are 112 possible estimated strength errors.

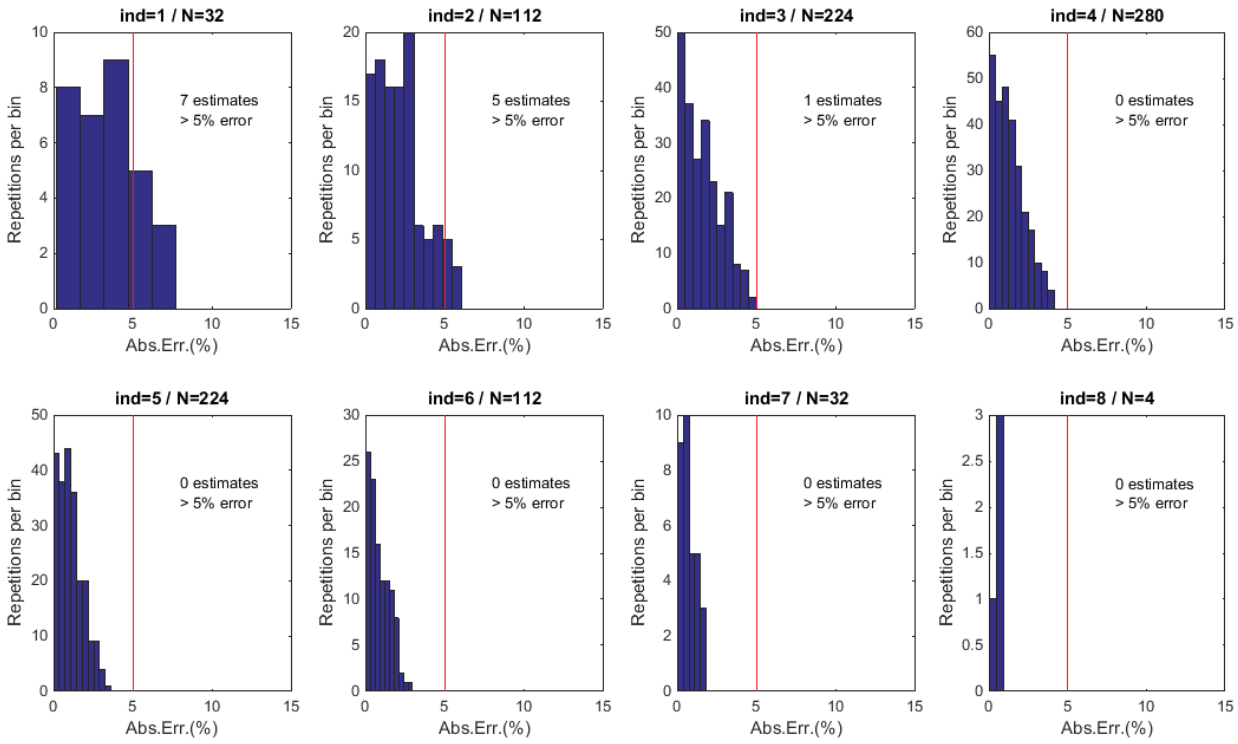

Figure D.2: Histograms of percent error of strength estimations in absolute value using a correction factor of 1.05 considering air-dried cores with no rebar and from PV/SI and PV/SI mixtures only (slabs R1, R2, R13 and R14). "ind" corresponds to the number of averaged core strength values to obtain the strength estimate and "N" is the total size of the dataset. The vertical red line defines the 5% strength error.

Figure D.2 shows the following:

- When strength was estimated using only one core, seven out of 32 possible strength estimates yielded an error higher than 5% (in absolute value); i.e., there is about a 78% chance of obtaining a 5% error or lower.
- When strength was estimated using the average of two cores, five out of 112 possible strength estimates yielded an error higher than 5% (in absolute value); i.e., there is about a 96% chance of obtaining 5% error or lower.
- When strength was estimated using the average of three cores, one out of 224 possible strength estimates yielded an error higher than 5% (in absolute value); i.e., there is a 99.6% chance of obtaining a 5% error or lower.
- When strength was estimated using the average of four or more cores, no estimated strength yielded an error higher than 5%.

D.5 SUMMARY AND DISCUSSION

Table D.1 summarizes the results presented in Figure D.2, which are based on the experimental results carried out in the project for this particular mixture set.

Table D.1: Results

		Number of cores used to estimate strength							
		1	2	3	4	5	6	7	8
% Data < 5%	A	78	96	100	100	100	100	100	100

When only one core is used to estimate the in-place strength of a concrete batch, at least 70% of the cores resulted in a strength estimate that agrees within 5% of the in-place strength. When the results of two cores were averaged, the estimates improved dramatically; that is, at least 84% of the cores provided a strength estimate that agreed within 5% of the in-place strength. The use of three or more averaged cores improved the strength estimate further—but only marginally.

APPENDIX E: RANDOM SAMPLING ANALYSIS RESULTS OF IN-PLACE STRENGTH ESTIMATED FROM CORES

E.1 EXPECTED ERROR CURVES AND HISTOGRAMS

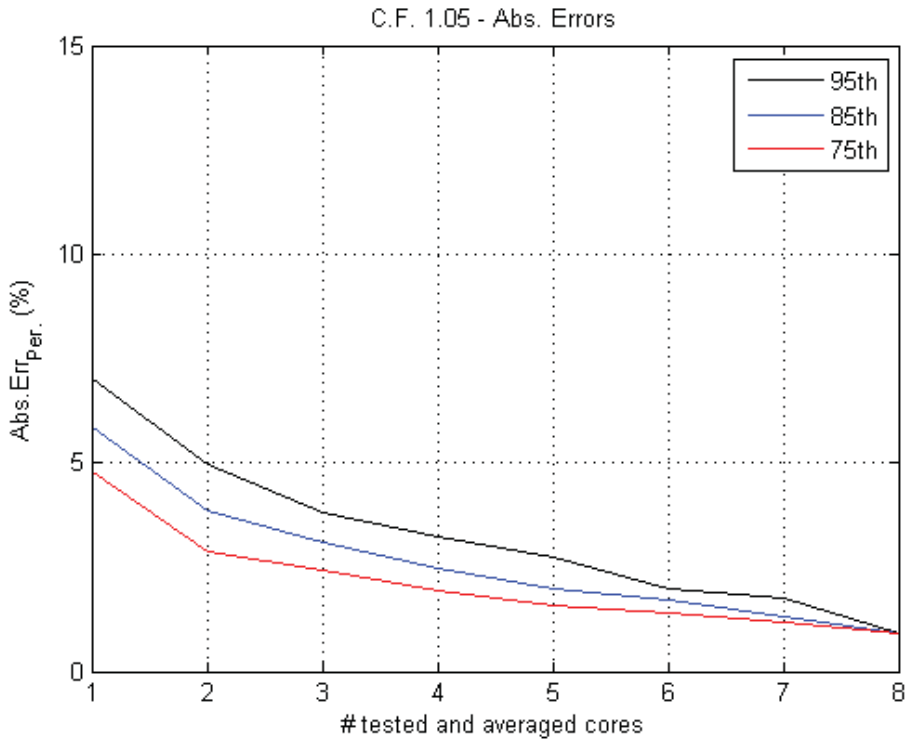

Figure E.1: Expected error curves of core random sampling analysis A.

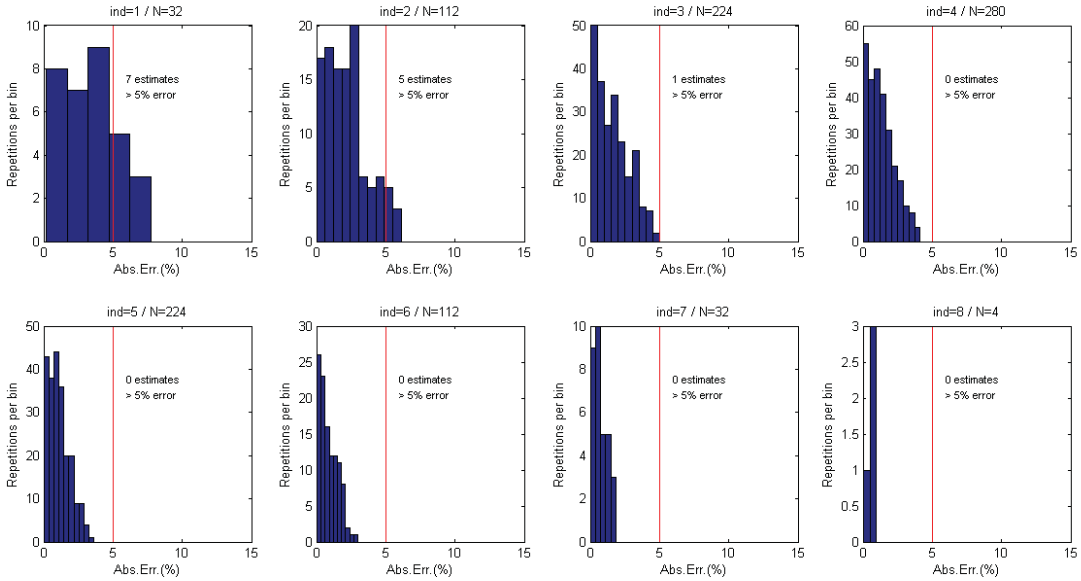

Figure E.2: Dataset histograms of core random sampling analysis A. The red line indicates the 5% error level. Text indicates the number of strength estimates having an error greater than 5%.

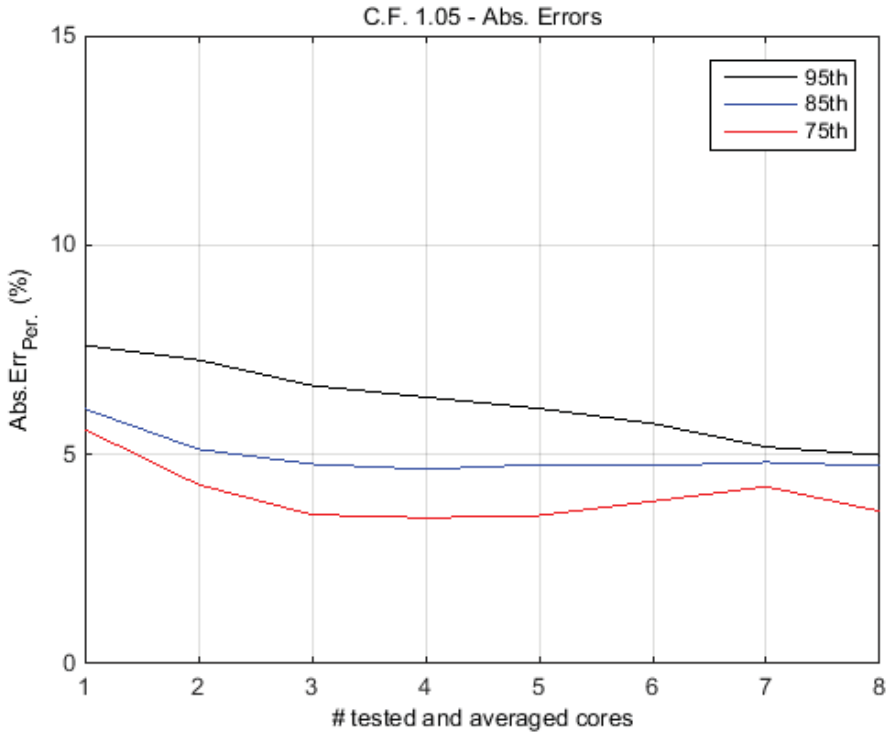

Figure E.3: Expected error curves of core random sampling analysis B.

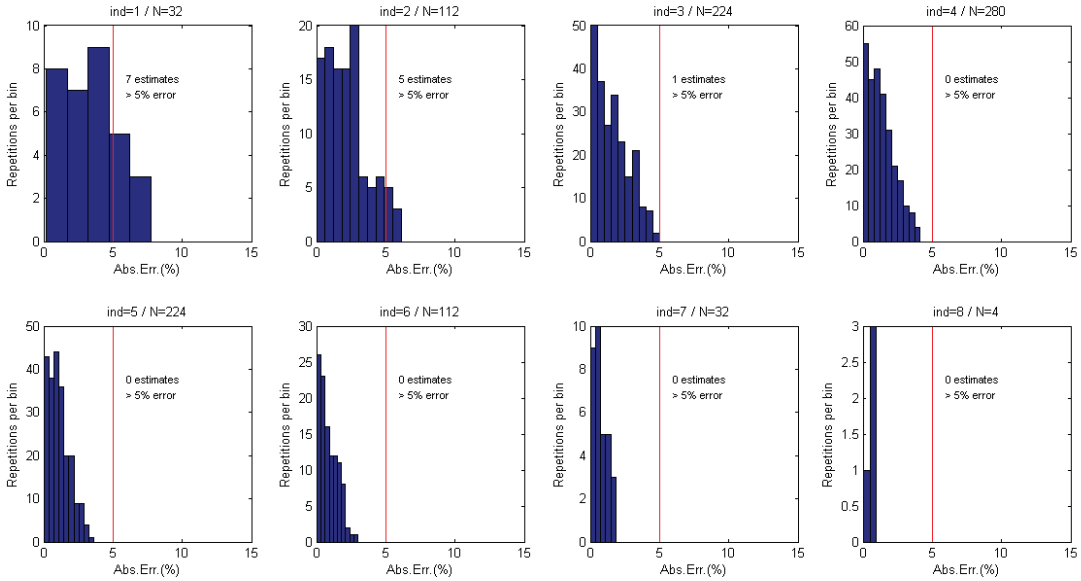

Figure E.4: Dataset histograms of core random sampling analysis B. The red line indicates the 5% error level. Text indicates the number of strength estimates having an error greater than 5%.

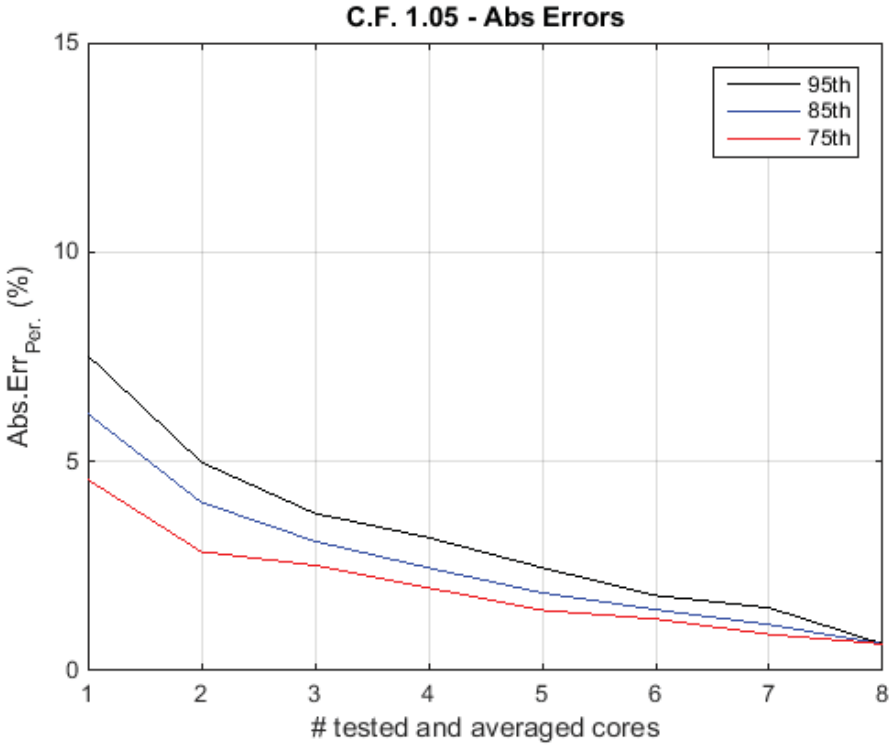

Figure E.5: Expected error curves of core random sampling analysis C.

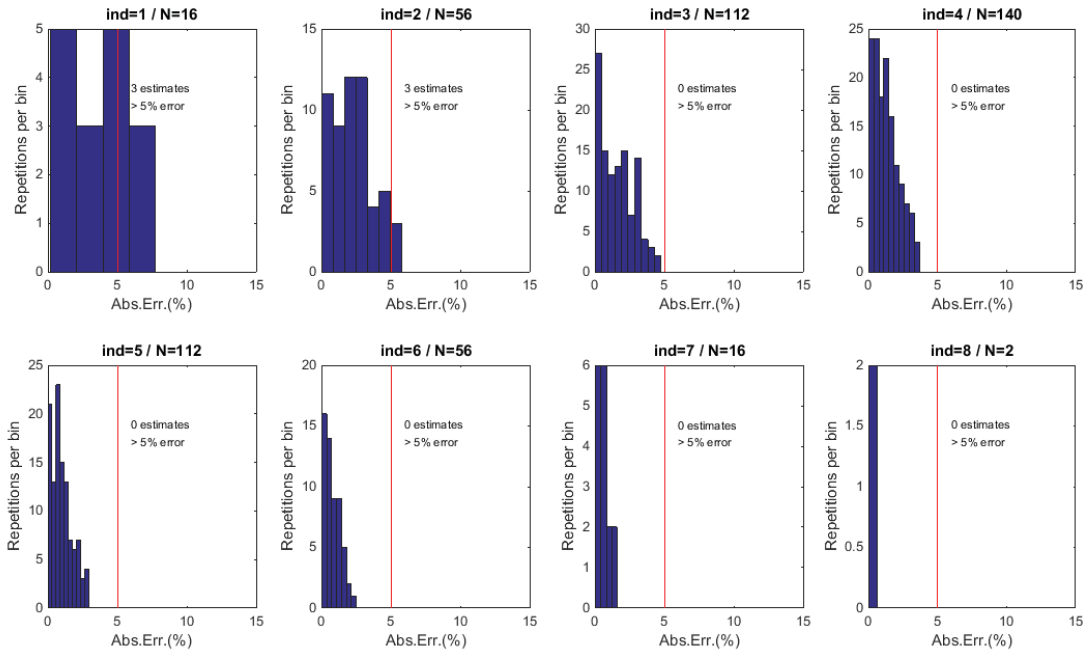

Figure E.6: Dataset histograms of core random sampling analysis C. The red line indicates the 5% error level. Text indicates the number of strength estimates having an error greater than 5%.

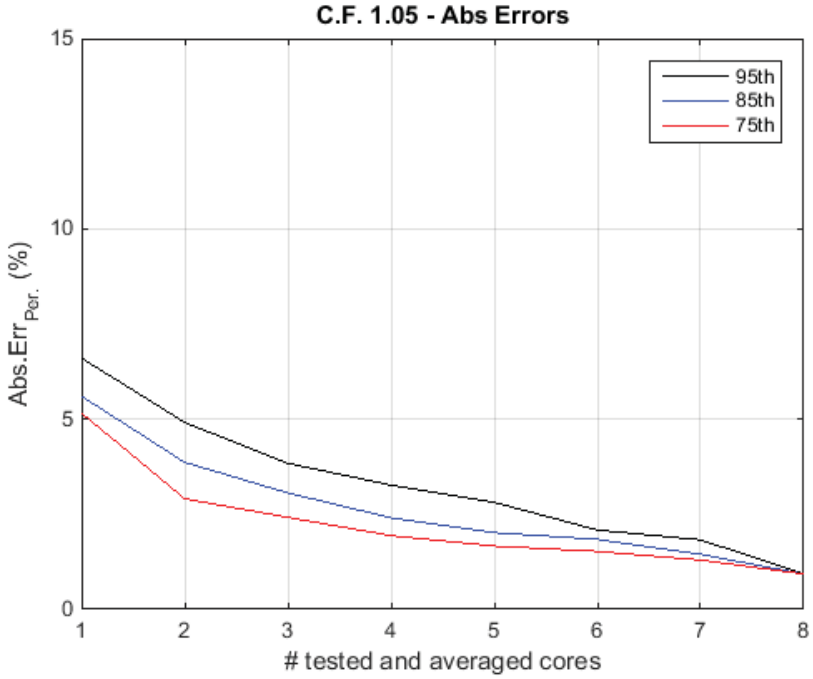

Figure E.7: Expected error curves of core random sampling analysis D.

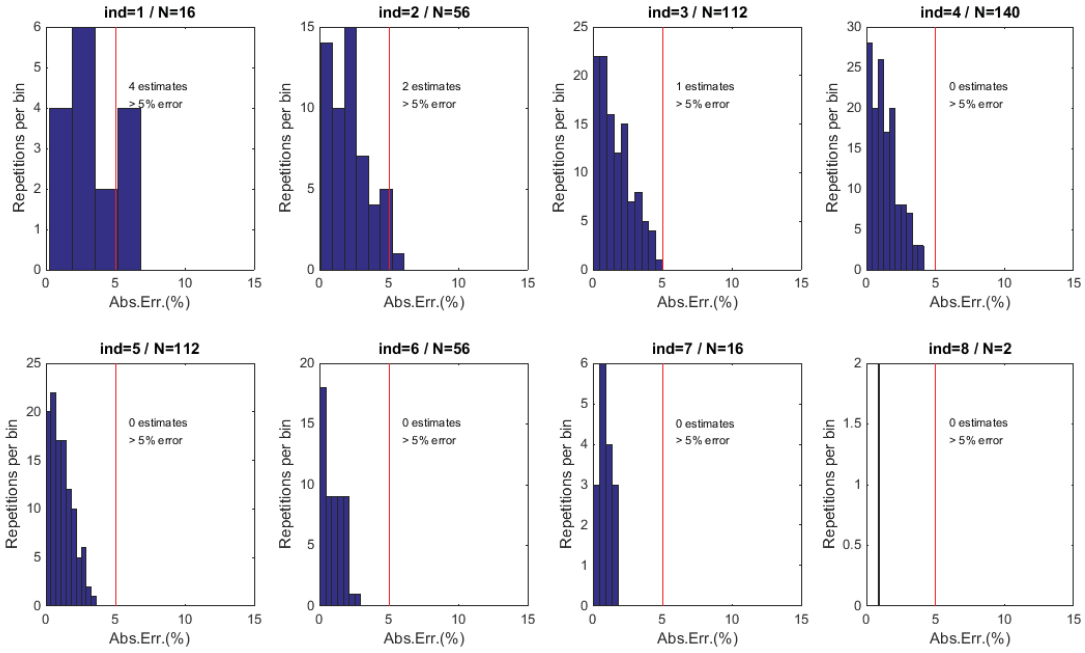

Figure E.8: Dataset histograms of core random sampling analysis D. The red line indicates the 5% error level. Text indicates the number of strength estimates having an error greater than 5%.

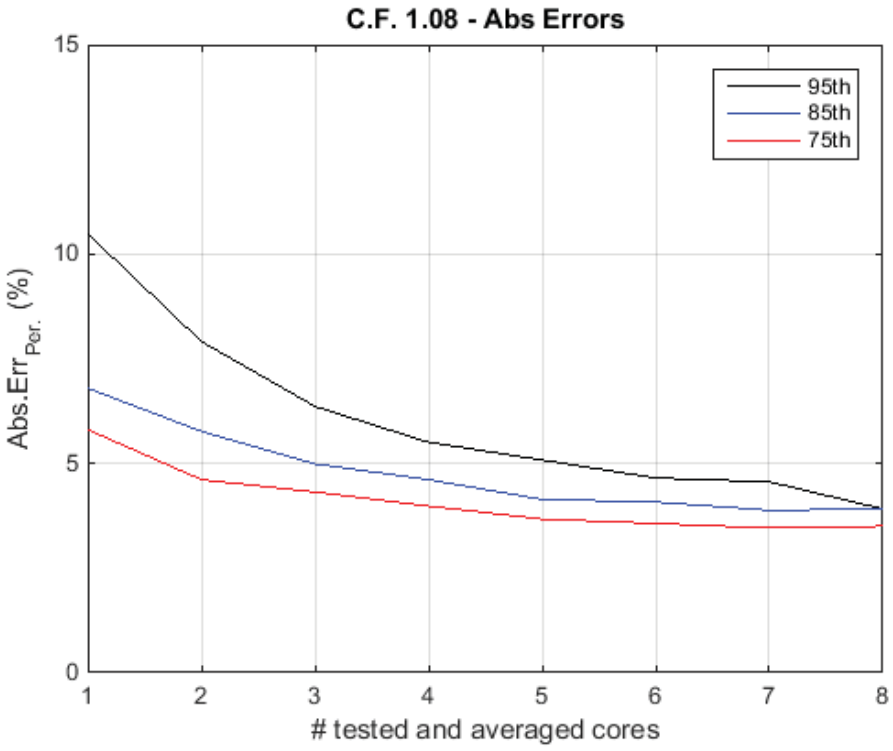

Figure E.9: Expected error curves of core random sampling analysis E.

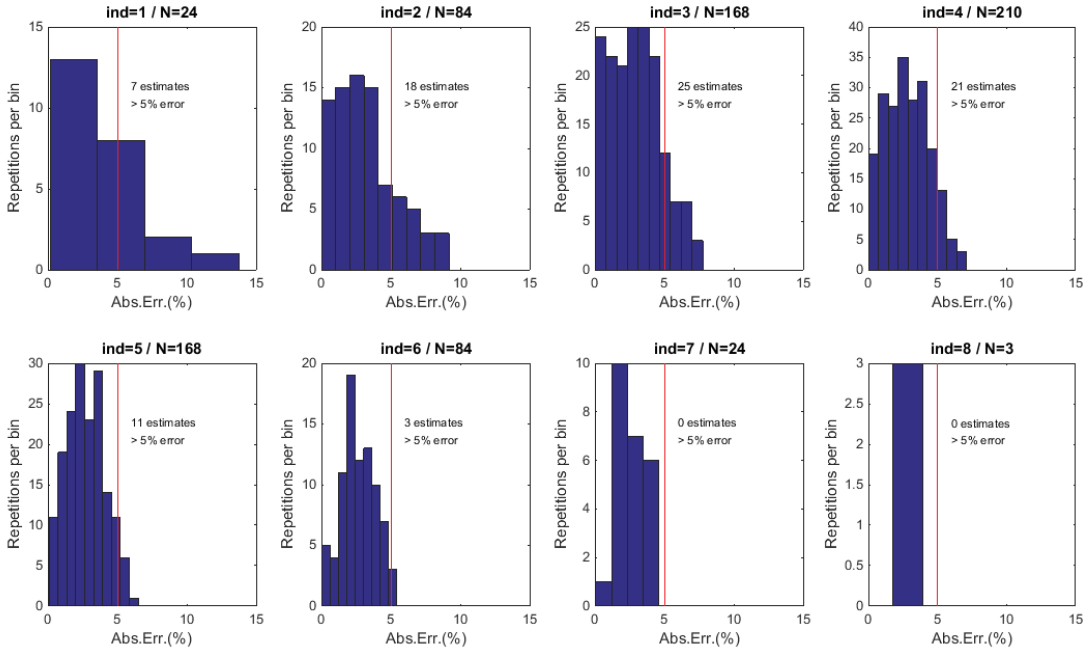

Figure E.10: Dataset histograms of core random sampling analysis E. The red line indicates the 5% error level. Text indicates the number of strength estimates having an error greater than 5%.

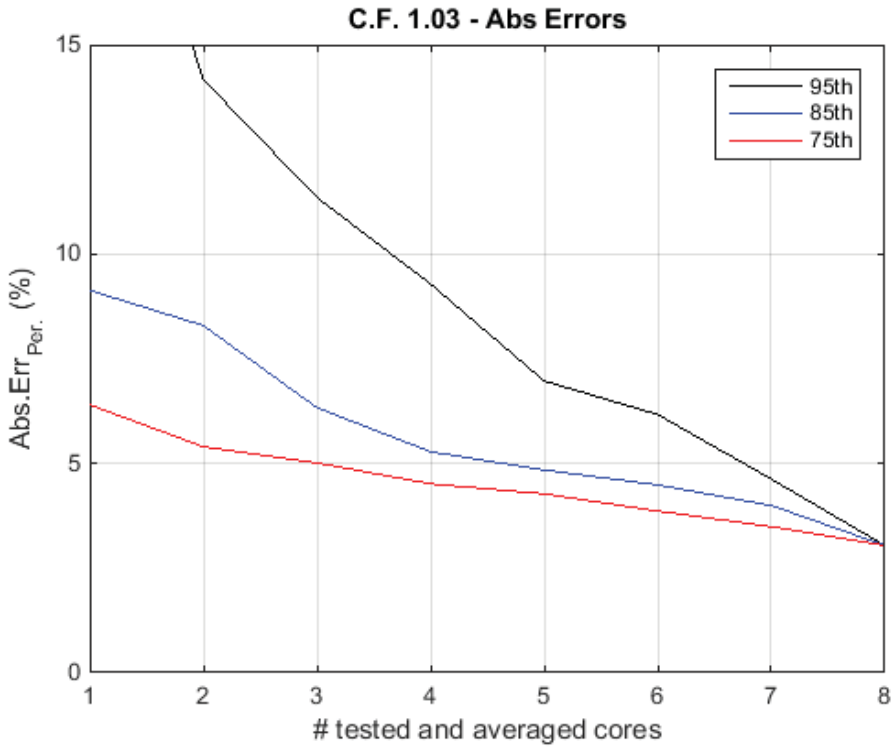

Figure E.11: Expected error curves of core random sampling analysis F.

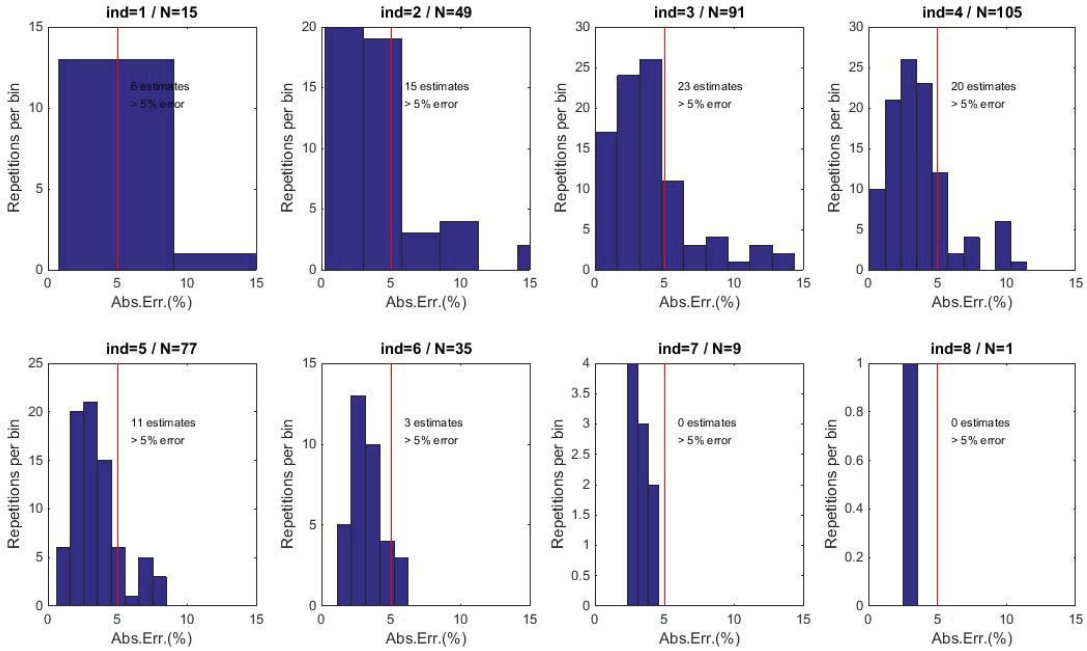

Figure E.12: Dataset histograms of core random sampling analysis F. The red line indicates the 5% error level. Text indicates the number of strength estimates having an error greater than 5%.

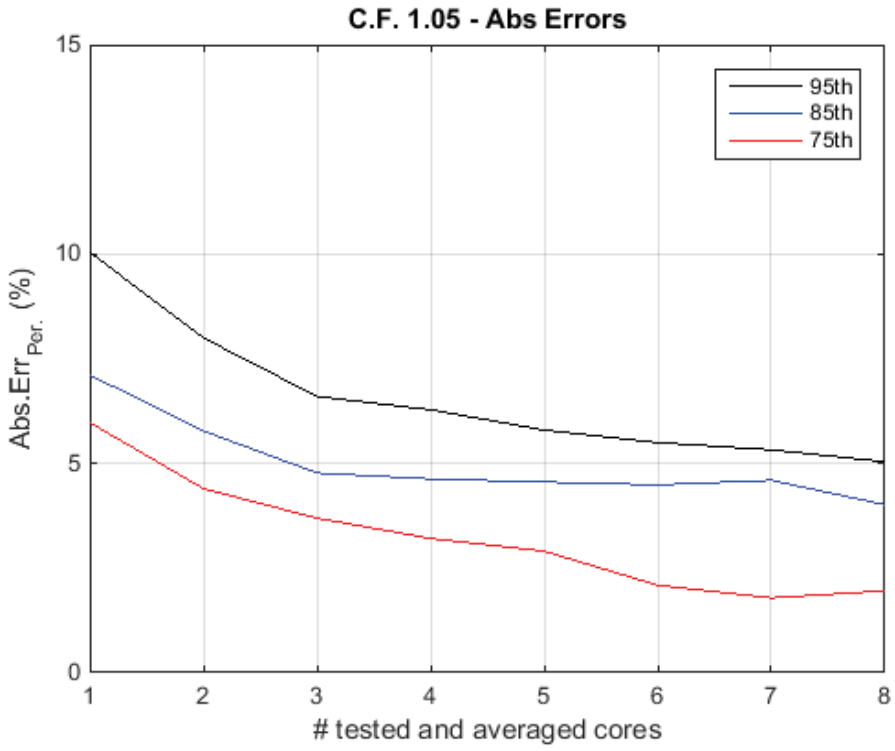

Figure E.13: Expected error curves of core random sampling analysis G.

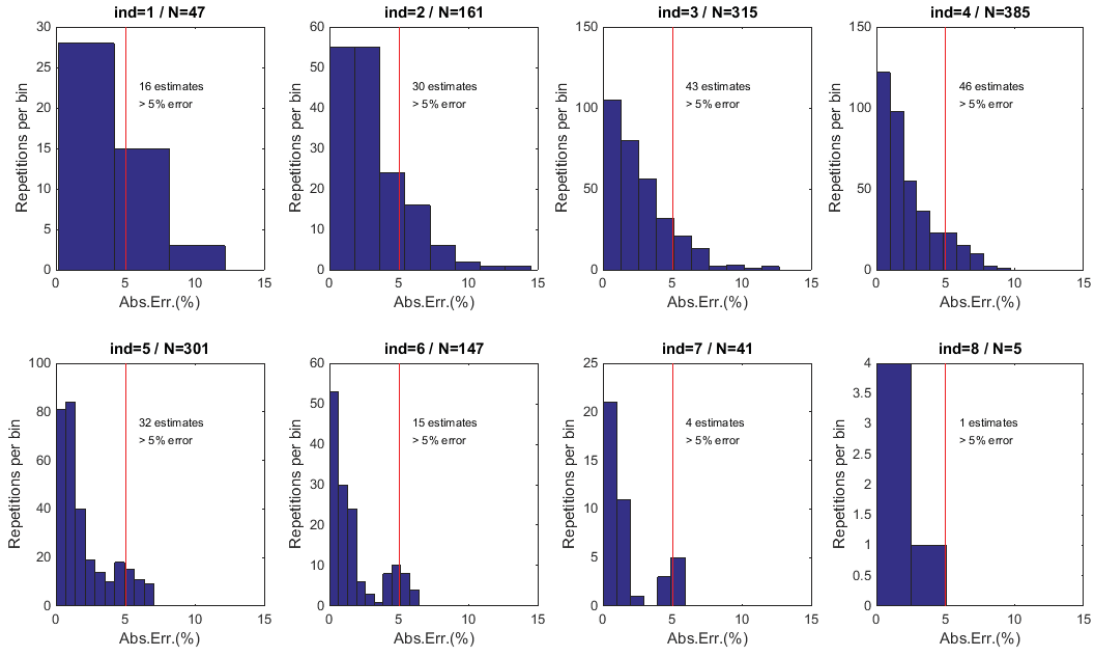

Figure E.14: Dataset histograms of core random sampling analysis G. The red line indicates the 5% error level. Text indicates the number of strength estimates having an error greater than 5%.

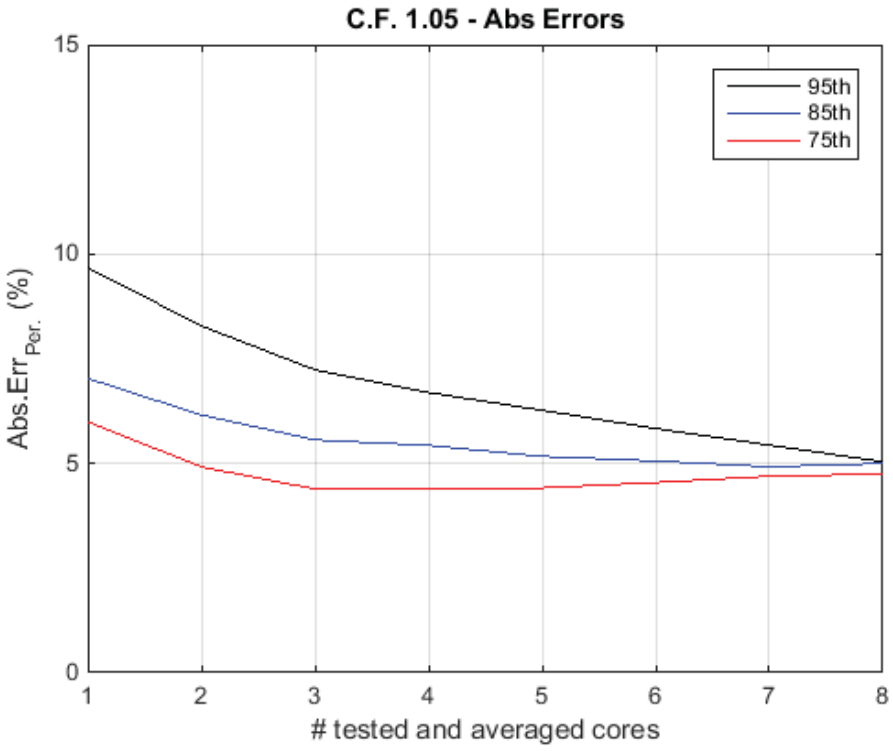

Figure E.15: Expected error curves of core random sampling analysis H.

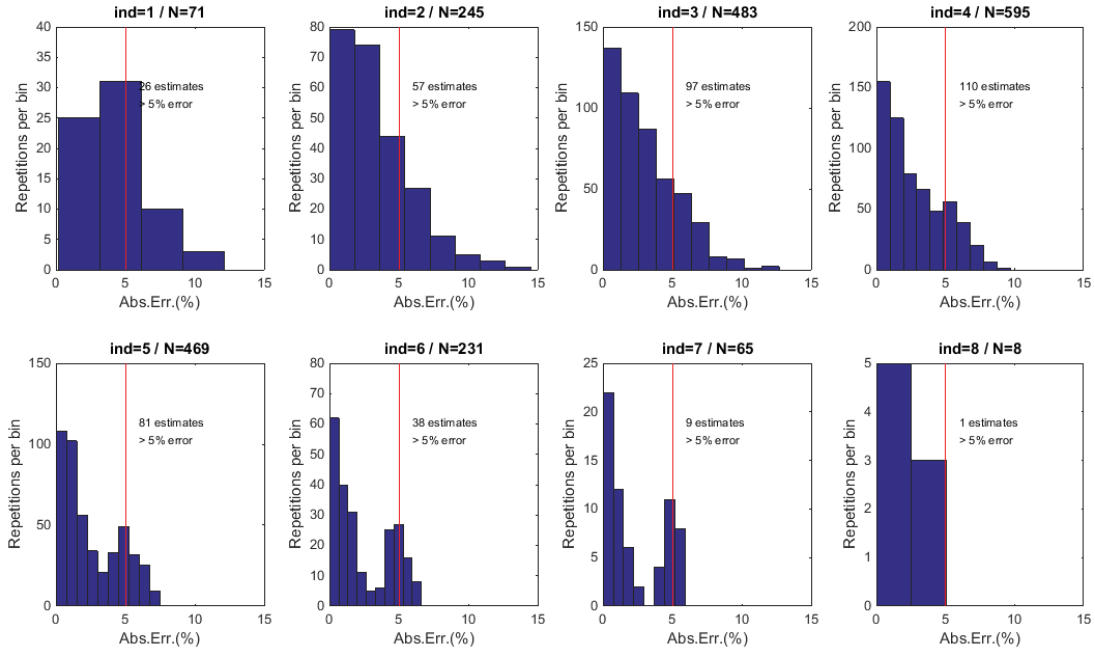

Figure E.16: Dataset histograms of core random sampling analysis H. The red line indicates the 5% error level. Text indicates the number of strength estimates having an error greater than 5%.

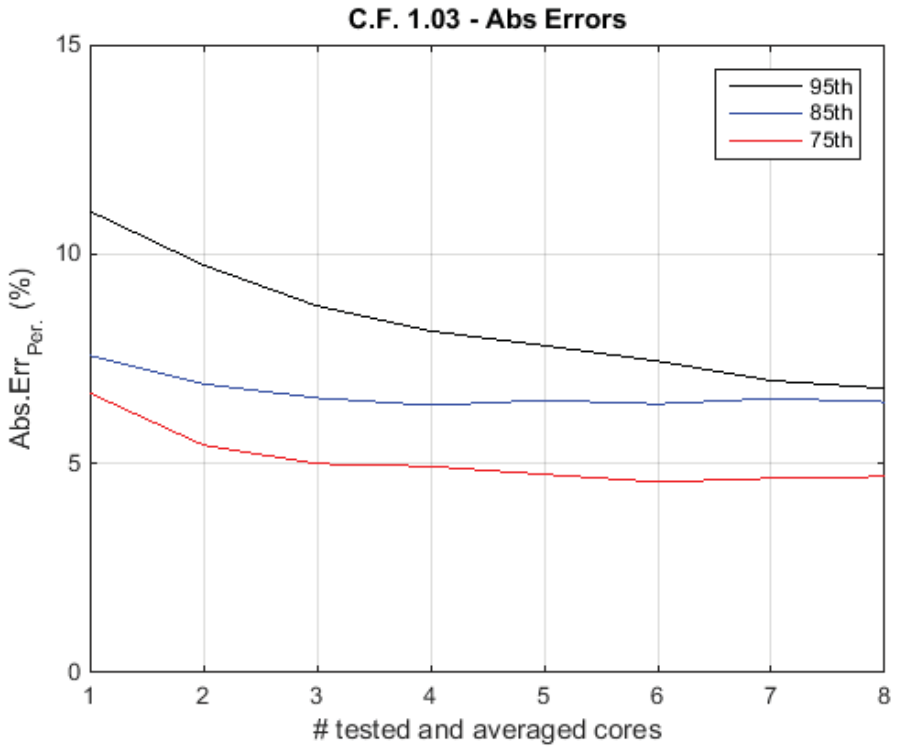

Figure E.17: Expected error curves of core random sampling analysis I.

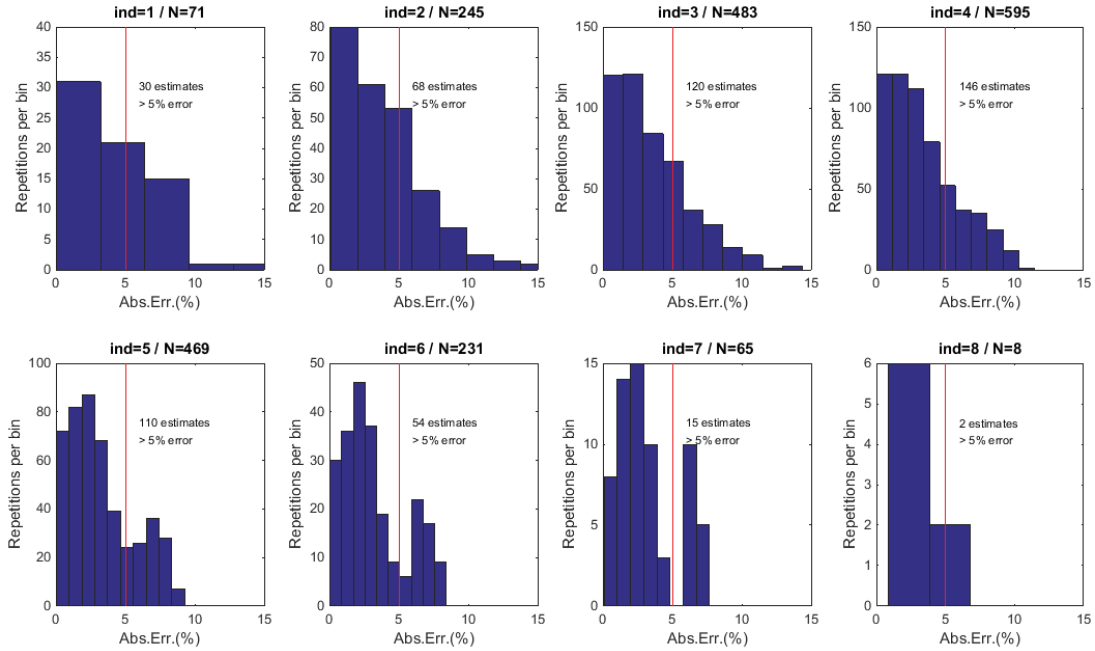

Figure E.18: Dataset histograms of core random sampling analysis I. The red line indicates the 5% error level. Text indicates the number of strength estimates having an error greater than 5%.

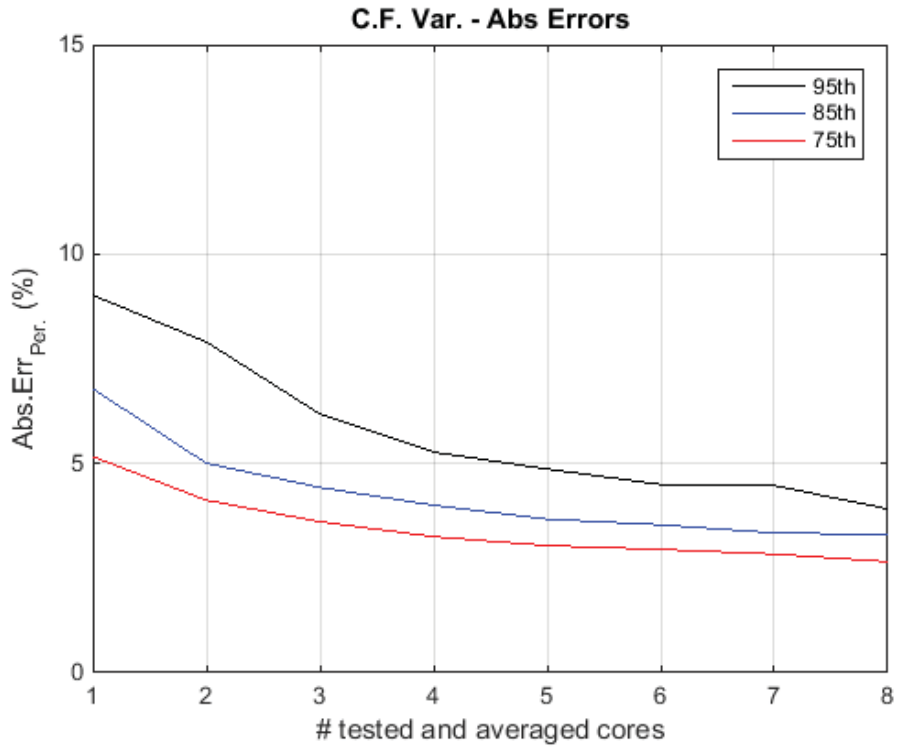

Figure E.19: Expected error curves of core random sampling analysis J.

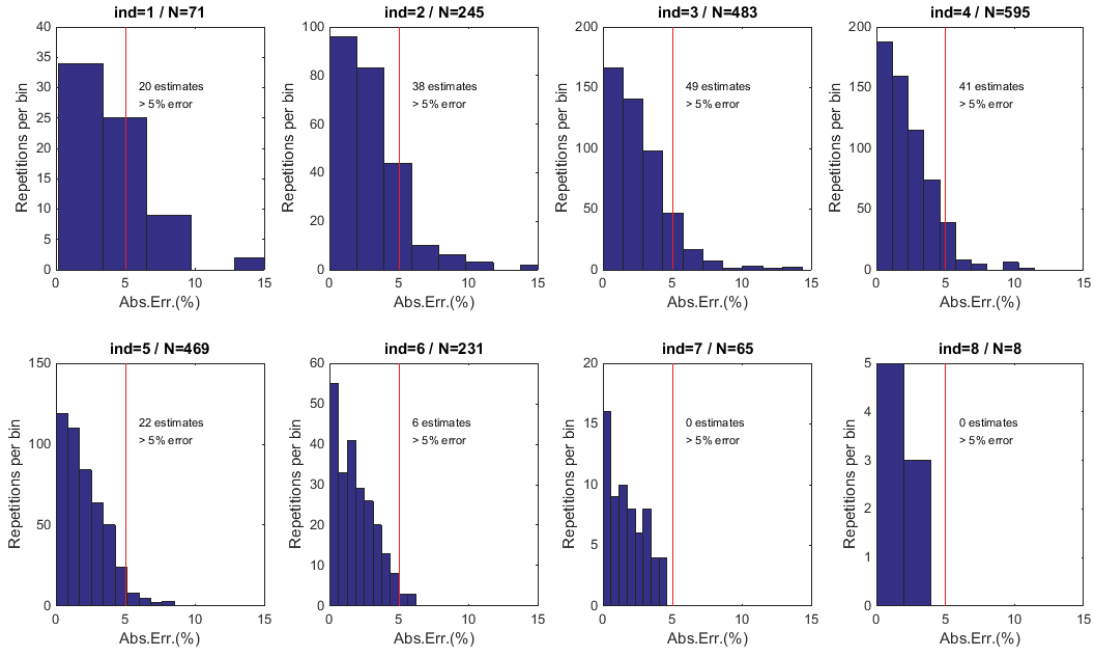

Figure E.20: Dataset histograms of core random sampling analysis J. The red line indicates the 5% error level. Text indicates the number of strength estimates having an error greater than 5%.

APPENDIX F: AGGREGATE GRADATIONS

F.1 COARSE AGGREGATE 1, CM16, KANKAKEE

Sieve/Test	Average	Unit
1/2" (12.5mm)	100.0	%
3/8" (9.5mm)	96.2	%
1/4" (6.3mm)	64.1	%
#4 (4.75mm)	39.8	%
#8 (2.36mm)	7.6	%
#16 (1.18mm)	3.0	%
#200 (75um)	1.77	%
Pan	0.00	%

Figure F.1: CM16 aggregate gradation expressed in terms of percentage of aggregate passing through the specified sieve. Provided by Prairie Materials.

F.2 COARSE AGGREGATE 2, CM11, KANKAKEE

Sieve/Test	Average	Unit
1 1/2" (37.5mm)	100.0	%
1" (25mm)	100.0	%
3/4" (19mm)	85.7	%
5/8" (16mm)	68.4	%
1/2" (12.5mm)	44.8	%
3/8" (9.5mm)	24.6	%
1/4" (6.3mm)	10.9	%
#4 (4.75mm)	6.9	%
#8 (2.36mm)	2.7	%
#16 (1.18mm)	2.0	%
#200 (75um)	1.56	%
Pan	0.00	%

Figure F.2: CM11 aggregate gradation expressed in terms of percentage of aggregate passing through the specified sieve. Provided by Prairie Materials.

F.3 FINE AGGREGATE, FA, MID-AMERICA, MAHOMET

Table F.1: Fine Aggregate Gradation (Provided by Prairie Materials)

Sieve	% Passing
3/8 (9.5 mm)	100
#4 (4.75 mm)	96.1
#8 (2.36 mm)	89.5
#16 (1.18 mm)	79.1
#30 (0.6 mm)	63.9
#40 (0.425 mm)	48.2
#50 (0.3 mm)	25.4
#100 (0.15 mm)	2.5
#200 (0.075 mm)	1.3
Pan	0


Illinois Department
of Transportation


ILLINOIS
UNIVERSITY OF ILLINOIS AT URBANA-CHAMPAIGN